MAGNETISM AND MAGNETIC EXCITATIONS IN NARROW BAND METALS AND RARE-EARTH COMPOUNDS

by

Abdulrahim A. Bahurmuz

A thesis submitted to the Faculty of Graduate Studies and Research of McGill University in partial fulfillment of the requirements for the Degree of Doctor of Philosophy

Baton Electronics Research Laboratory
Department of Physics
McGill University
Montreal, Quebec
Canada

January 1976

McGill University

Faculty of Graduate Studies & Research

Final Oral Examination
for the Degree of
Doctor of Philosophy
of

Abdulrahim Abdulla Bahurmuz

of the Department of Physics
on 9 February 1976 at 10:15 a.m.
in the Foster Radiation Seminar Room
McGill University

COMMITTEE:

Prof. M. Whitehead (Pro-Dean)
Prof. R. Harris
Prof. J.M. Robson
Prof. N. Rumin
Prof. M. Shapiro
Prof. J. Ström-Olsen
Prof. M. Zuckermann

W.F. HITSCHFELD,
Dean

Members of Faculty and Graduate
Students are invited to be present.

Abdulrahim Abdulla Bahurmuz

Ph.D. Department of Physics

MAGNETISM AND MAGNETIC EXCITATIONS IN NARROW-BAND METALS AND RARE-EARTH COMPOUNDS

In Part I of this thesis, we investigate the properties of a model for magnetism in narrow band metals which consists of localized orbitals hybridizing with a broad conduction band. We examine the static magnetic properties of this model and obtain the conditions under which a magnetic state exists. We also examine the magnetic excitations, spin waves and spin fluctuations, in this model. We show that the spin wave dispersion relation has the usual quadratic form in the long wavelength limit. We also show that the scattering of electrons off spin fluctuations leads to the usual T^2 term in the resistivity at low temperatures and discuss its application to the pressure effects in α-Ce.

In Part II, we consider the damping of magnetic excitations in singlet-ground-state systems by random fields (due to thermal fluctuations) using the coherent potential approximation (CPA) and discuss its application to Pr_3Tl. We find that, in addition to broadening, the scattering shifts the spin wave modes.

Abstract

In Part I of this thesis, we investigate the properties of a model for magnetism in narrow band metals which consists of localized orbitals hybridizing with a broad conduction band. We examine the static magnetic properties of this model and obtain the conditions under which a magnetic state exists. We also examine the magnetic excitations, spin waves and spin fluctuations, in this model. We show that the spin wave dispersion relation has the usual quadratic form in the long wavelength limit. We also show that the scattering of electrons off spin fluctuations leads to the usual T^2 term in the resistivity at low temperatures and discuss its application to the pressure effects in α-Ce.

In Part II, we consider the damping of magnetic excitations in singlet-ground-state systems by random fields (due to thermal fluctuations) using the coherent potential approximation (CPA) and discuss its application to Pr_3Tl. We find that, in addition to broadening, the scattering shifts the spin wave modes.

Résumé

La première partie de cette thèse concerne l'étude des propriétés d'un modèle pour le magnétisme dans les métaux à bande étroite, qui consiste d'orbitales localisées hybridées avec une large bande de conduction. Nous examinons les propriétes magnétiques statiques de ce modèle et obtenons les conditions sous lesquelles un état magnétique existe. Nous examinons aussi dans ce modèle les excitations magnétiques, les ondes de spin et les fluctuations de spin. Nous montrons que la relation de dispersion de l'onde de spin possède la forme quadratique usuelle dans la limite des grandes longueurs d'onde. Nous montrons aussi que la dispersion des électrons par les fluctuations de spins conduit au terme habituel en T^2 dans la résistivité à basse température et discutons son application aux effets de pression dans α-Ce.

Dans la 2^{ième} partie, nous considerons l'amortissement des excitations magnétiques par des champs aléatoires (dûs aux fluctuations thermiques) dans les systèmes ayant pour état fondamental un singulet, en utilisant l'approximation du potentiel cohérent (APC) et nous discutons son application à Pr_3Tl. Nous trouvons que, en plus de les élargir, la dispersion déplace les modes d'onde de spin.

Acknowledgements

I am very grateful to my supervisor Dr. M.J. Zuckermann for his help, guidance and encouragement throughout the course of this work.

I would like to thank Dr. D.J.W. Geldart for suggesting the problem discussed in Chapter V and Appendix B and for helpful discussions. I wish to acknowledge the close cooperation of Dr. W.J.L. Buyers in the work of Part II of this thesis and to thank him for helpful discussions. I would also like to thank Dr. R. Harris for helpful discussions and a critical reading of the manuscript and to Dr. M. Plischke for helpful discussions.

Finally I would like to thank B.G. Mulimani and D. Zobin for many useful discussions, and Deborah Terry for typing this thesis.

The financial support of the National Research Council of Canada is gratefully acknowledged.

TABLE OF CONTENTS

PREFACE

This thesis is concerned with the study of some problems related to magnetism in metallic systems. The magnetic moment associated with an atom results from the moments of electrons such as the 3d electrons in transition metals and the 4f electrons in the rare-earth metals. These two groups of metals, however, differ in a fundamental way: the 3d electrons in the transition metals are itinerant while the 4f electrons in the rare-earth metals are well localized at their respective atomic sites. Thus, in the transition metals such as Ni, Co and Fe a band picture is employed for the 3d electrons and the magnetization results from the splitting of the spin up and spin down bands. On the other hand the magnetic moments in the rare-earth metals (e.g. Gd) are well localized and they interact via the conduction electrons.

In certain metals the localized magnetic electrons can hybridize with a conduction band i.e. the localized orbitals and the conduction states are mixed and electrons can jump from one to the other. If the localized orbitals have appreciable overlap with orbitals on neighbouring sites they will form a narrow band and this band may also hybridize with a broad conduction band.

In other metals the localized moment is strongly affected by the electric charges of the neighbouring

ions. These charges produce an electrostatic potential (called the crystal-field potential) which can split the ground state multiplet of the central ion. This changes the character of the moment and leads to an interesting magnetic behaviour.

In Part I of this thesis we study the magnetic properties of metals in which the magnetic electrons hybridize with the conduction band. In particular we examine their static properties such as magnetization and Curie temperatures and also their collective excitations in both the ferromagnetic and paramagnetic states. In Part II we consider metallic systems with strong crystal-fields. Here we consider the damping or scattering of spin waves by fluctuating magnetic fields which result from thermal fluctuations of spins.

Statement of originality

The material in Chapters I-IV on the static and dynamic magnetic properties of the narrow band model is original. The extension of the double resonance theory for the interaction between two moments is also original. To the best of my knowledge, the coherent potential approximation is used for the first time in Part II to investigate the scattering of spin waves in singlet-ground-state systems.

PART I

Magnetism and magnetic excitations in narrow band metals

INTRODUCTION

Ferromagnetism has been a fascinating subject for many years. In 1907 Weiss put forward the "molecular field" hypothesis that each atom of a ferromagnetic material is a magnetic dipole and is acted upon by an intense magnetic field proportional to, and parallel to, the magnetization in the region surrounding it. This met with considerable success in accounting for spontaneous magnetization and its variation with temperature. Weiss realized that the molecular field has to be more intense than could be accounted for by ordinary magnetic forces but was unable to trace its origin. The strong interaction responsible for spontaneous magnetization was recognized by Heisenberg in 1926 as being the "exchange" interaction between electrons predicted by the then newly developed quantum mechanics. The exchange forces are basically electrostatic in origin and consequently may have an intensity many orders of magnitude greater than the ordinary magnetic forces between the spin moments.

The first theory of ferromagnetism based on exchange interactions was put forward independently by Heisenberg and

Dirac in 1928. They showed that the exchange interaction between electrons localized on different atomic sites can be written in terms of a coupling between their spins. The result is the Heisenberg Hamiltonian

$$H = - \sum_{ij} J_{ij} \, \underline{J}_i \cdot \underline{J}_j \qquad (1)$$

where $\underline{J}_i$ is the spin of the i^{th} atomic site and J_{ij} the exchange interaction between the i^{th} and the j^{th} atoms. The Heisenberg model of direct interaction is mainly applicable to insulators such as the ferromagnetic compounds EuO and $GdCl_3$.

In the iron-group metals Fe, Co and Ni, calculations show that the exchange coupling between electrons localized on atomic sites is too small to account for their strong ferromagnetism. There are, moreover, other reasons why a perfectly localized model is inadequate for these metals. In particular it is now known that the measured moments per atom are not integral numbers of Bohr magnetons. The 'collective electron' model first put forward by Stoner and by Slater explained this fact by taking into account the itinerant nature of the 3d electrons. These electrons now form bands and the effect of the exchange interaction is to split the spin up and spin down bands giving rise to a net magnetic moment. As in the Weiss molecular field theory,

the exchange field which splits the spin up and spin down bands is in turn proportional to the net magnetization. The band picture allows a non-integral occupation per atom and this can explain the fact that the moments in the iron-group metals are not integral numbers of Bohr magnetons.

Direct exchange between electrons localized on atomic sites is even less likely to be significant in rare-earth metals where the 4f orbitals, with radii of about 0.3Å, overlap very little with orbitals on neighbouring atoms which are separated by about 3Å. In the rare-earth metals, indirect exchange via the conduction electrons is responsible for the magnetic order. An example of such an interaction is the Ruderman-Kittel-Kasuya-Yosida or RKKY interaction. In this model, an exchange interaction between a localized spin and the conduction electrons causes a polarization of the conduction electrons which is centered around the local moment and falls off with distance in an oscillatory manner. Another localized spin sees this polarization and interacts with it thus leading to a coupling between the spins. For two spins $\underline{S}_1$ and $\underline{S}_2$ separated by a distance R the RKKY interaction energy is given by

$$E_{RKKY} = \frac{9\pi J^2 z^2}{\epsilon_F} \frac{2k_F R \cos 2k_F R - \sin 2k_F R}{(2k_F R)^4} \underline{S}_1 \cdot \underline{S}_2 \qquad (2)$$

where J is the exchange coupling between the localized spin and the conduction electrons, Z the number of conduction electrons per atom, ε_F the Fermi energy and k_F the Fermi wave vector given by

$$k_F = (3\pi^2 n)^{1/3} \qquad (3)$$

where n is the conduction electron concentration. The interaction (2) is oscillatory and we note that the coupling can be changed from ferromagnetic to anti-ferromagnetic by changing k_F i.e. by changing the electron concentration.

In the first part of this thesis we examine a new model for magnetism that is more suitable for certain metals and intermetallic compounds. An interesting example is presented by a group of intermetallic compounds known as Heusler alloys. Before describing the new model we give below a brief description of these alloys.

The Heusler alloys first became of interest in 1903 when F. Heusler discovered that it was possible to make ferromagnetic alloys entirely from non-ferromagnetic elements. These alloys were made from copper-maganese bronze alloyed with the elements tin, aluminum, arsenic, antimony, bismuth, or boron. Among the first to be discovered were the alloys Cu_2Mn Sn and Cu_2 Mn Al. A comprehensive crystallographic investigation of the structure of one of these alloys was carried out by Bradley and Rodgers (1934) on Cu_2 Mn Al. The structure is shown in Figure 1 and is best described in terms

of four interpenetrating face-centered cubic sublattices A, B, C and D. At the stoichiometric composition Cu_2MnAl the A and C sites are occupied by Cu atoms, the B sites by Mn and the D sites by Al. This arrangement corresponds to the Strukturbericht type $L2_1$. Heusler alloys are now commonly defined as ternary intermetallic compounds at the stoichiometric composition X_2YZ with the $L2_1$ structure.

The magnetic moment in the Heusler alloys was believed by early investigators to be carried by the Mn atoms. The first direct evidence in support of this view was obtained by Felcher et al (1963) from neutron diffraction measurements. They investigated the magnetic moment distribution in Cu_2MnAl and were able to show that within the accuracy of the experiment the entire moment of the molecule could be attributed to the Mn atom. Later experiments have confirmed that in most Heusler alloys containing Mn the magnetic moment is confined to the Mn sites. The only exceptions are a series containing cobalt (Webster (1971)) in which the magnetic moment is shared with the cobalt atoms.

A summary of the properties of the principal ferromagnetic Heusler alloys is shown in Table 1. The lattice parameter is of the order of 6Å in these alloys. The magnetic moment per formula is of the order of $4\mu_B$ (where μ_B is the Bohr magneton) in the non-cobalt alloys and of the order of $5\mu_B$ in the cobalt ones. In the latter, between 25-30 per cent of the moment is on the Co atoms and the rest on the Mn atoms. In contrast to the lattice constant and

Alloy	Lattice Parameter $2a_o$ (Å)	Curie Temperature T_c (K)	Magnetic Moment per formula μ (Bohr magnetons)
Cu_2MnAl	5.95	600	3.8
Cu_2MnIn	6.2	520	4.0
Cu_2MnSn	6.1	(530)	4.1
Pd_2MnSn	6.380	189	4.23
Pd_2MnSb	6.424	247	4.40
Ni_2MnIn	6.068	323	4.40
Ni_2MnSn	6.052	344	4.05
Ni_2MnSb	6.000	360	3.27
Co_2MnSi	5.654	985	5.07
Co_2MnGa	5.770	694	4.05
Co_2MnGe	5.743	905	5.11
Co_2MnSn	6.000	829	5.08

Table 1. Properties of some of the ferromagnetic Heusler alloys. (Taken from Webster (1969)).

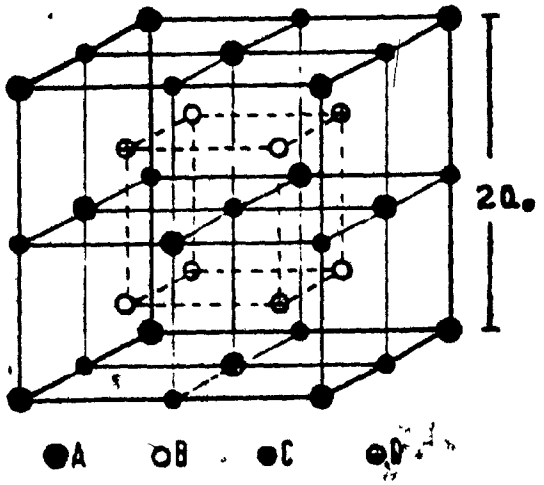

Fig. 1. The Heusler structure.

magnetic moment the Curie temperature varies widely in these alloys being highest in the cobalt alloys.

The interaction responsible for the alignment of the moments was first discussed in terms of direct exchange. According to the early theory, ferromagnetism requires the presence of atoms with an incomplete shell of electrons to provide a permanent moment, usually the d and f shells. These atoms must have neighbours with which they can interact to produce a positive value of the exchange integral, and hence the distance between the atoms must not be too great, or else the interaction energy becomes insufficient to stabilize the ferromagnetic condition. Coles et al (1949) used these ideas to compare Cu_2MnAl and Cu_2MnIn. These two alloys are strictly analogous as regards valencies, structures and electron concentration. However, the In atom (which is below Al in the periodic table) has a larger radius and consequently the lattice constant and the resultant Mn-Mn separation is larger in Cu_2MnIn than Cu_2MnAl. Assuming approximately the same moment on the Mn atoms in both alloys they concluded that in the direct exchange picture the lower Curie temperature in the In alloy is due to the larger Mn-Mn separation in this compound.

However, objections have been raised against direct exchange between the Mn atoms because the Mn-Mn separation in these alloys is $\sim 4.2\text{Å}$ which is thought to be too large to account for the strong ferromagnetism in the non-cobalt

alloys. (In alloys containing cobalt the situation is more complicated in that the Co atoms also carry a moment and one can have Co-Co, Co-Mn and Mn-Mn interactions. The Co-Co distance is $\sim 3.0\text{Å}$ while the Co-Mn separation is $\sim 2.6\text{Å}$ and it is likely that there would be direct exchange in these alloys. The exchange mechanism in the cobalt alloys is expected to be quite complex and in what follows we will concentrate on the simpler case of non-cobalt alloys.) It is also known that the conduction electrons play an important role in the magnetism of these alloys. The series Pd_2MnIn, Pd_2MnSn and Pd_2MnSb illustrates this point. The last two alloys are ferromagnetic with Curie temperatures of 189 and 247K respectively (see Table 1) while Pd_2MnIn is antiferromagnetic with a Néel temperature of 142K. The lattice parameter for Pd_2MnIn is $2a_o = 6.373\text{Å}$ and its magnetic moment per formula is $4.3\ \mu_B$. Although small changes in the lattice parameter and the magnetic moment may have some effect on the exchange forces, it is the conduction electron concentration (assuming that In contributes 3 electrons to the conduction band while Sn and Sb contribute 4 and 5 electrons respectively) that determines whether ferromagnetic or anti-ferromagnetic order will predominate. This suggests that the interaction between the Mn atoms might be an indirect one via the conduction electrons such as the RKKY interaction. In this way it would be possible

to explain the change from anti-ferromagnetism in Pd_2MnIn to ferromagnetism in Pd_2MnSn and Pd_2MnSb as resulting from a change in the electron concentration as mentioned earlier.

The magnetic moment of the Mn atoms in an alloy such as Cu_2MnAl results from the unfilled d-shells of Mn. The outer s and p electrons of Cu, Mn and Al form broad conduction bands while the d-orbitals of Mn remain well localized. However the broad conduction bands overlap the d-levels and mixing or hybridization takes place between these states. Thus any theory for the Heusler alloys must take into account this hybridization and in the first part of this thesis we consider such a model. To simplify matters we take an idealized situation and consider a model consisting of the following:

(i) a broad free-like conduction band for the outer-shell electrons

(ii) a periodic lattice of N magnetic atoms each with a localized non-degenerate orbital

(iii) mixing between the conduction and localized states via a hybridization matrix element which allows electrons to jump from a localized state into a conduction state and vice versa

(iv) a Coulomb repulsion between opposite spin electrons on the localized orbital. This spin-splitting interaction is responsible for the magnetic moment formation on the localized levels.

The Mn atoms in the Heusler alloys are well separated

and we have assumed the 3d orbitals to be well localized. In reality, however, there would be some overlap between orbitals on neighbouring atoms and the 3d electrons would form a very narrow band. Although we have neglected the overlap of the 3d orbitals we still refer to this model as the narrow band model. We also note that this model is also suitable for the 4f electrons in the rare-earth metals and the 5f electrons in the actinide metals.

The properties of the narrow band model are investigated in the first three chapters. In chapter I we examine the static magnetic properties of this system. The Coulomb repulsion(U) favors a ferromagnetic or spin split state while the mixing or hybridization potential(V) has the opposite effect. In the Hartree-Fock approximation, we discuss under what conditions a ferromagnetic state is stable as U and V are varied. We thus obtain a magnetic phase diagram which shows the magnetic and non-magnetic regions in U-V space. In the ferromagnetic state we obtain the variation of the magnetization and Curie temperature as a function of U and as expected both increase with U. Finally, we plot the temperature dependence of the magnetization and the static susceptibility.

In chapter II we consider the ferromagnetic state and examine the collective excitations or spin waves of the system. These spin waves are single particle excitations which propagate through the crystal with energy ω and wave vector q. In the long wavelength limit, we show that the dispersion

relation for these excitations has the usual quadratic form $\omega \sim Dq^2$. The stiffness coefficient D is evaluated for different values of magnetization and it is shown that for small values of the magnetization D increases linearly with magnetization.

We then consider, in chapter III, the excitations of the system in the paramagnetic state. These excitations are known as "spin fluctuations" and their spectral density is obtained. We then consider the effect of the spin fluctuations on the resistivity and show that the temperature dependence of the spin fluctuation part of the resistivity has the usual form i.e. aT^2 behaviour at low temperatures going over to a linear dependence at higher temperatures. At still higher temperatures the resistivity deviates below the linear law.

In chapter IV we discuss the application of this model to the ferromagnetic Heusler alloys. We also discuss qualitatively the possible application to α-Ce and in particular attempt to explain the pressure dependence of the resistivity found in α-Ce.

For the Heusler alloys we find that the Curie temperatures obtained are higher than the observed values and hence, in chapter V we examine another model. This is the double resonance model which considers the interaction of two Mn atoms. The d levels of each Mn atom form resonances by hybridization with the conduction band and the interaction between the atoms is via the conduction band. This interaction

was derived by Caroli (1967) who showed that, for a large separation R of the Mn atoms, it varies as $1/R^3$. This is valid for dilute alloys where the separation of the magnetic atoms is very large but is expected to be a poor approximation for concentrated alloys such as the Heusler alloys. In chapter V we obtain the $1/R^4$ correction term to this interaction and show that we can obtain a better fit to the Heusler alloys than that given by Caroli's expression.

Chapter I

The narrow band model

The magnetic moment on atoms arises from unfilled inner shells such as the 3d electrons in the transition metals, the 4f electrons in the rare-earth metals and the 5f electrons in the actinide metals. When such atoms condense into a solid the outer valence electrons form broad conduction bands. The inner shell electrons may or may not form bands depending on the extent of the overlap of the wave functions on neighbouring atoms. In the rare-earth metals the 4f electrons are well localized and retain much of their atomic character. In the iron-group metals the 3d wavefunctions on neighbouring atoms overlap to some extent and the 3d electrons form narrow bands. The same is true of some of the actinide metals where the overlap of 5f wavefunctions is appreciable. On the other hand, when transition metal or actinide atoms combine with non-magnetic metals to form intermetallic compounds the overlap is reduced and the inner shell wavefunctions remain well localized. However, when the broad conduction band formed from the outer electrons overlaps the localized orbitals, mixing or hybridization takes place as electrons jump from the localized orbitals into the conduction band and vice versa. We are thus lead to consider an idealized model consisting of a broad conduction band hybridizing with localized orbitals centred on atomic sites of a periodic lattice. The localized orbitals can

be considered as the limit of an infinitely narrow band (ie. zero overlap) and we call this model the narrow band model.

We begin in section 1.1 with a brief description of the Anderson model which considers the simpler case of one magnetic atom dissolved in a metallic host. Then in section 1.2 we describe the narrow band model and examine its static magnetic properties.

1.1 The Anderson model

The characteristic property of transition metal atoms is an unfilled inner shell of d-electrons, which gives rise to interesting magnetic properties. When such an atom is dissolved in another metal, its d-shells retain much of their localized character, the d-electron wavefunction being mostly contained within the impurity cell, while the outer s-electrons go into the conduction band of the host. However, the state of magnetization of the impurity depends strongly on the host. For example in some metals Fe group impurities appear to lose their magnetic moments completely. Figure 1.1 shows what happens to the magnetic moment of Fe when dissolved into alloys of the second-row transition metals. We see, for example, that iron forms a local moment in molybdenum but not in rhenium.

In the atomic d-shell, exchange and Coulomb correlations produce alignments of spins to give a magnetic moment (Hund's rule). In a metallic host the d-levels of a transition metal

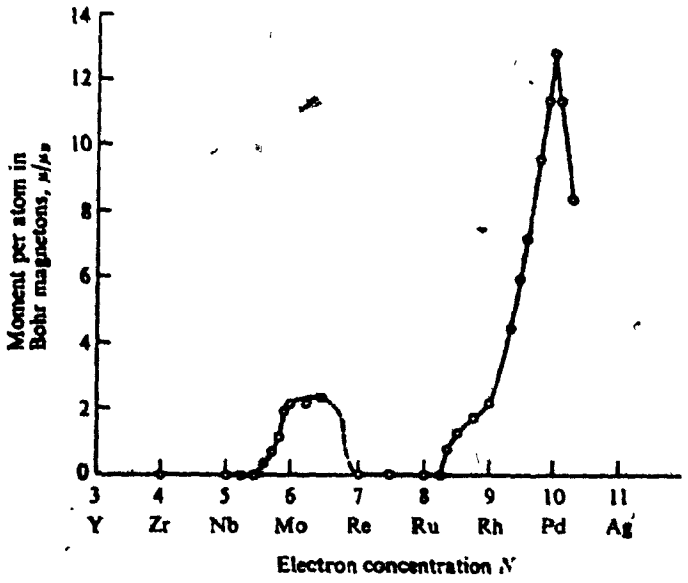

Figure 1.1

Magnetic moment in Bohr magnetons of an iron atom dissolved in various second-row transition metals and alloys as a function of electron concentration. (After A. Clogston et al (1962)).

impurity may lie somewhere in the conduction band, so d-electron wavefunctions hybridize with conduction electron states and this can change the atomic character of the impurity wavefunctions. The hybridization produces a resonance or a virtual bound state (v.b.s.) i.e. the sharp d-level is broadened. Friedel (1958) argues that a narrow v.b.s. will retain a localized moment, while for a broad state the magnetic splitting will be swamped out and the state will be degenerate with respect to spin and non-magnetic.

Following the above ideas, Anderson (1961) proposed a model for localized magnetic states in metals. He considered a potentially magnetic atom dissolved in a metallic host. The host is represented by a conduction band and the impurity by a non-degenerate localized d-orbital which is allowed to mix or hybridize with the host conduction states. Including a Coulomb repulsion between opposite spin electrons in the localized state, the Hamiltonian in the second quantized notation is:

$$H = \sum_{\underline{k}\sigma} \epsilon_{\underline{k}} C^{\dagger}_{\underline{k}\sigma} C_{\underline{k}\sigma} + \sum_{\sigma} E_d C^{\dagger}_{d\sigma} C_{d\sigma}$$

$$+ \sum_{\underline{k}\sigma} (V_{\underline{k}d} C^{\dagger}_{\underline{k}\sigma} C_{d\sigma} + V_{d\underline{k}} C^{\dagger}_{d\sigma} C_{\underline{k}\sigma}) + U n_{d\uparrow} n_{d\downarrow} \qquad (1.1)$$

where $\epsilon_{\underline{k}}$ is the kinetic energy of a conduction electron with momentum $\underline{k}$ and $C^{\dagger}_{\underline{k}\sigma}$ and $C_{\underline{k}\sigma}$ are the creation and annihilation operators for conduction electrons with momentum $\underline{k}$ and spin σ.

$C^{\dagger}_{d\sigma}$ and $C_{d\sigma}$ are the creation and annihilation operators for the localized d-level with spin σ and E_d is the energy of this level. The third term in (1.1) represents the hybridization and $V_{\underline{k}d}$ is the mixing matrix element. The fourth term is the Coulomb repulsion between states of opposite spins and the Coulomb interaction U is given by

$$U = \int\int |\phi_d(\underline{r}_1)|^2 \frac{e^2}{|\underline{r}_1 - \underline{r}_2|} |\phi_d(\underline{r}_2)|^2 \, d\underline{r}_1 d\underline{r}_2$$

where $\phi_d(\underline{r})$ is the wavefunction for the d-level. In (1.1) $n_{d\sigma} = C^{\dagger}_{d\sigma} C_{d\sigma}$ is the number operator.

In the Hartree-Fock approximation the operator $n_{d\uparrow}n_{d\downarrow}$ is replaced by

$$n_{d\uparrow}n_{d\downarrow} = \langle n_{d\downarrow} \rangle n_{d\uparrow} + \langle n_{d\uparrow} \rangle n_{d\downarrow}$$

where $\langle n_{d\sigma} \rangle$ is the average occupation. The d-part of the Green's function is then (Anderson (1961)):

$$G_{d\sigma}(\omega) = \frac{1}{\omega - E_{d\sigma} - (\Gamma - i\Delta)} \qquad (1.2)$$

where

$$E_{d\sigma} = E_d + U\langle n_{d-\sigma} \rangle \qquad (1.3)$$

and

$$\Gamma - i\Delta = \sum_{\underline{k}} \frac{|V_{\underline{k}d}|^2}{\omega - \varepsilon_{\underline{k}} + i\delta} \qquad (1.4)$$

where δ is a positive infinitesimal. The real part Γ represents a shift in the d-level and can be absorbed into E_d. The resulting d-part of the density of states is

$$\rho_{d\sigma}(\omega) = \frac{1}{\pi} \frac{\Delta}{(\omega - E_{d\sigma})^2 + \Delta^2} \qquad (1.5)$$

This is a Lorentzian of width Δ as shown in figure 1.2.

Integrating (1.5) to the Fermi level ε_F gives the average occupation number

$$\langle n_{d\sigma} \rangle = \frac{1}{\pi} \mathrm{Cot}^{-1} \frac{E_{d\sigma} - \varepsilon_F}{\Delta} \qquad (1.6)$$

Because of (1.3), equation (1.6) represents a pair of coupled equations in $\langle n_{d\uparrow} \rangle$ and $\langle n_{d\downarrow} \rangle$. For $U\rho_{d\sigma}(\varepsilon_F) < 1$ the only solution is non-magnetic i.e. $\langle n_{d\uparrow} \rangle = \langle n_{d\downarrow} \rangle$ while for $U\rho_{d\sigma}(\varepsilon_F) > 1$, a magnetic solution ($\langle n_{d\uparrow} \rangle \neq \langle n_{d\downarrow} \rangle$) is stable. The phase boundary between magnetic and non-magnetic states is given by $U\rho_{d\sigma}(\varepsilon_F) = 1$ and this is shown in figure 1.3.

1.2 The narrow band model

We now generalize the Anderson model from a one impurity problem to a system with N atoms situated on an ordered lattice. The N localized levels form a flat band which hybridizes with

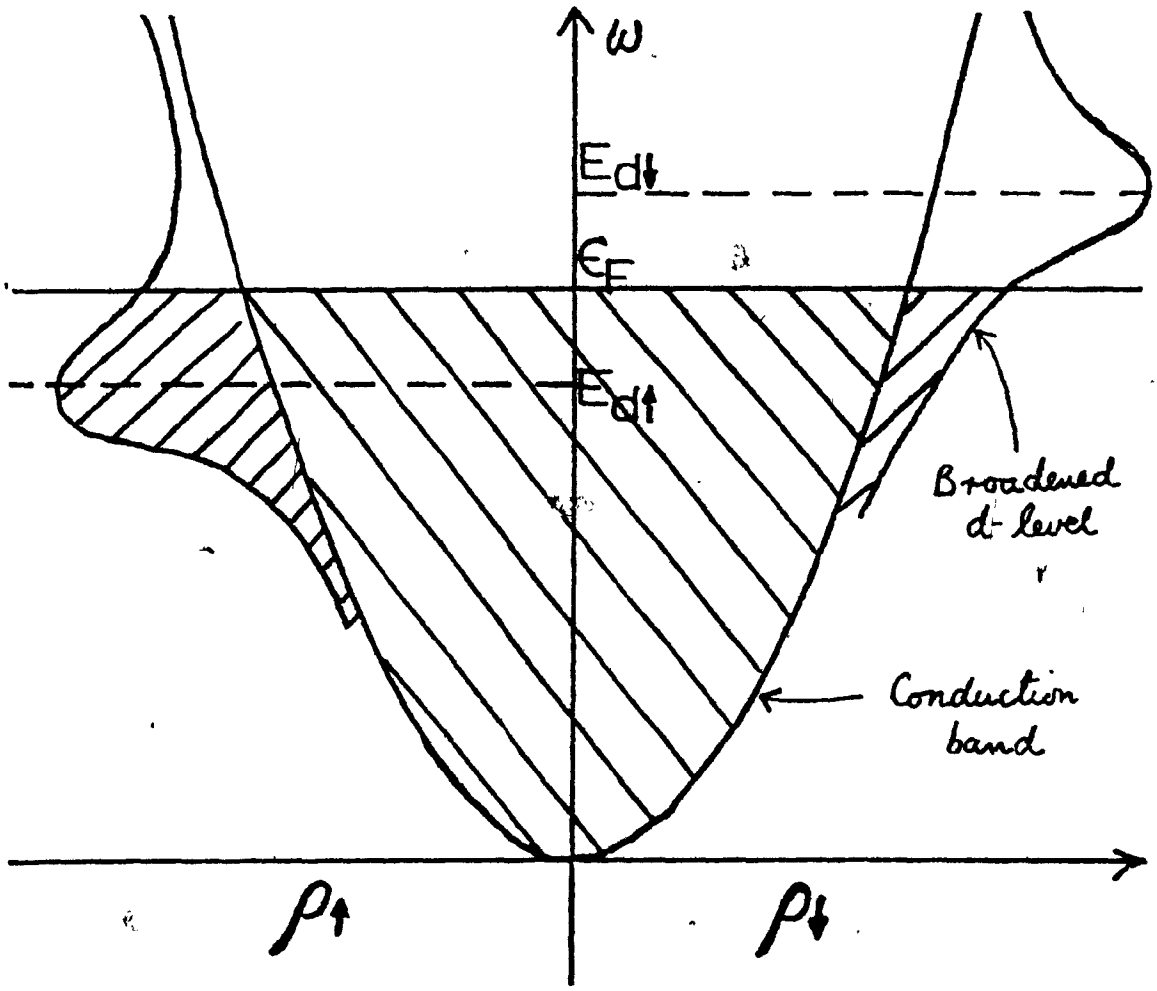

Figure 1.2

Schematic plot of the density of state distributions in the Anderson model in a magnetic case.

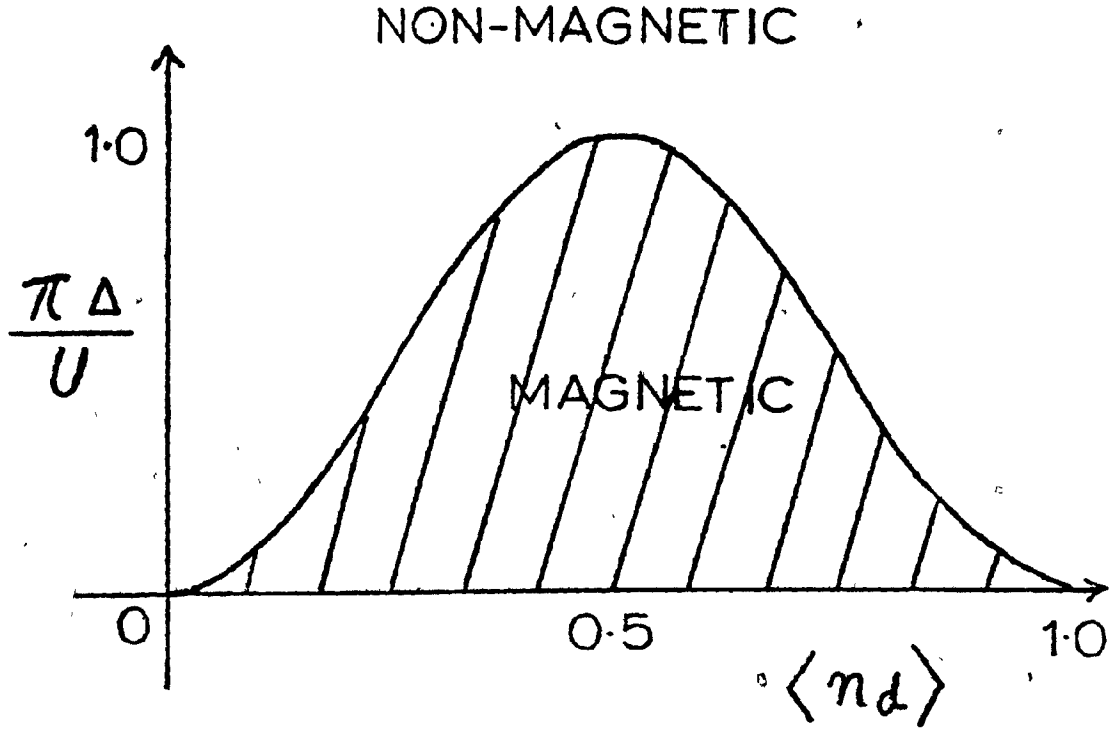

Figure 1.3

Regions of magnetic and non-magnetic behaviour in the Anderson model.

a broad conduction band. The Hamiltonian can then be written as:

$$H = H_s + H_d + H_{sd} + H_{dd} \qquad (1.7a)$$

H_s is the conduction band part given, as before, by

$$H_s = \sum_{\underline{k}\sigma} \varepsilon_{\underline{k}} C^{\dagger}_{\underline{k}\sigma} C_{\underline{k}\sigma} \qquad (1.7b)$$

H_d is the flat localized band

$$H_d = \sum_{i\sigma} E_d C^{\dagger}_{di\sigma} C_{di\sigma} \qquad (1.7c)$$

where i runs over the N sites (we refer to this as the d-band, but it could also represent a narrow f-band). The mixing term H_{sd} and the interaction term H_{dd} are similarly given by

$$H_{sd} = \frac{1}{\sqrt{N}} \sum_{\underline{k}i\sigma} (V_{\underline{k}di} C^{\dagger}_{\underline{k}\sigma} C_{di\sigma} + V_{di\underline{k}} C^{\dagger}_{di\sigma} C_{\underline{k}\sigma}) \qquad (1.7d)$$

and

$$H_{dd} = \sum_i U n_{di\uparrow} n_{di\downarrow} \qquad (1.7e)$$

with

$$n_{di\sigma} = C^{\dagger}_{di\sigma} C_{di\sigma} \qquad (1.7f)$$

To obtain the various densities of states we employ the Green's function method of Zubarev (1960). For two operators, A and B, we define the retarded Green's function as:

$$G_{AB}(t-t') = \langle\langle A(t) | B(t') \rangle\rangle$$

$$= -i\theta(t) \langle [A(t), B(t')]_{\pm} \rangle \quad (1.8)$$

where θ is the step function and $\langle \ldots \rangle$ denotes a thermal average. The + or - sign indicates an anticommutator for Fermion operators and a commutator for Boson operators respectively. The time dependence of the operators is in the Heisenberg representation i.e. for any operator 0 we have

$$0(t) = e^{iHt}\, 0 e^{-iHt} \quad (1.9)$$

where H is the Hamiltonian of the system and we have taken $\hbar = 1$. Using (1.9) it is straightforward to show that the equation of motion for the Green's function is:

$$i\frac{\partial}{\partial t} G_{AB}(t-t') = \delta(t-t') \langle [A,B]_{\pm} \rangle$$

$$+ \langle\langle [A(t), H] | B(t') \rangle\rangle \quad (1.10)$$

Fourier transforming this equation we obtain:

$$\omega\, G_{AB}(\omega) = \langle [A,B]_{\pm} \rangle + \langle\langle [A(t),H] \,|B(t')\rangle\rangle_{\omega} \qquad (1.11)$$

where $\langle\langle \ldots \ldots \rangle\rangle_{\omega}$ indicates Fourier transform. It can also be shown (Zubarev (1960)) that

$$\langle BA \rangle = \int_{-\infty}^{\infty} J(\omega)\, f(\omega)\, d\omega \qquad (1.12)$$

where J is the spectral function given by

$$J(\omega) = -\frac{1}{\pi}\, \mathrm{Im}\, G_{AB}\,(\omega + i\delta) \qquad (1.13)$$

and for Fermion operators $f(\omega)$ is the Fermi function

$$f(\omega) = (e^{\beta\omega} + 1)^{-1} \qquad (1.14)$$

with $\beta = 1/KT$.

Since we are interested in the average occupation numbers for the localized and conduction states we define the following Green's functions:

$$G_{ij\sigma}(t-t') = \langle\langle C_{di\sigma}(t) \,|C^{\dagger}_{dj\sigma}(t')\rangle\rangle \qquad (1.15)$$

and

$$G_{\underline{k}\underline{k}'\sigma}(t-t') = \langle\langle C_{\underline{k}\sigma}(t) \mid C^{\dagger}_{\underline{k}'\sigma}(t')\rangle\rangle \qquad (1.16)$$

For the first Green's function the equation of motion (1.11) gives

$$\omega\, G_{ij\sigma}(\omega) = \delta_{ij} + \langle\langle [C_{di\sigma}(t),\, H] \mid C^{\dagger}_{dj\sigma}(t')\rangle\rangle_{\omega} \qquad (1.17)$$

The commutator on the right hand side is easily evaluated giving:

$$[C_{di\sigma}, H] = E_d\, C_{di\sigma} + \frac{1}{\sqrt{N}} \sum_{\underline{k}} V_{di\underline{k}}\, C_{\underline{k}\sigma} + U\, n_{di-\sigma}\, C_{di\sigma} \qquad (1.18)$$

Hence

$$\omega\, G_{ij\sigma}(\omega) = \delta_{ij} + E_d\, G_{ij\sigma}(\omega) + \frac{1}{\sqrt{N}} \sum_{\underline{k}} V_{di\underline{k}}\, G_{\underline{k}j\sigma}(\omega) + U \langle\langle n_{di-\sigma}(t)\, C_{di\sigma}(t) \mid C^{\dagger}_{dj\sigma}(t')\rangle\rangle_{\omega} \qquad (1.19)$$

where, in an obvious notation

$$G_{\underline{k}j\sigma}(t-t') = \langle\langle C_{\underline{k}\sigma}(t) \mid C^{\dagger}_{dj\sigma}(t')\rangle\rangle$$

The last term of (1.19) represents a higher order Green's function and its equation of motion would generate a Green's function of still higher order leading to a hierachy of coupled Green's functions equations. To decouple these equations we use the Hartree-Fock approximation which is equivalent in this case to replacing the number operator $n_{di-\sigma}$ in (1.19) by its average value $\langle n_{di-\sigma}\rangle = \langle n_{d-\sigma}\rangle$ independent of site. With this simplication, equation (1.19) reduces to

$$(\omega - E_{d\sigma})\, G_{ij\sigma}(\omega) = \delta_{ij} + \frac{1}{\sqrt{N}} \sum_{\underline{k}} V_{di\underline{k}}\, G_{\underline{k}j\sigma}(\omega) \qquad (1.20)$$

with

$$E_{d\sigma} = E_d + U\langle n_{d-\sigma}\rangle \qquad (1.21)$$

The equation of motion for $G_{\underline{k}j\sigma}$ gives

$$\omega\, G_{\underline{k}j\sigma}(\omega) = \langle\langle [C_{\underline{k}\sigma}(t),\, H]\, | C^{\dagger}_{dj\sigma}(t')\rangle\rangle_{\omega}$$

$$= \varepsilon_{\underline{k}}\, G_{\underline{k}j\sigma}(\omega) + \frac{1}{\sqrt{N}} \sum_{\ell} V_{\underline{k}d\ell}\, G_{\ell j\sigma}(\omega)$$

or

$$(\omega - \varepsilon_{\underline{k}})\, G_{\underline{k}j\sigma}(\omega) = \frac{1}{\sqrt{N}} \sum_{\ell} V_{\underline{k}d\ell}\, G_{\ell j\sigma}(\omega) \qquad (1.22)$$

Substituting (1.22) into (1.20) gives

$$G_{ij\sigma}(\omega) = \frac{\delta_{ij}}{\omega - E_{d\sigma}} + \frac{1}{N}\sum_{\underline{k},\ell} \frac{V_{dik}\, V_{kd\ell}\, G_{\ell j\sigma}(\omega)}{(\omega - E_{d\sigma})\,(\omega - \varepsilon_{\underline{k}})} \qquad (1.25)$$

This is an integral equation for $G_{ij\sigma}$ which can easily be solved by introducing the Fourier transform:

$$G_{ij\sigma}(\omega) = \frac{1}{N}\sum_{\underline{q}} G_{\underline{q}\sigma}(\omega)\, e^{i\underline{q}\cdot(\underline{R}_i - \underline{R}_j)} \qquad (1.24a)$$

and its inverse

$$G_{\underline{q}\sigma}(\omega) = \frac{1}{N}\sum_{ij} G_{ij\sigma}(\omega)\, e^{i\underline{q}\cdot(\underline{R}_i - \underline{R}_j)} \qquad (1.24b)$$

where $\underline{R}_i$ is the position of the i^{th} site and $\underline{q}$ runs over the Brillouin zone. Hence from (1.24) and using the relation

$$V_{di\underline{k}} = V_{do\underline{k}}\, e^{i\underline{k}\cdot\underline{R}_i} \qquad (1.25)$$

we find

$$G_{\underline{q}\sigma}(\omega) = \frac{1}{\omega - E_{d\sigma}} + \frac{|V_{d\sigma\underline{q}}|^2}{(\omega - E_{d\sigma})(\omega - \varepsilon_{\underline{q}})}\, G_{\underline{q}\sigma}(\omega)$$

Hence

$$G_{\underline{q}\sigma}(\omega) = \frac{1}{\omega - E_{d\sigma} - \dfrac{|V_{d\sigma\underline{q}}|^2}{\omega - \varepsilon_{\underline{q}}}} \qquad (1.26)$$

which can be rewritten as a sum of two "quasi-particle" Green's function as:

$$G_{q\sigma}(\omega) = \sum_{\lambda=\pm} \frac{Z^{\lambda}_{q\sigma}}{\omega - \varepsilon^{\lambda}_{q\sigma}} \tag{1.27}$$

where

$$\varepsilon^{\lambda}_{q\sigma} = \frac{1}{2}\left(\varepsilon_q + E_{d\sigma} + \lambda\sqrt{(\varepsilon_q - E_{d\sigma})^2 + 4|V_{dq}|^2}\right) \tag{1.28}$$

and

$$Z^{\lambda}_{q\sigma} = \frac{\lambda(\varepsilon^{\lambda}_{q\sigma} - \varepsilon_q)}{(\varepsilon^{+}_{q\sigma} - \varepsilon^{-}_{q\sigma})} \tag{1.29}$$

Similarly for $G_{\underline{k}\underline{k}'\sigma}(\omega)$ we find that

$$(\omega - \varepsilon_{\underline{k}})\, G_{\underline{k}\underline{k}'\sigma}(\omega) = \delta_{\underline{k}\underline{k}'} + \frac{1}{\sqrt{N}} \sum_{\ell} V_{\underline{k}d\ell}\, G_{\ell\underline{k}'\sigma}(\omega)$$

with

$$(\omega - E_{d\sigma})\, G_{\ell\underline{k}'\sigma}(\omega) = \frac{1}{\sqrt{N}} \sum_{\underline{k}''} V_{d\ell\underline{k}''}\, G_{\underline{k}''\underline{k}'\sigma}(\omega)$$

Substituting the second equation into the first gives

$$G_{\underline{k}\underline{k}'\sigma}(\omega) = \frac{\delta_{\underline{k}\underline{k}'}}{\omega - \varepsilon_{\underline{k}}} + \frac{1}{N} \sum_{\ell\underline{k}''} \frac{V_{\underline{k}d\ell}\, V_{d\ell\underline{k}''}\, G_{\underline{k}''\underline{k}'\sigma}(\omega)}{(\omega - \varepsilon_{\underline{k}})\,(\omega - E_{d\sigma})}$$

$$= \frac{\delta_{\underline{k}\underline{k}'}}{\omega - \varepsilon_{\underline{k}}} + \frac{|V_{d\underline{k}}|^2\, G_{\underline{k}\underline{k}'\sigma}(\omega)}{(\omega - \varepsilon_{\underline{k}})(\omega - E_{d\sigma})}$$

using (1.25). As before this can be rewritten in the "quasi-particle" form as.

$$G_{\underline{k}\underline{k}'\sigma}(\omega) = \sum_{\lambda=\pm} \frac{Y^{\lambda}_{\underline{k}\sigma}\ \delta_{\underline{k}\underline{k}'}}{\omega - \varepsilon^{\lambda}_{\underline{k}\sigma}} \tag{1.30}$$

where

$$Y^{\lambda}_{\underline{k}\sigma} = 1 - Z^{\lambda}_{\underline{k}\sigma} \tag{1.31}$$

The "quasi-particle" energies $\varepsilon^{\lambda}_{q\sigma}$ are shown in figure 1.4 together with the unperturbed conduction band and the flat localized band at E_d. Here, we have made the following simplifying assumptions:

(i) V_{doq} is independent of q and we write

$$V_{doq} = V \tag{1.32}$$

(ii) the conduction band is parabolic i.e.

$$\varepsilon_{\underline{k}} = \frac{\hbar^2 k^2}{2m} \tag{1.33}$$

As seen in figure 1.4, the hybridization between the conduction band and the N localized states is coherent and instead of localized Lorentzian resonances (as found in the one impurity case) we find two new hybrid bands split by an energy gap.

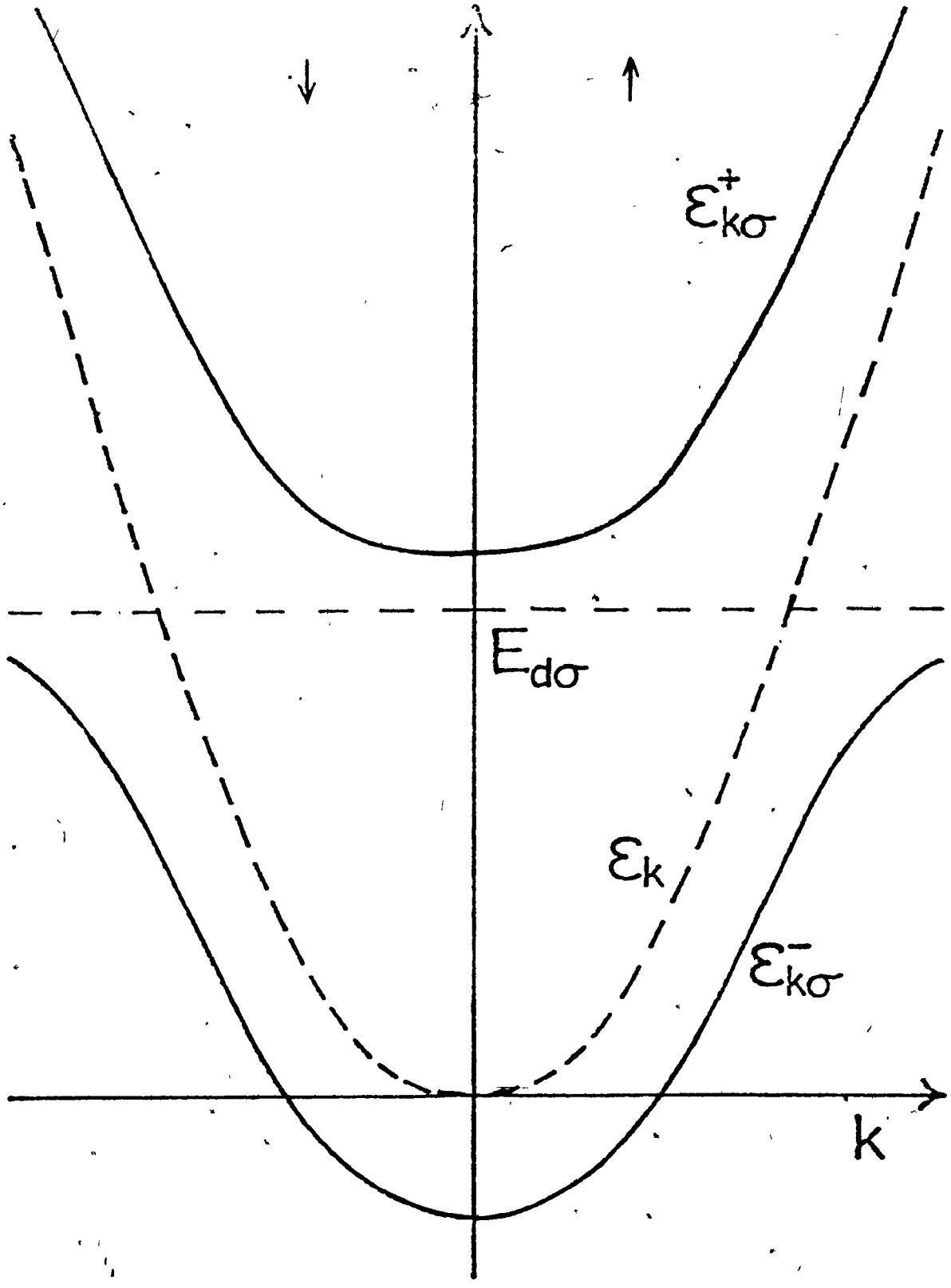

Figure 1.4

Hybridized bands in the non-magnetic state in the narrow band model (schematic). In the magnetic case the spin up bands will be shifted downwards relative to the spin down bands.

Having found the Green's function we can now go ahead and obtain the average occupation numbers using equation (1.12). Thus the average occupation per atom of the localized states for spin σ is

$$N_{d\sigma} = \frac{1}{N} \sum_i \langle C^{\dagger}_{di\sigma} C_{di\sigma} \rangle$$

$$= \frac{1}{N} \sum_i \int_{-\infty}^{\infty} \left(-\frac{1}{\pi} \operatorname{Im} G_{ii\sigma}(\omega+i\delta)\right) f(\omega)\, d\omega$$

$$= \int_{-\infty}^{\infty} \rho_{d\sigma}(\omega)\, f(\omega)\, d\omega \qquad (1.34)$$

where the last line defines the density of states per atom of spin σ for the localized states

$$\rho_{d\sigma}(\omega) = \frac{1}{N} \sum_i \left(-\frac{1}{\pi} \operatorname{Im} G_{ii\sigma}(\omega+i\delta)\right) \qquad (1.35)$$

Substituting (1.24) and (1.27) into (1.35) gives

$$\rho_{d\sigma}(\omega) = \frac{1}{N} \sum_{q\lambda} Z^{\lambda}_{q\sigma}\, \delta(\omega - \epsilon^{\lambda}_{q\sigma}) \qquad (1.36)$$

where we have used the relation

$$\operatorname{Im} \frac{1}{x+i\delta} = -\pi\, \delta(x) .$$

Similarly the average occupation of the conduction states per atom and of spin σ is

$$N_{c\sigma} = \frac{1}{N} \sum_{\underline{k}} \langle c^{\dagger}_{\underline{k}\sigma} C_{\underline{k}\sigma} \rangle$$

$$= \frac{1}{N} \sum_{\underline{k}} \int_{-\infty}^{\infty} \left(-\frac{1}{\pi} \operatorname{Im} G_{\underline{k}\underline{k}\sigma}(\omega+i\delta)\right) f(\omega)\, d\omega$$

$$= \int_{-\infty}^{\infty} \rho_{c\sigma}(\omega)\, f(\omega)\, d\omega \qquad (1.37)$$

where again we have introduced the density of states per atom of spin σ for the conduction states

$$\rho_{c\sigma}(\omega) = \frac{1}{N} \sum_{\underline{k}} \left(-\frac{1}{\pi} \operatorname{Im} G_{\underline{k}\underline{k}\sigma}(\omega+i\delta)\right) \qquad (1.38)$$

Substituting (1.30) into (1.38) gives

$$\rho_{c\sigma}(\omega) = \frac{1}{N} \sum_{\underline{k}\lambda} Y^{\lambda}_{\underline{k}\sigma}\, \delta(\omega-\varepsilon^{\lambda}_{\underline{k}\sigma}) \qquad (1.39)$$

The densities of states given by equation (1.36) and (1.39) are the main results of this section. As they stand, these equations are not in a very convenient form. They can be simplified by performing the sum over the wave-vectors and thereby removing the δ-functions. It follows from (1.32) and (1.33) that $\varepsilon^{\lambda}_{q\sigma}$ is a function only of the magnitude of q and hence so are $Z^{\lambda}_{q\sigma}$ and $Y^{\lambda}_{q\sigma}$. This enables us to make a further approximation and replace the sums in (1.36) and (1.39), which are taken over the Brillouin zone, by an integral over a sphere of the same volume. Thus, if the radius of the sphere is q_s we have

$$\frac{4\pi}{3} q_s^3 = 8\pi^3/v$$

i.e. $$q_s = (6\pi^2 v)^{1/3} \tag{1.40}$$

where v is the unit cell volume. The replacement is then

$$\frac{1}{N}\sum_{q} \rightarrow \frac{3}{q_s^3}\int_0^{q_s} q^2 dq$$

Using this we find, after a little algebra, that

$$\rho_{c\sigma}(\omega) = \frac{3/2}{\varepsilon_s^{3/2}}\left(\frac{(\omega-\varepsilon^+_{o\sigma})(\omega-\varepsilon^-_{o\sigma})}{(\omega-E_{d\sigma})}\right)^{1/2} \text{ for } \varepsilon^-_{o\sigma} < \omega < \varepsilon^+_s$$

$$= 0 \text{ otherwise} \tag{1.41}$$

and

$$\rho_{d\sigma}(\omega) = \rho_{c\sigma}(\omega)\frac{V^2}{(\omega-E_{d\sigma})^2} \tag{1.42}$$

where

$$\varepsilon_s = \hbar^2 q_s^2/2m \tag{1.43}$$

and the band edges are given by

$$\varepsilon^{\lambda}_{s\sigma} = \frac{1}{2}\left(\varepsilon_s + E_{d\sigma} + \lambda\sqrt{(\varepsilon_s - E_{d\sigma})^2 + 4V^2}\right) \tag{1.44a}$$

and

$$\varepsilon^{\lambda}_{o\sigma} = \frac{1}{2}\left(E_{d\sigma} + \lambda\sqrt{E^2_{d\sigma} + 4V^2}\right) \tag{1.44b}$$

Typical density of states curves are drawn schematically in figure 1.5 and shows the qualitative features of the densities of states for finite values of V.

We note here that these densities of states do not have a simple integrable form and to obtain the occupation numbers the integrations have to be done numerically.

To investigate the properties of the system described above we perform model calculations treating U and V as variable parameters. We are especially interested in the effects of U and V on the static magnetic properties. From the results of section 1.1, we expect U to favour a magnetic or spin-split state and V to have the opposite effect. We begin by rewriting equation (1.34) for the average occupation number of the localized state as:

$$N_{d\sigma} = \int_{-\infty}^{\infty} \rho_{d\sigma}(\omega, E_{d\sigma})\ f(\omega)\ d\omega \qquad (1.45)$$

where we have now explicitly indicated that the density of states $\rho_{d\sigma}$ depends on $E_{d\sigma}$. But from (1.21), $E_{d\sigma}$ depends on $\langle n_{d-\sigma} \rangle = N_{d-\sigma}$. Hence equation (1.45) is really a pair of coupled equations for $N_{d\uparrow}$ and $N_{d\downarrow}$:

$$N_{d\uparrow} = \int_{-\infty}^{\infty} \rho_{d\sigma}(\omega, N_{d\downarrow})\ f(\omega)\ d\omega \qquad (1.46a)$$

and

$$N_{d\downarrow} = \int_{-\infty}^{\infty} \rho_{d\sigma}(\omega, N_{d\uparrow})\ f(\omega)\ d\omega \qquad (1.46b)$$

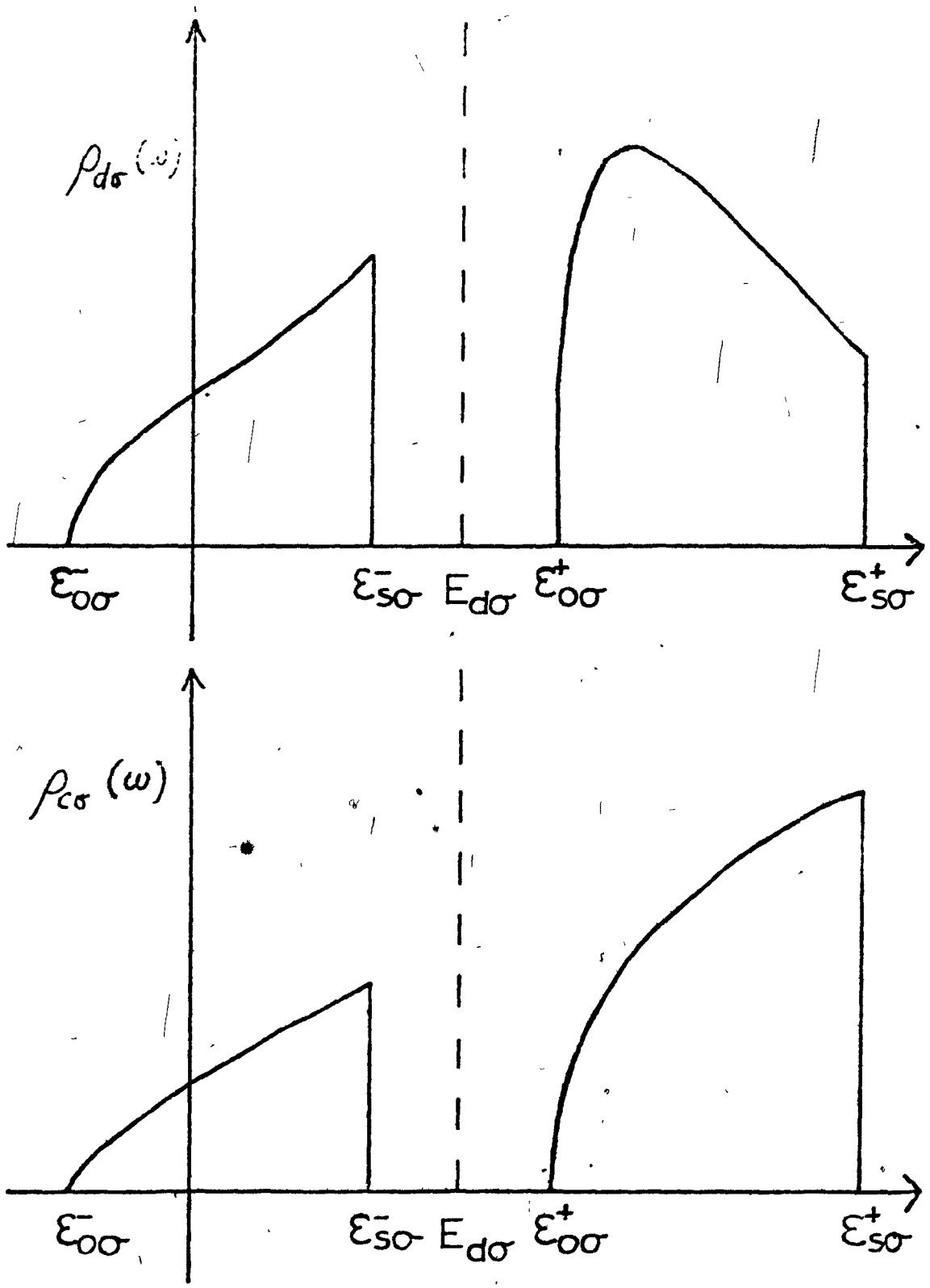

Figure 1.5

Density of states for the localized and conduction states in the narrow band model (schematic).

These two equations must be solved self-consistently and, depending on the relative strengths of U and V, we may have a non-magnetic solution ($N_{d\uparrow} = N_{d\downarrow}$) or a magnetic one ($N_{d\uparrow} \neq N_{d\downarrow}$). Thus we can draw a U-V phase diagram showing the magnetic and non-magnetic regions and this is done below. We then examine other properties of this model such as the magnetization, the Curie temperature and the susceptibility.

(i) Phase diagram at T = 0.

The simplest way to obtain the condition under which equation (1.46) has a magnetic solution is through the d-part of the static susceptibility X_s. The dynamic susceptibility is derived in appendix A and taking the static limit we find

$$X_s = \frac{X_s^\circ}{1 - UX_s^\circ} \tag{1.47}$$

When the denominator is zero the susceptibility diverges and this indicates a transition from a non-magnetic to a ferromagnetic state. Thus the phase boundary is given by

$$UX_s^\circ = 1 \tag{1.48}$$

In the above equation X_s° is evaluated in the non-magnetic state and it is then easy to show that

$$UX_s^\circ = \int_{-\infty}^{\infty} \rho_1(\omega)\ f(\omega)\ d\omega + \int_{-\infty}^{\infty} \rho_2(\omega)\ \frac{-\partial f}{\partial \omega}(\omega)\ d\omega \tag{1.49}$$

where

$$\rho_1(\omega) = -2\,UV^2\rho_{c\sigma}(\omega)\;\frac{(\omega-E_{d\sigma})}{((\omega-E_{d\sigma})^2+V^2)^2} \qquad (1.50)$$

and

$$\rho_2(\omega) = UV^2\,\rho_{d\sigma}(\omega)\;\frac{1}{((\omega-E_{d\sigma})^2+V^2)^2} \qquad (1.51)$$

with $\rho_{c\sigma}$ and $\rho_{d\sigma}$ given by (1.41) and (1.42) respectively. Since we are working in the paramagnetic state we have $N_{d\uparrow} = N_{d\downarrow} = N_d$ and $E_{d\sigma}$ is independent of σ.

Before we can proceed further we need to know the total number of electrons in the system. The densities of states $\rho_{c\sigma}$ and $\rho_{d\sigma}$ each have room enough for one electron per atom per spin i.e. the maximum possible number of electrons is 4 per atom. 4 electrons per atom represents completely full bands and this is not an interesting case. We do not consider here the case of 2 electrons per atom because this represents a special case of full lower bands at zero temperature. For our model calculations we have chosen 3 electrons per atom i.e we have

$$N_{d\uparrow} + N_{d\downarrow} + N_{c\uparrow} + N_{c\downarrow} = 3 \qquad (1.52)$$

This is done by introducing a chemical potential μ in the Fermi function $f(\omega)$ as

$$f(\omega) = (e^{\beta(\omega-\mu)} + 1)^{-1}$$

and μ is chosen to satisfy condition (1.52). The choice of 3 electrons per atom represents a model calculation and cannot be applied to realistic systems such as the Heusler alloys. The main reason is that the simple model we consider does not take into account the degeneracy of the localized level. This is discussed further in chapter IV.

It is convenient to normalize all energies to ε_s (given by (1.43)) which is typically of the order of a few eV for the Heusler alloys of interest to us (e.g. in Cu_2MnAl and Cu_2MnIn $\varepsilon_s \sim 4$ eV). U and V are also of the order of a few eV and we have therefore taken the range of normalized U and V to be $\sim 0 - 1$. We assume E_d lies in the middle of the band and thus take $E_d = 0.5$.

To obtain the phase diagram we proceed as follows: for fixed U and V we solve the self-consistent equations (1.46) with $N_{d\uparrow} = N_{d\downarrow}$ and satisfying (1.52). We search for pairs of values of U and V which satisfy the critical condition $UX_s^\circ = 1$. These form the phase boundary shown in figure 1.6. For $UX_s^\circ < 1$ we have a non-magnetic solution to (1.46) and for $UX_s^\circ > 1$ a magnetic solution is the stable one. As expected, we see that as U increases we go from a non-magnetic to a magnetic region and vice versa for V.

(ii) Magnetization at T = 0

From the phase diagram of figure 1.6 we know the values of U and V for which a magnetic solution to (1.46) exists. We investigate here how the magnetization varies with U for a fixed value of V. The simplest way to obtain the magnetic solution is to plot $N_{d\uparrow}$ as a function of $N_{d\downarrow}$ for a given value of the Fermi energy ε_F. Typical plots are shown schematically in figure 1.7 for two values of U, one in the non-magnetic region (figure 1.7a) and the other in the magnetic region (figure 1.7b). In these figures AB' is the reflection of AB about the line OP which corresponds to $N_{d\uparrow} = N_{d\downarrow}$. We see from figure 1.7a that there is only one possible self-consistent solution and it is the non-magnetic solution at A. In figure 1.7b there are two self-consistent solutions, a magnetic one at C and a non-magnetic one at A. The magnetic solution at C is the stable one and we can converge to it by following the path indicated by the arrows. Having found this solution we then vary ε_F to satisfy (1.52).

We obtain the magnetic solution for various values of U and plot the magnetization in figure 1.8. The d-part of the magnetization M_d, the conduction part M_c and the total magnetization M are defined as

$$M_d = N_{d\uparrow} - N_{d\downarrow} \qquad (1.53a)$$

$$M_c = N_{c\uparrow} - N_{c\downarrow} \qquad (1.53b)$$

$$M = M_d + M_c \qquad (1.53c)$$

For low values of U the magnetization is zero. As U increases beyond a critical value U_c the magnetization increases

from zero, at first very sharply, and tends to saturate for high values of U. The value of U_c is consistent with figure 1.6. We also note that $M_d >> M_c$ and this is reasonable since the magnetic interactions are in the d-band.

(iii) Curie temperatures

The magnetization shown in figure 1.8 is the maximum value obtained at T = 0. As the temperature increases we expect this value to decrease steadily and to drop to zero at a transition or Curie temperature T_c. Above this temperature the system would be non-magnetic. To find this temperature we again look at the static susceptibility and its temperature dependence. At high temperatures, the unenhanced susceptibility X_s° is small (and $UX_s^\circ << 1$) but as T decreases it increases. The critical temperature is reached when $UX_s^\circ = 1$ at which point the static susceptibility X_s diverges, signalling a phase transition to the ferromagnetic state. Thus T_c is defined by

$$UX_s^\circ (T_c) = 1 \qquad (1.54)$$

As in the case of magnetization we have obtained T_c as a function of U for a fixed value of V and this is shown in figure 1.9. Again, for small U the Curie temperature is zero but at U_c it starts increasing in a manner similar to the magnetization.

(iv) Magnetization as a function of temperature

For a point in the magnetic region of the phase diagram we solve (1.46) self-consistently for various temperatures and plot the magnetization as a function of temperature in figure 1.10. As expected, the magnetization decreases as the temperature increases and drops to zero at the value of T_c given by (1.54).

(v) Paramagnetic susceptibility as a function of T

At temperatures above the Curie temperature we plot, in figure 1.11, the inverse of the static susceptibility as a function of temperature. The linear dependence with temperature indicates that the static susceptibility has the following Curie-Weiss form

$$\chi_s(T) = \frac{C}{T-T_c} \qquad (1.55)$$

where C is the Curie constant.

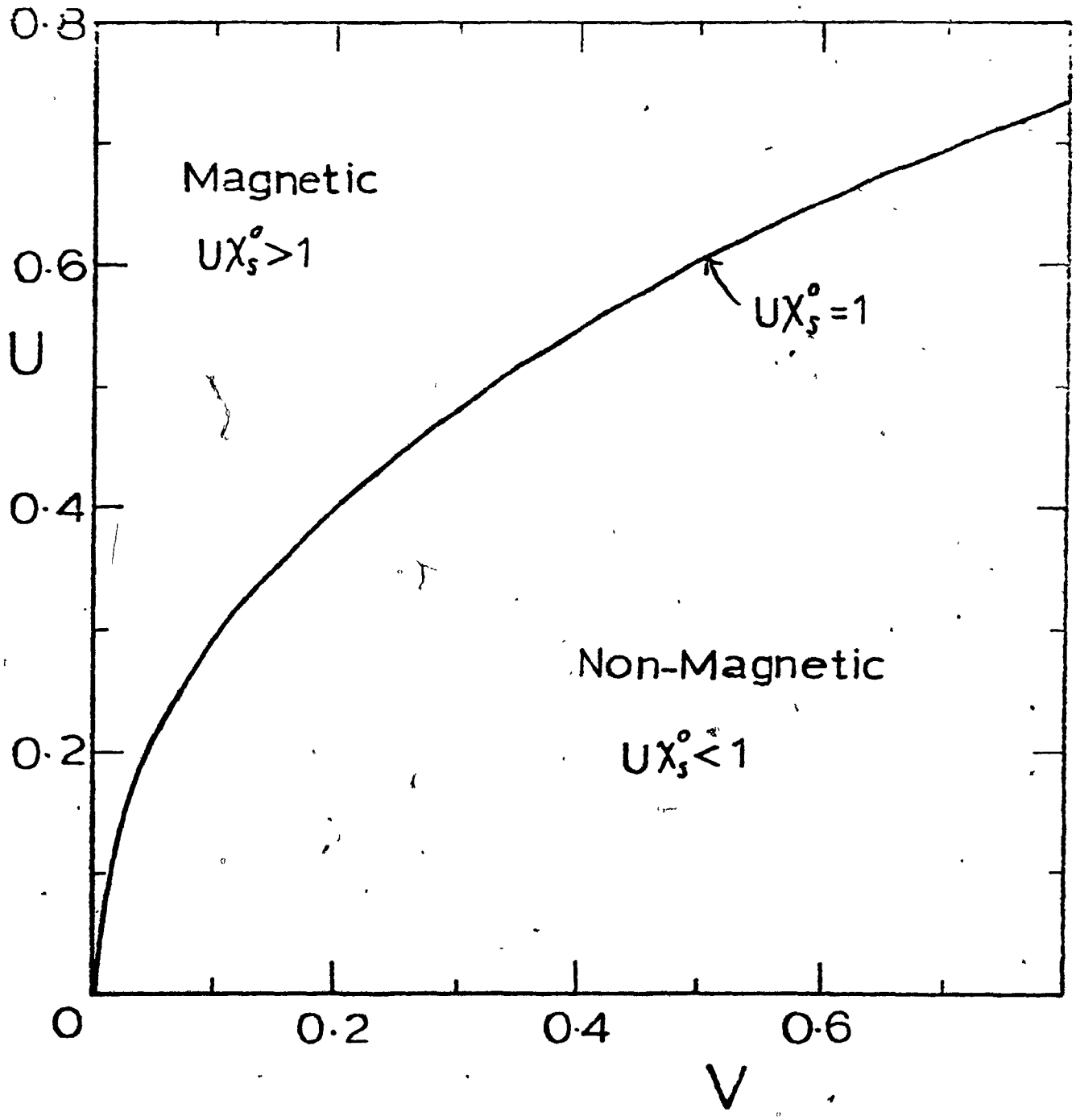

Figure 1.6

Phase diagram for the narrow band model. All energies are normalized to ϵ_s (equation(1.43)).

Figure 1.7a

Figure 1.7b

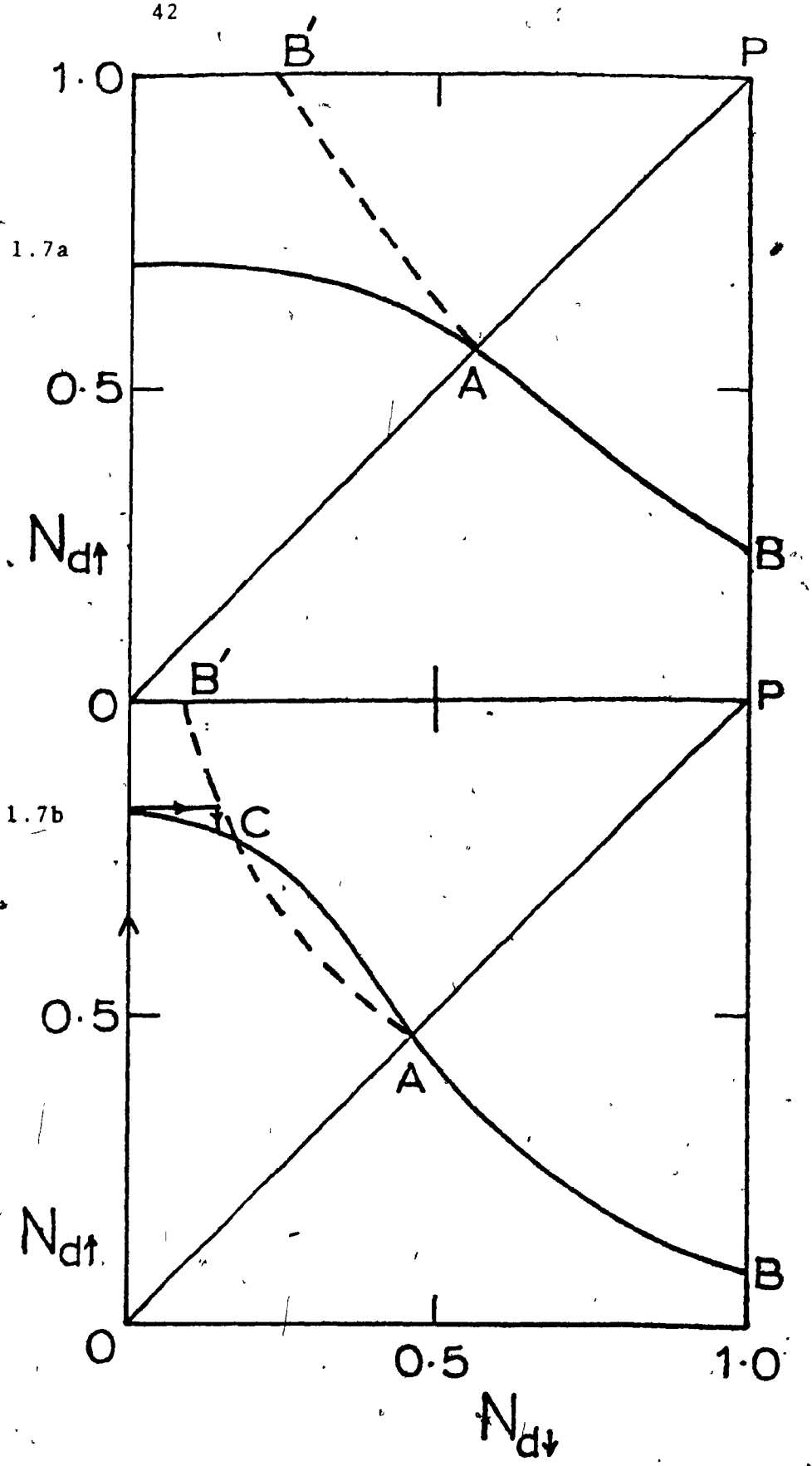

Figure 1.7
Schematic plot of $N_{d\uparrow}$ versus $N_{d\downarrow}$ in the non-magnetic (top) and magnetic (bottom) states.

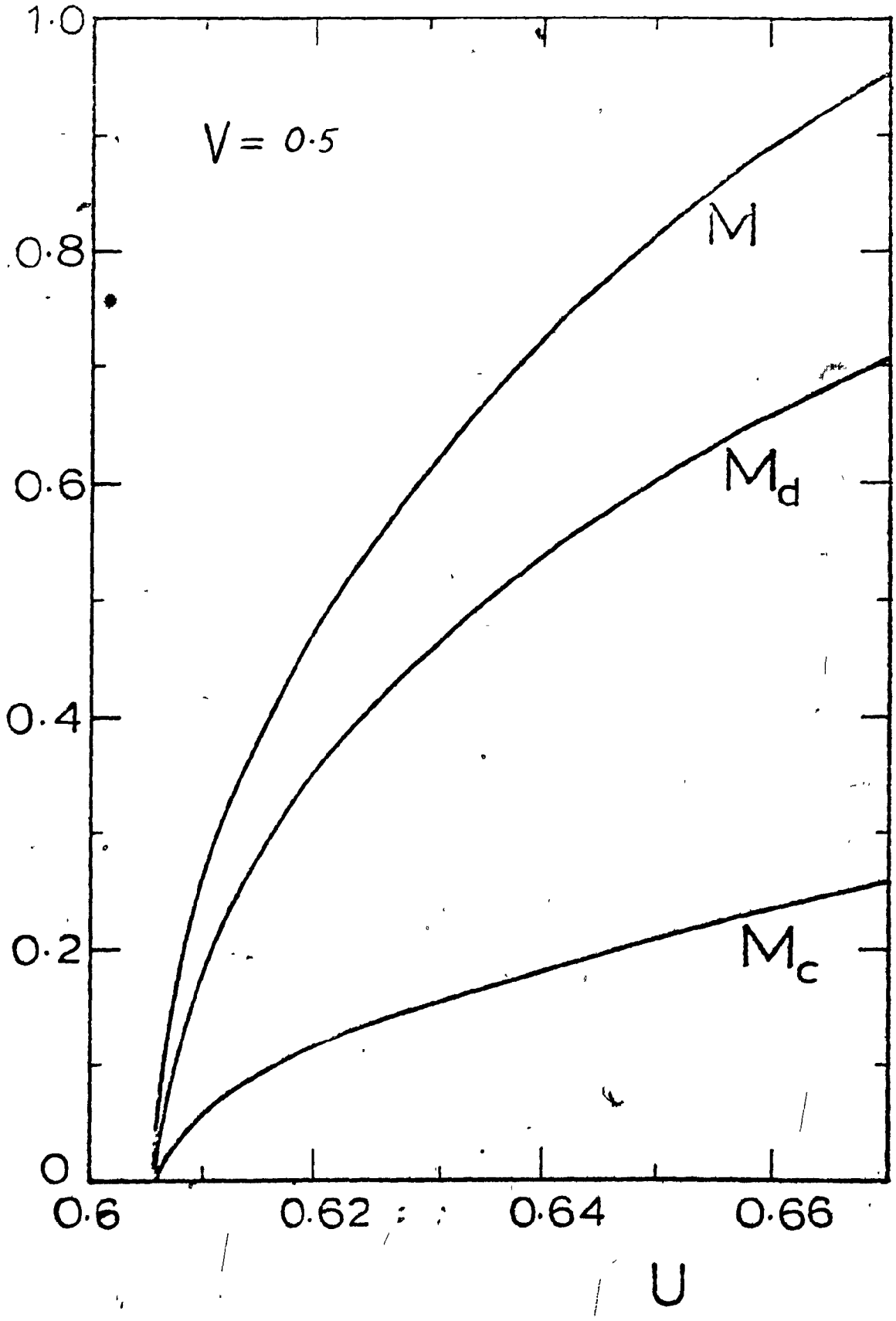

Figure 1.8
Magnetization as a function of U in the narrow band model. M_d, M_c and M are defined by (1.53). All energies are normalized to ϵ_s (equation (1.45)).

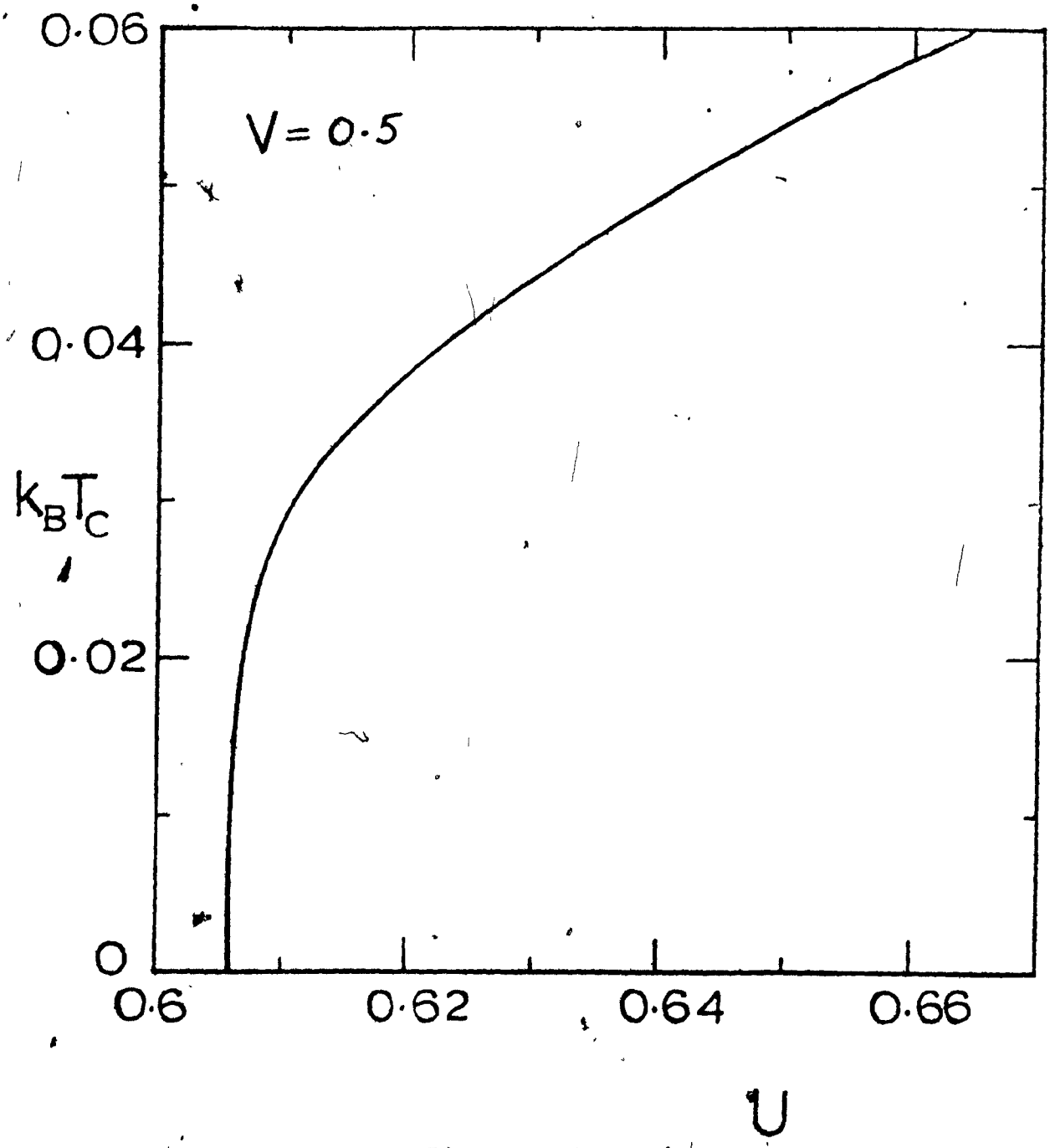

Figure 1.9

Curie temperature as a function of U in the narrow band model. All energies are normalized to $-\epsilon_s$ (equation (1.43)).

Figure 1.10

Magnetization as a function of temperature in the narrow band model. M_d, M_c and M are defined in (1.53). All energies are normalized to ϵ_s (equation (1.43)).

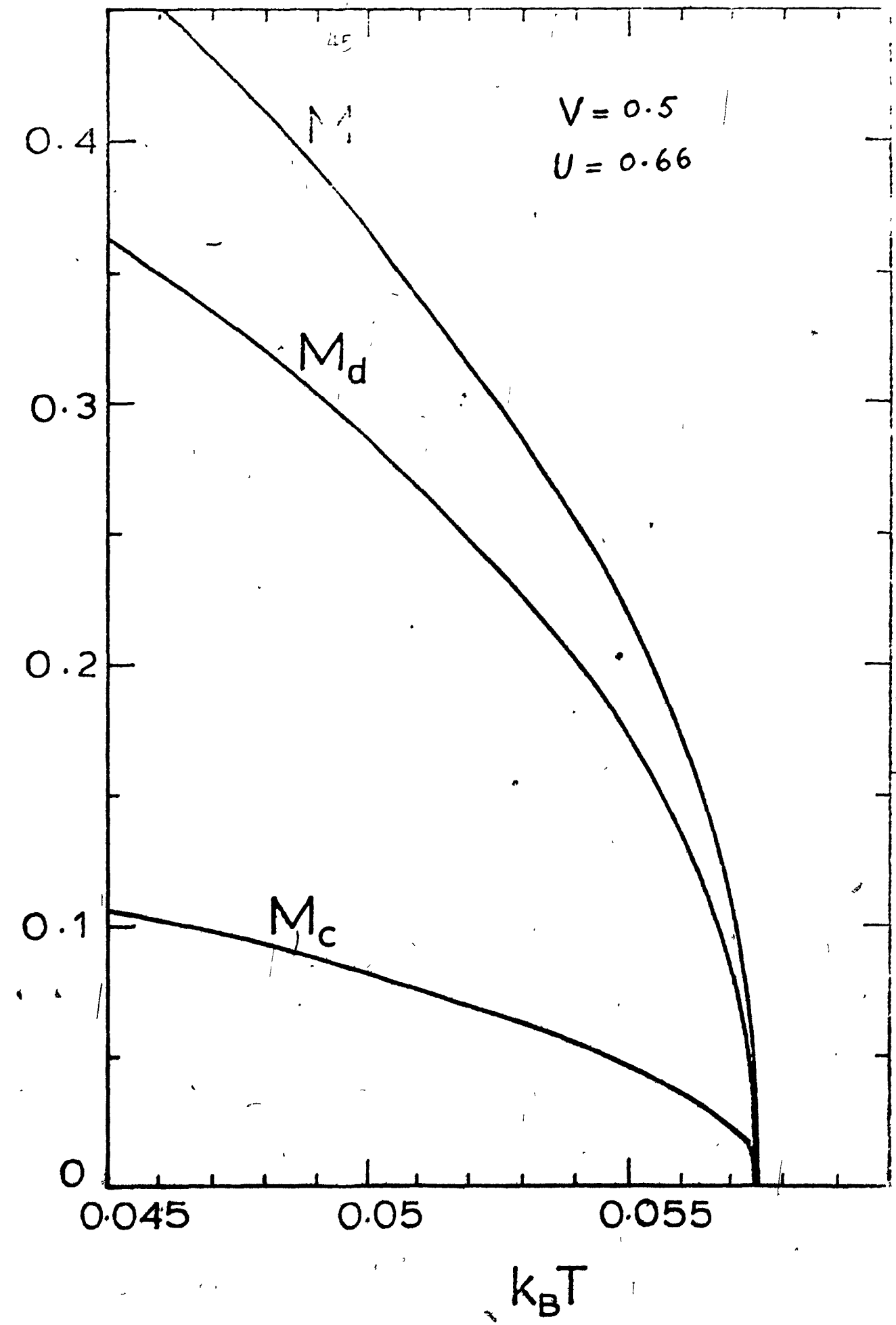

Figure 1.10

Figure 1.11

Inverse static susceptibility as a function of temperature in the narrow band model. All energies are normalized to ϵ_s (equation (1.43)).

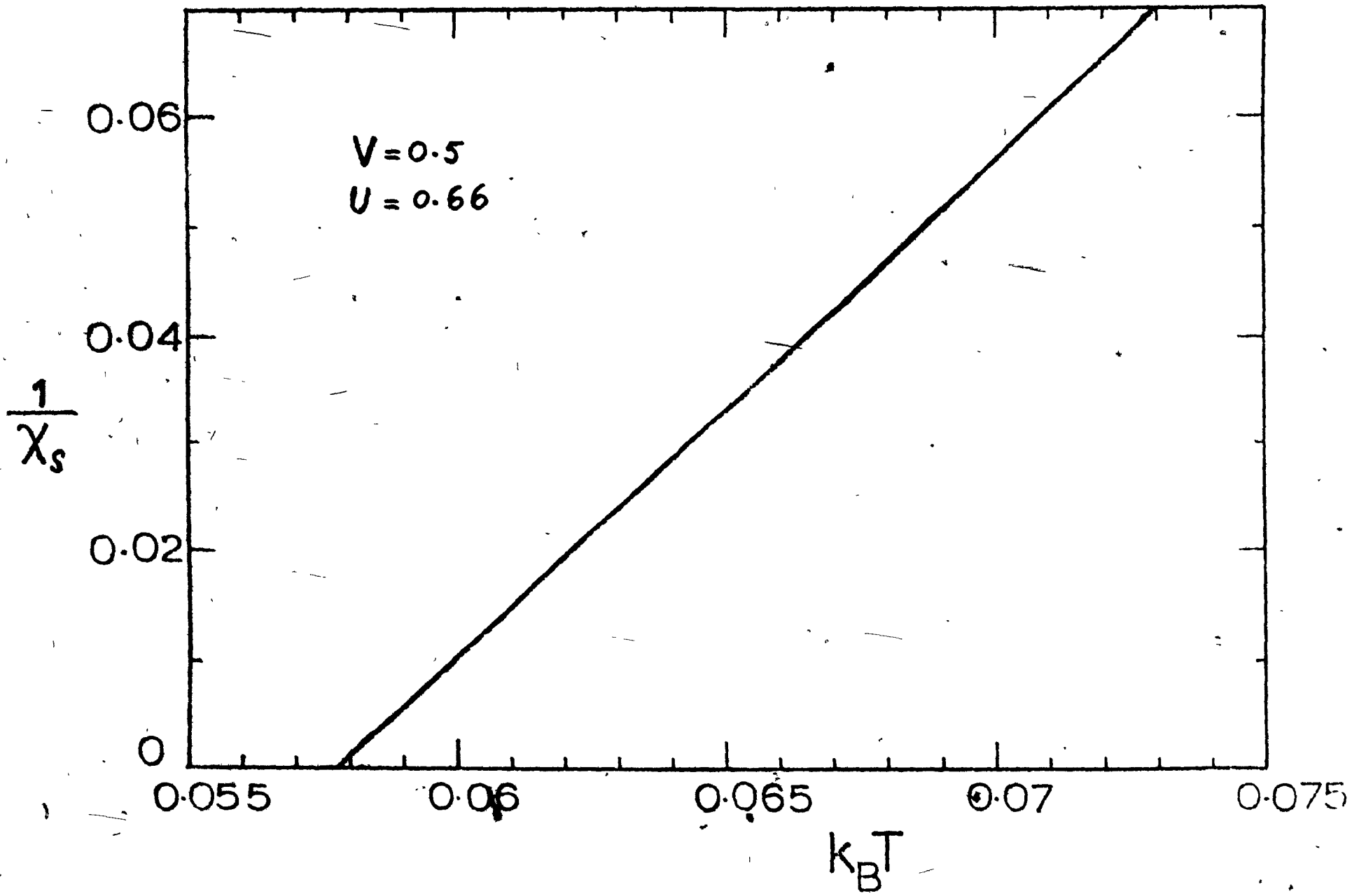

Figure 1.11

Chapter II

Spin waves in the narrow band model

In ferromagnets, at zero temperature, all moments are aligned resulting in maximum magnetization. At finite temperatures there will always be some misorientation of the moments because of thermal activation and hence the spontaneous magnetization of a sample will decrease as the temperature is raised. At low temperatures the magnetization M(T) is found to vary with temperature in the following simple manner:

$$M(T) = M(o)\ (1 - AT^{3/2}) \qquad (2.1)$$

where A is a constant. Although the application of Boltzmann statistics to the Weiss molecular field theory gives an expression for the temperature dependence of the magnetization which is in qualitative agreement with experiment , the theory does not yield the $T^{3/2}$ behaviour observed at low temperatures.

Bloch (1930) introduced the idea of spin waves in order to explain the observed temperature dependence of the magnetization. In section 2.1 we give a brief review of spin waves in the localized theory of ferromagnetism. Then, in section 2.2, we discuss how these concepts are extended to itinerant electrons. Finally, in section 2.3, we examine spin waves in the narrow band model.

2.1 Spin waves in the localized model

In 1930, Bloch proposed a theory to describe the behaviour of a ferromagnet in which a small fraction of the total spin is not aligned to the magnetization. The simplest excited states of the system are those in which the magnetic moment is reduced by a single deviation of the total spin. This deviation is not static since an exchange interaction of some type will ensure that it travels through the lattice. Thus the spin deviation may be considered to be associated with all the ions in the crystal and forming a collective excitation. If the deviation were maintained on a particular lattice site it would be a single particle excitation and would require much more energy. Thus the collective excitations, which are called spin waves, are the magnetic excitations of lowest energy. At finite temperatures, the complicated motion of the spins can be considered as a superposition of spin waves. This idea is similar to that used in treating the complicated thermal motion of ions in a solid which is considered to be composed of a superposition of normal vibrational modes. The normal vibrational modes are called phonons and by analogy a spin wave may be considered as a quasi-particle referred to as a magnon.

The dispersion relation for spin waves is of fundamental interest and for the localized model it can be obtained in a straightforward way. We begin with the Heisenberg Hamiltonian

$$H = -2 \sum_{i>j} J_{ij} \underline{S}_i \cdot \underline{S}_j \qquad (2.2)$$

Introducing transverse spin operators

$$S_j^{\pm} = S_j^x \pm i S_j^y \qquad (2.3)$$

and assuming only nearest neighbour interaction J, the Hamiltonian can be rewritten as:

$$H = -2J \sum_{i>j} (S_i^z S_j^z + \tfrac{1}{2} S_i^+ S_j^- + \tfrac{1}{2} S_i^- S_j^+) \qquad (2.4)$$

Following Holstein and Primakoff (1940) we write S_j^z and $S_j^{\pm}$ in terms of boson annihilation and creation operators a_j and a_j^+ :

$$S_j^+ = (2S)^{1/2} \left(1 - \frac{a_j^+ a_j}{2S}\right)^{1/2} a_j \qquad (2.5a)$$

$$S_j^- = (2S)^{1/2} a_j^+ \left(1 - \frac{a_j^+ a_j}{2S}\right)^{1/2} \qquad (2.5b)$$

$$S_j^z = S - a_j^+ a_j \qquad (2.5c)$$

Using the expansion

$$\left(1 - \frac{a_j^+ a_j}{2S}\right)^{1/2} = 1 - \frac{1}{4S} a_j^+ a_j - \frac{1}{32S^2} a_j^+ a_j a_j^+ a_j + \ldots\ldots \qquad (2.6)$$

and neglecting terms higher than quadratic in a_j's the Hamiltonian becomes

$$H = - JS^2 NZ - 2JS \sum_{ij} (a_i^+ a_j - a_j^+ a_j) \qquad (2.7)$$

where Z is the number of nearest neighbours. This can now be diagonalized by a transformation from the atomic operators a_j to spin wave operators $b_{\underline{k}}$:

$$b_{\underline{k}} = \frac{1}{\sqrt{N}} \sum_j e^{i\, \underline{k}.\underline{R}_j}\, a_j \qquad (2.8)$$

where $\underline{R}_j$ is the position of the j^{th} ion. Substituting this into (2.7) and neglecting the constant first term we find:

$$H = \sum_{\underline{k}} \omega_{\underline{k}}\, b_{\underline{k}}^+\, b_{\underline{k}} \qquad (2.9)$$

where

$$\omega_{\underline{k}} = 2JSZ \left(1 - \frac{1}{Z} \sum_{\underline{\delta}} e^{i\, \underline{k}.\underline{\delta}}\right) \qquad (2.10)$$

and $\underline{\delta}$ are vectors to the nearest neighbours. In (2.9) $b_{\underline{k}}^+ b_{\underline{k}}$ is the number operator for a magnon of wavevector $\underline{k}$ and energy $\omega_{\underline{k}}$. The dispersion relation (2.10) has a very simple form in the longwavelength limit. Thus for $k \to 0$ and for a cubic lattice

$$\omega_{\underline{k}} \approx Dk^2 \qquad (2.11)$$

where the stiffness coefficient D is given by

$$D = 2JS\,a^2 \qquad (2.12)$$

and a is the lattice constant.

It is instructive to look at spin waves from the classical point of view which gives a more physical picture The spin $\underline{S}$ is now considered as a classical spin which will precess around a magnetic field. The state of one spin deviation now becomes a state in which a wave travels through the precessing spins in such a manner that, in the direction of the wave, the phase angle between neighbouring spins differ by a constant amount. Figure 2.1 shows the usual classical picture of a spin wave. If we consider a spin $\underline{S}_i$ surrounded by neighbours $\underline{S}_j$, the Hamiltonian is $-2J\,\underline{S}_i \cdot \sum_j \underline{S}_j$. Thus we may represent the effect of the exchange on spin $\underline{S}_i$ by an effective field which is proportional to $2J \sum_j \underline{S}_j$. The classical equation of motion for $\underline{S}_i$ is then

$$\frac{\partial \underline{S}_i}{\partial t} = 2J\,\underline{S}_i \wedge \sum_j \underline{S}_j \qquad (2.13)$$

Without going into details of the calculation (see for example Kittel (1971))equation (2.13) has a solution for $\underline{S}_i$ of a travelling wave form $e^{i(\omega t - \underline{k}\cdot\underline{R}_i)}$ with ω given in terms of $\underline{k}$ by (2.10).

There is now a sound body of experimental work which demonstrate that spin waves really do exist in magnetic materials. One of the most direct methods of probing spin waves is by neutron inelastic scattering. The neutron has a spin of 1/2 and a magnetic moment of about -1.9 nuclear magnetons, and so it will interact magnetically with the magnetization of a lattice and thus be scattered. In inelastic scattering the neutrons can be thought of as creating or destroying a magnon in the scattering process. Conservation of energy and momentum allows the determination of the energy and momentum of the spin waves i.e. the determination of the dispersion relation for magnons. Results of experiments on face-centered cubic crystals of Co + 8% Fe by Sinclair and Brockhouse (1960) are shown in figure 2.2. The dispersion relation is of the form:

$$\omega_{\underline{k}} = \Delta + Dk^2 \qquad (2.14)$$

where Δ is a gap introduced by anisotropy fields. The value of D in (2.14) was found to be 5.9×10^{-29} erg cm^2 or approximately 370 meV $\AA^2$.

The effect of spin waves on magnetization can be easily derived. The spin deviation operator for the whole system is ,

$$NS - \sum_j S_j^z = \sum_{\underline{k}} n_{\underline{k}} \qquad (2.15)$$

where $n_{\underline{k}} = b^{+}_{\underline{k}} b_{\underline{k}}$. This equation states that each excited spin wave reduces the z-component of the total spin by one unit. The magnetization is thus given by

$$M(T) = M(o) - g\mu_\beta \sum_{\underline{k}} \langle n_{\underline{k}} \rangle$$

where the average occupation numbers are determined by Bose-Einstein statistics. Hence,

$$M(T) = M(o) - g\mu_\beta \sum_{\underline{k}} \frac{1}{(e^{\beta\omega_{\underline{k}}} - 1)}$$

At low temperatures, it is a good approximation to use the long wavelength expression for $\omega_{\underline{k}}$ (equation (2.11)) and, replacing the sum over $\underline{k}$ by an integral, we find

$$M(T) = M(o) - g\mu_\beta \zeta(3/2)\left(\frac{kT}{4\pi D}\right)^{3/2} \qquad (2.16)$$

where ζ is the Riemann-Zeta function. This is the Bloch $T^{3/2}$ law. Although the first experiments to see how the magnetization of Fe, Ni and Co changed on cooling to very low temperatures were made as early as 1910, it was not until 1936 that a proper investigation of the magnetization of Fe and Ni was made down to 20K (Fallot (1936)). This work was specifically done to see if the magnetization at low temperatures followed the $1-AT^{3/2}$ law predicted by the Bloch theory or whether it was closer to the $1-BT^2$ dependence which other investigators had found was applicable at higher

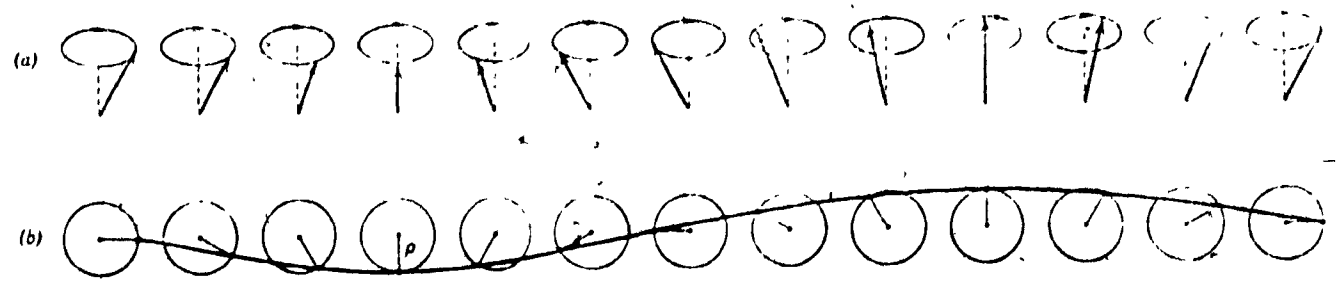

Figure 2.1

Classical picture of a spin wave: (a) The ends of the spin vectors precess on the surface of cones, with successive spins advanced in phase by a constant angle. (b) Spins viewed from above, showing one wavelength.

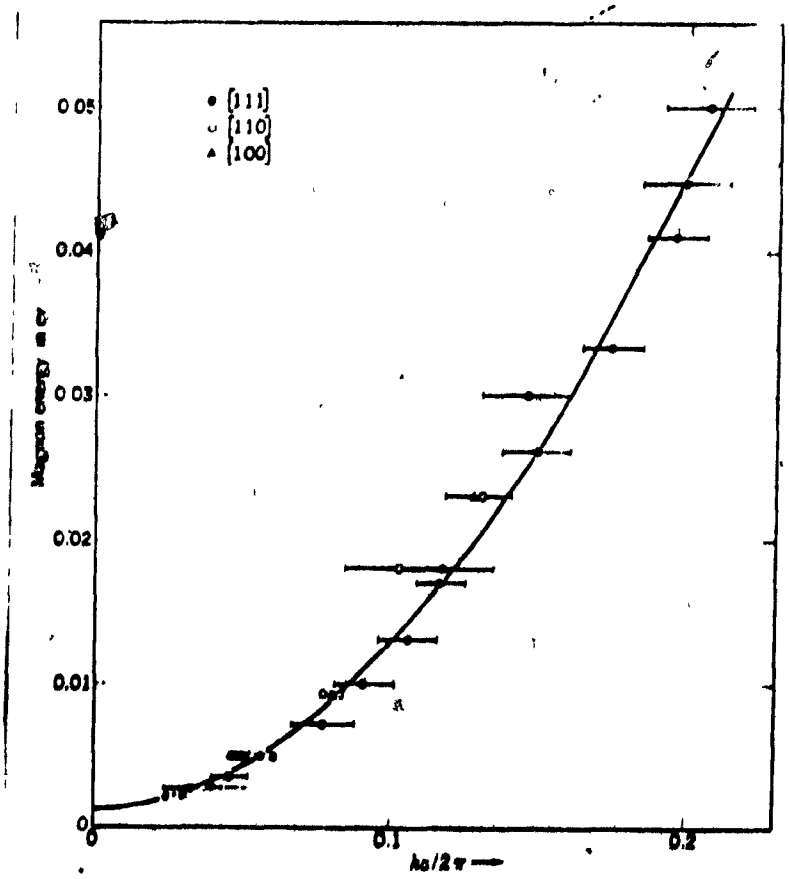

Figure 2.2

Spin wave dispersion in fcc Co + 8% Fe (after Sinclair and Brockhouse (1960)).

temperatures. Fallot found that $1-AT^{3/2}$ gave a better fit. More recent work (such as that of Elliot et al (1953) on Gd) does confirm the $T^{3/2}$ dependence at very low temperatures.

2.2 Spin waves in the itinerant model

For a considerable time it was not clear whether spin waves could exist in metals where the magnetic electrons are itinerant. The earlier band model of ferromagnetism (Stoner (1938), Wohlfarth (1953)) did not contain any spin wave excitations because it used the molecular field approximation which precludes spin wave excitations from the outset. However, Herring and Kittel (1951) proposed that spin waves did exist in metals, and since that time a new theory of itinerant electron ferromagnetism has been evolved by Izuyama (1960), Izuyama and Kubo (1964) and Mattis (1963). In essence these treatments investigate more fully the features of the Stoner-Wohlfarth model. However, the interaction is now treated in a proper dynamic form, rather than the static approximation method used earlier.

As a starting point we consider the Hubbard Hamiltonian (Hubbard (1963)) which describes a band of interacting electrons. The interaction is a Coulomb repulsion between electrons of opposite spins when they are at the same atomic site. The Hamiltonian is then a sum of a kinetic energy term and an interaction term

$$H = \sum_{k\sigma} \epsilon_{\underline{k}} C^{\dagger}_{\underline{k}\sigma} C_{\underline{k}\sigma} + \sum_{i} I\, n_{i\uparrow}\, n_{i\downarrow} \qquad (2.17)$$

where I is the Coulomb repulsion and $n_{i\sigma} = C^{\dagger}_{i\sigma} C_{i\sigma}$ where $C^{\dagger}_{i\sigma}$ and $C_{i\sigma}$ are creation and annihilation operators for Wannier states for site i and are related to the conduction state wave functions by:

$$C_{i\sigma} = \frac{1}{\sqrt{N}} \sum_{\underline{k}} e^{i\underline{k}\cdot\underline{R}_i} C_{\underline{k}\sigma} \qquad (2.18)$$

Substituting this into (2.17) gives

$$H = \sum_{\underline{k}\sigma} \epsilon_{\underline{k}} C^{\dagger}_{\underline{k}\sigma} C_{\underline{k}\sigma} + \frac{I}{N} \sum_{\underline{q}'\underline{k}'\underline{k}''} C^{\dagger}_{\underline{q}'+\underline{k}''\uparrow} C_{\underline{q}'+\underline{k}'\uparrow} C^{\dagger}_{\underline{k}'\downarrow} C_{\underline{k}''\downarrow} \qquad (2.19)$$

The molecular field (MF) approximation applied to (2.17) is equivalent to replacing the four operator product by two operator products as

$$n_{i\uparrow}\, n_{i\downarrow} = \langle n_{i\uparrow} \rangle\, n_{i\downarrow} + \langle n_{i\downarrow} \rangle\, n_{i\uparrow} \qquad (2.19a)$$

and using (2.18) we find that in the MF approximation the Hamiltonian becomes

$$H_0 = \sum_{k\sigma} \epsilon_{\underline{k}\sigma} C^{\dagger}_{\underline{k}\sigma} C_{\underline{k}\sigma} \qquad (2.20)$$

where

$$\varepsilon_{\underline{k}\sigma} = \varepsilon_{\underline{k}} + I\langle n_{i-\sigma}\rangle \qquad (2.21)$$

Thus in the MF approximation the band is spin-split (figure 2.3a) by an amount proportional to the magnetization and this is equivalent to the Stoner-Wohlfarth model. We now consider a spin-flip excitation of an electron from a state $\underline{k}$ to $\underline{k} + \underline{q}$ as shown in figure 2.3a. The energy of this single-particle excitation is:

$$\omega_{\underline{q}}^{sp} = \varepsilon_{\underline{k}+\underline{q}\downarrow} - \varepsilon_{\underline{k}\uparrow}$$

$$= \varepsilon_{\underline{k}+\underline{q}} - \varepsilon_{\underline{k}} + I\langle m\rangle \qquad (2.22)$$

where $\langle m\rangle = \langle n_\uparrow\rangle - \langle n_\downarrow\rangle$ is the magnetization. These single-particle excitations are known as Stoner excitations and their spectrum is given by (2.22) and shown by the shaded region of figure 2.3b. We note that there is a gap in the excitation energy at small $\underline{q}$ and at $\underline{q} = 0$ this gap is equal to the band splitting $I\langle m\rangle$.

We can also form excitations of lower energy by taking a linear combination of the single-particle excitations i.e. by forming a collective excitation or a spin wave. The excitation corresponding to (2.22) is given by the operator $C^{\dagger}_{\underline{k}+\underline{q}\downarrow} C_{\underline{k}\uparrow}$ and we now define a spin wave operator $B_{\underline{q}}$ as a superposition of these i.e.

$$B_{\underline{q}} = \sum_{\underline{k}} \alpha_{\underline{k}} \, C^{\dagger}_{\underline{k}+\underline{q}\downarrow} \, C_{\underline{k}\uparrow} \qquad (2.23)$$

If the excitation energy for this spin wave is $\omega^{SW}_{\underline{q}}$, then $B_{\underline{q}}$ satisfies the following equation of motion

$$[H, B_{\underline{q}}] = \omega^{SW}_{\underline{q}} \, B_{\underline{q}} \qquad (2.24)$$

It is straightforward to show from (2.19) and (2.23) that

$$[H, B_{\underline{q}}] = \sum_{\underline{k}} \alpha_{\underline{k}} \, (\varepsilon_{\underline{k}+\underline{q}} - \varepsilon_{\underline{k}}) \, C^{\dagger}_{\underline{k}+\underline{q}\downarrow} \, C_{\underline{k}\uparrow}$$

$$+ \frac{I}{N} \sum_{\underline{q}'\underline{k}'\underline{k}} \alpha_{\underline{k}} \, (C^{\dagger}_{\underline{q}'+\underline{k}+\underline{q}\uparrow} \, C_{\underline{q}'+\underline{k}'\uparrow} C^{\dagger}_{\underline{k}'\downarrow} \, C_{\underline{k}\uparrow} - C^{\dagger}_{\underline{k}+\underline{q}\downarrow}$$

$$C_{\underline{q}'+\underline{k}'\uparrow} C^{\dagger}_{\underline{k}'\downarrow} \, C_{\underline{k}-\underline{q}'\downarrow})$$

We treat the second term in the random phase approximation (RPA) by replacing the 4-particle operators by 2-particle operators as:

$$C^{\dagger}_{\underline{q}'+\underline{k}+\underline{q}\uparrow} C_{\underline{q}'+\underline{k}\uparrow} \; C^{\dagger}_{\underline{k}'\downarrow} \; C_{\underline{k}\uparrow} = \delta_{\underline{k}',\underline{k}+\underline{q}} \langle n_{\underline{q}'+\underline{k}'\uparrow} \rangle \, C^{\dagger}_{\underline{k}'\downarrow} \, C_{\underline{k}\uparrow}$$

$$- \delta_{\underline{q},-\underline{q}'} \langle n_{\underline{k}\uparrow} \rangle C^{\dagger}_{\underline{k}'\downarrow} \, C_{\underline{q}'+\underline{k}'\downarrow}$$

$$C^{\dagger}_{\underline{k}+\underline{q}\downarrow} \, C_{\underline{q}'+\underline{k}\uparrow} \; C^{\dagger}_{\underline{k}'\downarrow} \, C_{\underline{k}-\underline{q}'\downarrow} = \delta_{\underline{k}',\underline{k}-\underline{q}'} \langle n_{\underline{k}'\downarrow} \rangle C^{\dagger}_{\underline{k}+\underline{q}\downarrow} \, C_{\underline{q}'+\underline{k}\uparrow}$$

$$- \delta_{\underline{q},-\underline{q}'} \langle n_{\underline{k}+\underline{q}\downarrow} \rangle \, C^{\dagger}_{\underline{k}'\downarrow} \, C_{\underline{q}'+\underline{k}'\downarrow}$$

Replacing $\langle n_{\underline{k}\sigma} \rangle$ by the Fermi function $f(\varepsilon_{\underline{k}\sigma})$ we get:

$$[H, B_{\underline{q}}] = \sum_{\underline{k}} \alpha_{\underline{k}} (\varepsilon_{\underline{k}+\underline{q}\uparrow} - \varepsilon_{\underline{k}\uparrow}) \, C^{\dagger}_{\underline{k}+\underline{q}\uparrow} \, C_{\underline{k}\uparrow}$$

$$+ \frac{I}{N} \sum_{\underline{k}\underline{k}'} \alpha_{\underline{k}'} (f(\varepsilon_{\underline{k}'+\underline{q}\downarrow}) - f(\varepsilon_{\underline{k}'\downarrow})) \, C^{\dagger}_{\underline{k}+\underline{q}\uparrow} C_{\underline{k}\uparrow}$$

where we have used the relation

$$\langle n_{\sigma} \rangle = \frac{1}{N} \sum_{\underline{k}} \langle n_{\underline{k}\sigma} \rangle$$

Hence from (2.24) we have

$$\sum_{\underline{k}} \left\{ \alpha_{\underline{k}} (\varepsilon_{\underline{k}+\underline{q}\uparrow} - \varepsilon_{\underline{k}\uparrow}) + \frac{I}{N} \sum_{\underline{k}'} \alpha_{\underline{k}'} (f(\varepsilon_{\underline{k}'+\underline{q}\downarrow}) - f(\varepsilon_{\underline{k}'\downarrow})) \right\} C^{\dagger}_{\underline{k}+\underline{q}\uparrow} \, C_{\underline{k}\uparrow}$$

$$= \sum_{\underline{k}} \omega^{sw}_{\underline{q}} \, \alpha_{\underline{k}} \, C^{\dagger}_{\underline{k}+\underline{q}\uparrow} \, C_{\underline{k}\uparrow}$$

Equating coefficients of $C^{\dagger}_{\underline{k}+\underline{q}\uparrow} \, C_{\underline{k}\uparrow}$ gives:

$$(\omega^{sw}_{\underline{q}} - (\varepsilon_{\underline{k}+\underline{q}\uparrow} - \varepsilon_{\underline{k}\uparrow}))\alpha_{\underline{k}} = \frac{I}{N} \sum_{\underline{k}'} \alpha_{\underline{k}'} (f(\varepsilon_{\underline{k}'+\underline{q}\downarrow}) - f(\varepsilon_{\underline{k}'\downarrow}))$$

(2.25)

The left hand side is a constant and denoting it by A' we get

$$\alpha_{\underline{k}} = \frac{A'}{\omega^{sw}_{\underline{q}} - (\varepsilon_{\underline{k}+\underline{q}\uparrow} - \varepsilon_{\underline{k}\uparrow})}$$

Substituting this back into (2.25) we obtain the following

equation for the spin wave energy ω_q^{sw} :

$$1 = \frac{I}{N} \sum_{\underline{k}} \frac{f(\varepsilon_{\underline{k}+\underline{q}\downarrow}) - f(\varepsilon_{\underline{k}\uparrow})}{\omega_q^{sw} - (\varepsilon_{\underline{k}+\underline{q}\downarrow} - \varepsilon_{\underline{k}\uparrow})} \qquad (2.26)$$

The same expression was obtained by Izuyama, Kim and Kubo (1963) from the dynamic susceptibility. These authors also showed that in the long-wavelength limit (2.26) yields the following dispersion relation

$$\omega_q^{sw} = Dq^2 \qquad (2.27)$$

where

$$D = \frac{I}{3N} \sum_{\underline{k}} \frac{(f(\varepsilon_{\underline{k}\uparrow}) + f(\varepsilon_{\underline{k}\downarrow}))\nabla^2\varepsilon_{\underline{k}}}{2K\langle m\rangle} - \frac{(f(\varepsilon_{\underline{k}\uparrow}) - f(\varepsilon_{\underline{k}\downarrow}))(\nabla\varepsilon_{\underline{k}})^2}{(K\langle m\rangle)^2}$$

Although the spin wave stiffness coefficient D has a different microscopic origin from that of the localized model, the spin wave energy is once more of the form Dq^2 (figure 2.3b) in the long-wave length limit. Hence the magnetization at low temperatures in the itinerant model will also follow the Bloch $T^{3/2}$ law.

2.3 Spin waves in the narrow band model.

As in the itinerant case, spin waves in the narrow band model can be built up from a linear combination of single-particle excitations. To do this we first obtain the Hartree-Fock expression for the model Hamiltonian described in Chapter

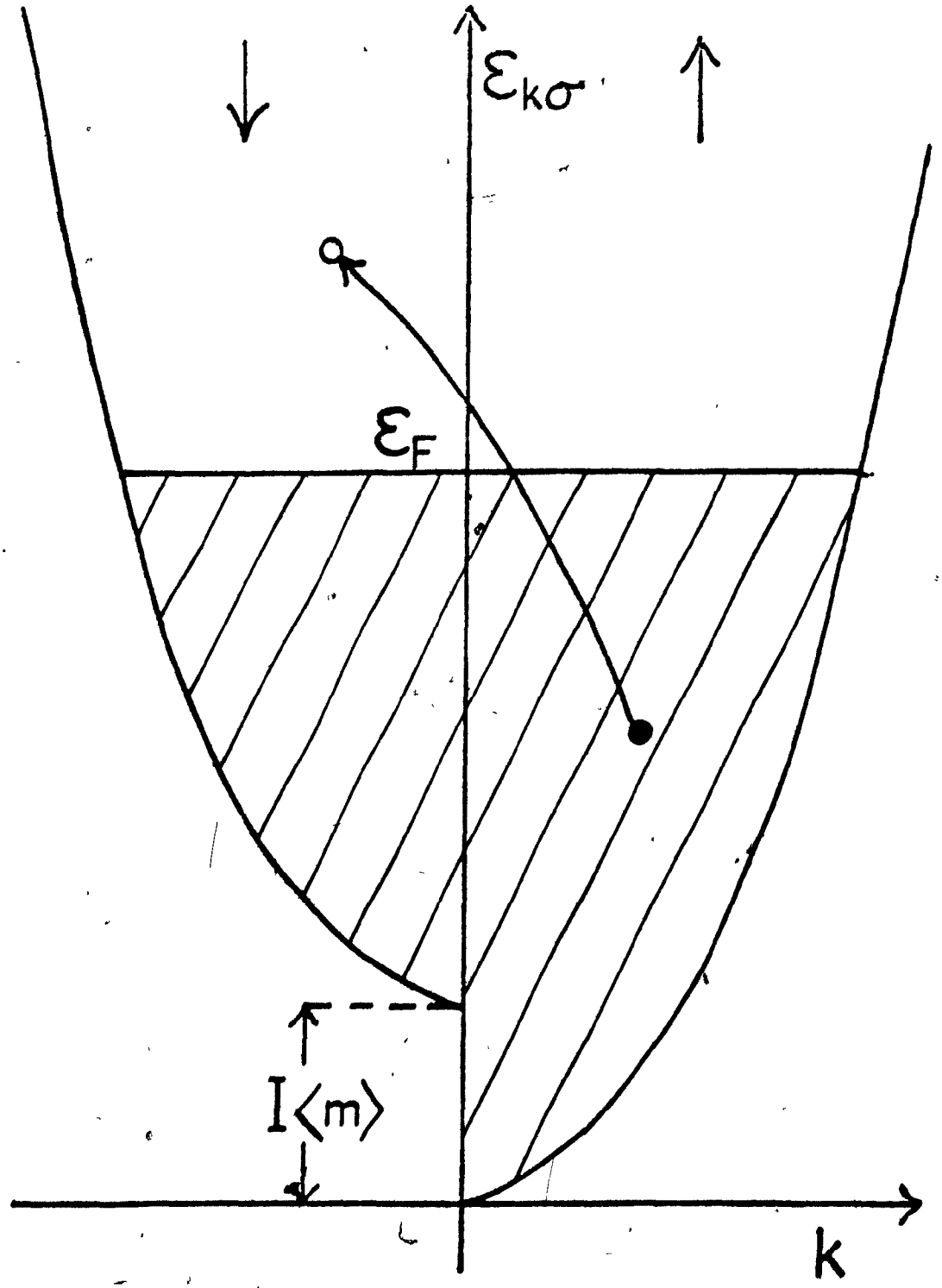

Figure 2.3(a)

Spin-split bands of the itinerant model showing a single-particle excitation (schematic). $\langle m\rangle = \langle n_\uparrow\rangle - \langle n_\downarrow\rangle$ is the magnetization.

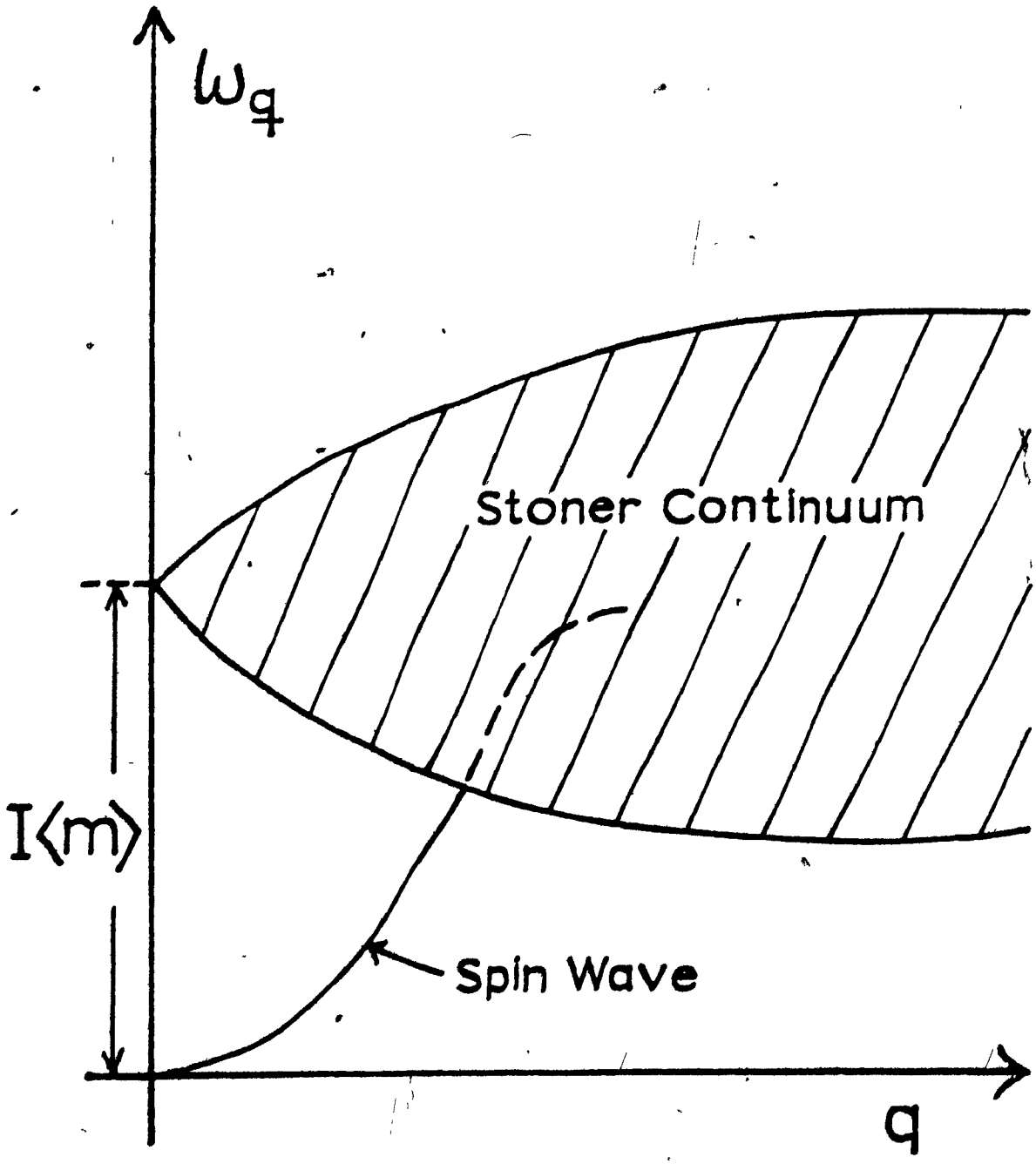

Figure 2.3(b)

Spectrum of single-particle (Stoner continuum) and spin wave excitations in the itinerant model (schematic).

I (equation (1.7)). In this approximation the interaction term is treated in exactly the same way as for the itinerant model i.e.as in equation (2.19a). The Hamiltonian thus reduces to

$$H_o = \sum_{\underline{k}\sigma} \varepsilon_{\underline{k}} C^{\dagger}_{\underline{k}\sigma} C_{\underline{k}\sigma} + \sum_{i\sigma} E_{d\sigma} C^{\dagger}_{di\sigma} C_{di\sigma} + \sum_{\underline{k}i\sigma} (V_{\underline{k}di} C^{\dagger}_{\underline{k}\sigma} C_{di\sigma} + V_{di\underline{k}} C^{\dagger}_{di\sigma} C_{\underline{k}\sigma}) \tag{2.28}$$

This can be simplified further by transforming $C_{di\sigma}$ to momentum representation:

$$C_{di\sigma} = \frac{1}{\sqrt{N}} \sum_{\underline{q}} e^{i\underline{q}\cdot\underline{R}_i} C_{d\underline{q}\sigma} \tag{2.29}$$

Substituting this into (2.28) and using (1.25) we get:

$$H_o = \sum_{\underline{q}\sigma} [\varepsilon_{\underline{q}} C^{\dagger}_{\underline{q}\sigma} C_{\underline{q}\sigma} + E_{d\sigma} C^{\dagger}_{d\underline{q}\sigma} C_{d\underline{q}\sigma} + V_{do\underline{q}} (C^{\dagger}_{\underline{q}\sigma} C_{d\underline{q}\sigma} + C^{\dagger}_{d\underline{q}\sigma} C_{\underline{q}\sigma})] \tag{2.30}$$

where we have taken $V_{do\underline{q}}$ to be real. It is straightforward to show that equation (2.30) is diagonalized by the following unitary transformation:

$$\begin{pmatrix} C_{q\uparrow\sigma} \\ C_{q\downarrow\sigma} \end{pmatrix} = \begin{pmatrix} \cos\theta & -\sin\theta \\ \sin\theta & \cos\theta \end{pmatrix} \begin{pmatrix} a_{q\uparrow\sigma} \\ a_{q\downarrow\sigma} \end{pmatrix} \quad (2.31)$$

with

$$\sin^2\theta = Z^{\uparrow}_{q\downarrow\sigma}$$

where $Z^{\uparrow}_{q\downarrow\sigma}$ is given by (1.29). Equation (2.30) can then be written as

$$H_0 = \sum_{q\lambda} \epsilon^{\lambda}_{q\uparrow\sigma}\, a^{\dagger}_{\lambda q\uparrow\sigma}\, a_{\lambda q\uparrow\sigma} \quad (2.32)$$

with $\epsilon^{\lambda}_{q\uparrow\sigma}$ given by (1.28). This is not a surprising result and we could have guessed it from the form of (1.27) and (1.28) for the Green's functions in the Hartree-Fock approximation.

We use the states in (2.32) as the single-particle states from which we build up the collective excitations. The energy of a transition from a spin up state in the λ' band with wave-vector $\underline{k}+\underline{q}$ to a spin down state in the λ band with wave vector $\underline{k}$ is $\omega^{sp}_{q\lambda\lambda'}$ given by

$$\omega^{sp}_{q\lambda\lambda'} = \epsilon^{\lambda}_{\underline{k}\uparrow} - \epsilon^{\lambda'}_{\underline{k}+\underline{q}\uparrow} \quad (2.33)$$

The operator for such a transition is $a^{\dagger}_{\lambda\,\underline{k}\uparrow}\, a_{\lambda'\underline{k}+\underline{q}\uparrow}$ and the four possible transitions for $\lambda = \pm$ and $\lambda' = \pm$ are shown in figure 2.4a. The continuum spectrum represented by (2.33) is shown schematically in figure 2.4b. As in the itinerant model there are gaps in these excitations for $q = 0$, and

again we can form collective excitations of lower energy by taking linear combinations of the single-particle excitations. The spin wave operator is now defined as

$$B_q = \sum_{q'\lambda\lambda'} \alpha_q^{\lambda\lambda'} a^+_{\lambda q''} + a_{\lambda' -q''} + q+ \qquad (2.33)$$

and its equation of motion is again (2.24). We now write the full Hamiltonian H in terms of the Hartree-Fock Hamiltonian H_o as:

$$H = H_o + H_{dd} - H_{add} \qquad (2.34)$$

where H_{dd} is given by (1.7e) and H_{add} is

$$H_{add} = \sum_{i\sigma} U \langle n_{d-\sigma} \rangle C^+_{di\sigma} C_{di\sigma} \qquad (2.35)$$

We need to express H in terms of the operators $a^+_{\lambda q\sigma}$ and $a_{\lambda q\sigma}$. H_o is already in this form and we can put H_{dd} and H_{add} into the required form by using (2.29) and (2.31). We have from (2.31) that

$$C_{dq\sigma} = \sum_{\lambda //} X^{\lambda}_{q\sigma} a_{\lambda q\sigma} \qquad (2.36)$$

where

$$(X^{\lambda}_{q\sigma})^2 = Z^{\lambda}_{q\sigma}$$

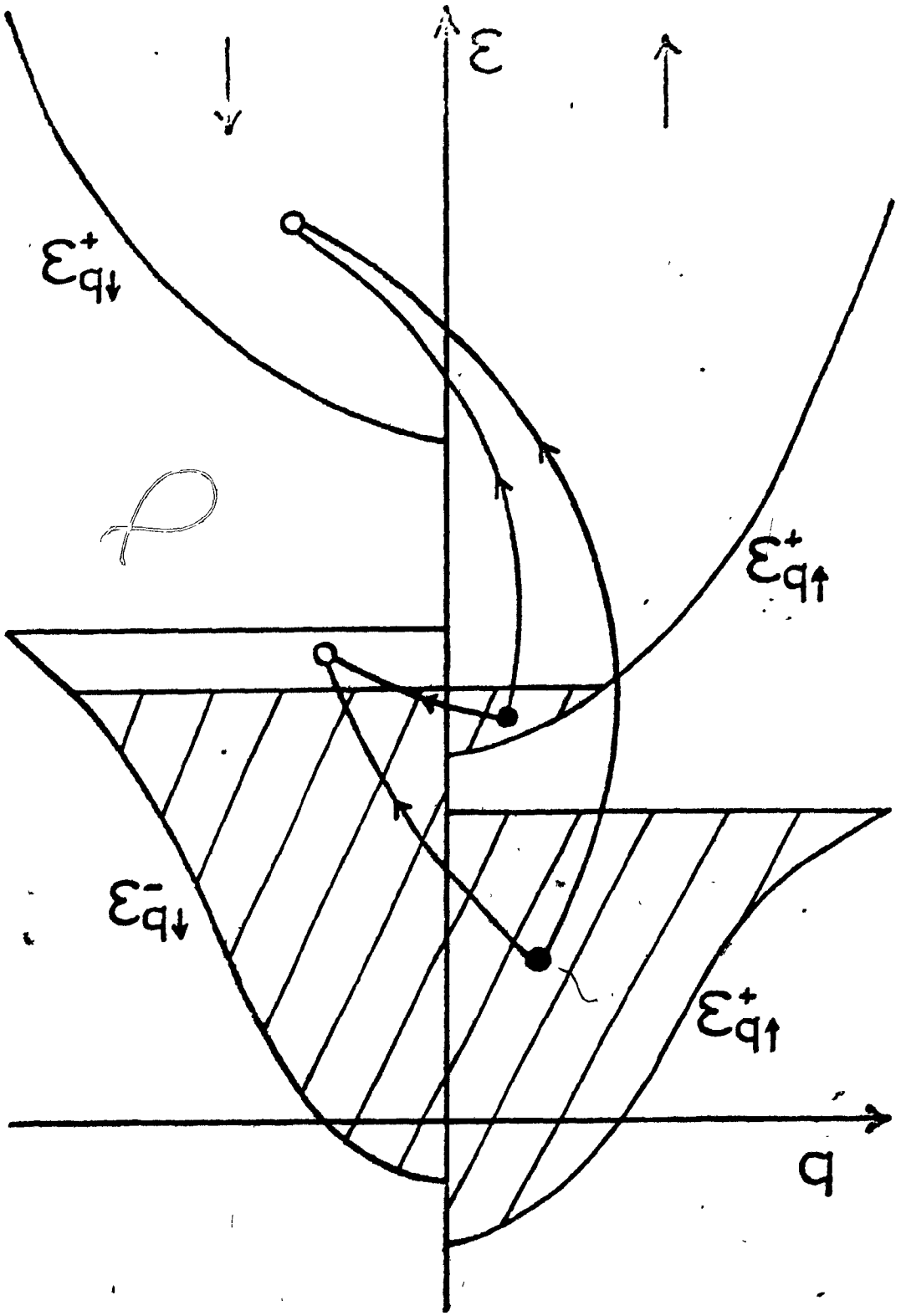

Figure 2.4(a)

Single-particle excitations in the narrow band model (schematic).

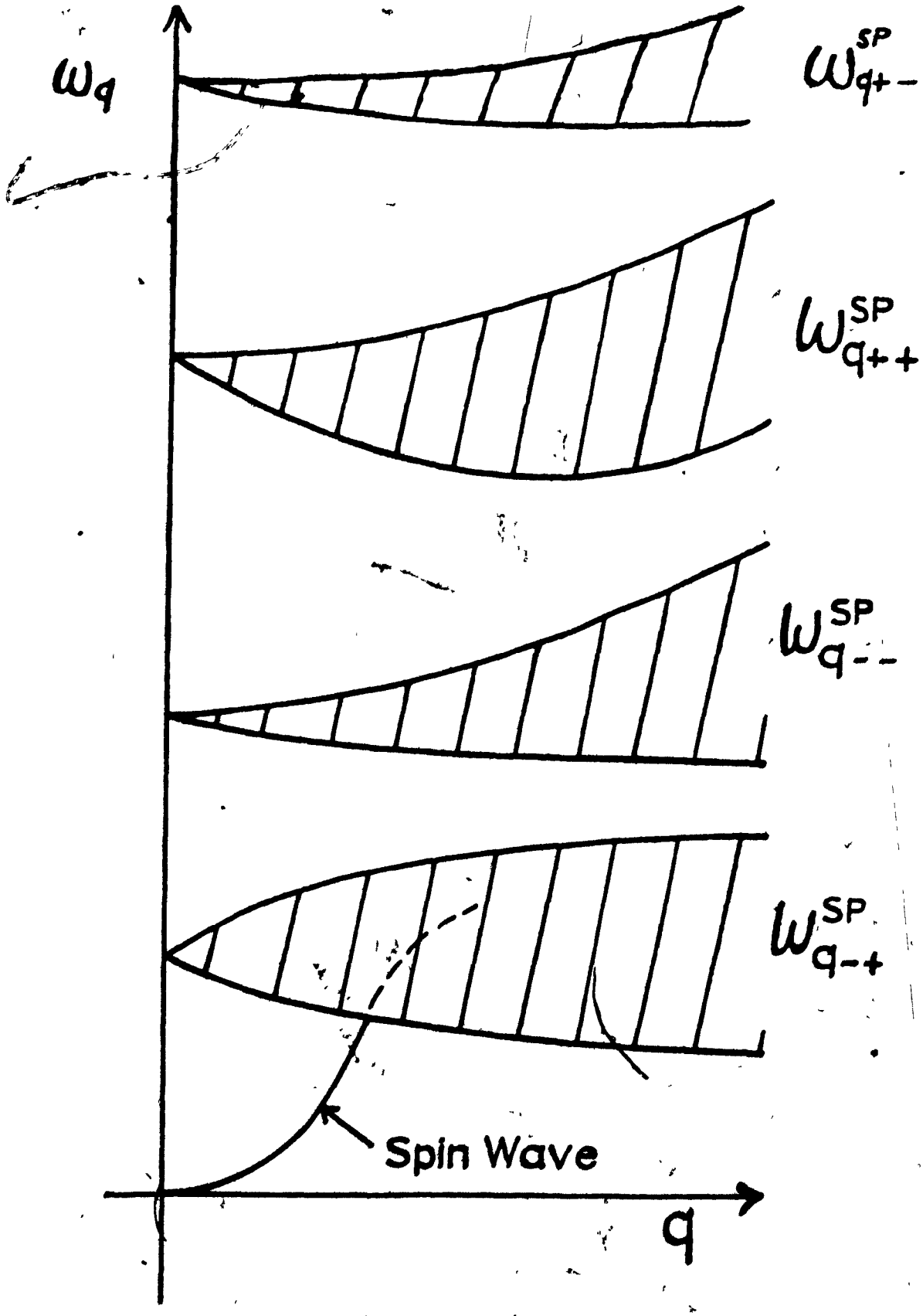

Figure 2.4(b)
Spectrum of single-particle and spin wave excitations in the narrow band model (schematic).

We finally find:

$$H_{dd} = \frac{U}{N} \sum_{\substack{q_3 q_4 q_5 \\ \lambda_1 \lambda_2 \lambda_3 \lambda_4}} X^{\lambda_1}_{q_4 - q_5 \uparrow} X^{\lambda_2}_{q_3 - q_5 \uparrow} X^{\lambda_3}_{q_3 \downarrow} X^{\lambda_4}_{q_4 \downarrow} a^{+}_{\lambda_1 q_4 - q_5 \uparrow} a_{\lambda_2 q_3 - q_5 \uparrow} a^{+}_{\lambda_3 q_3 \downarrow} a_{\lambda_4 q_4 \downarrow} \tag{2.37}$$

and

$$H_{add} = \sum_{\substack{q_1 \sigma \\ \lambda_1 \lambda_2}} U \langle n_{d-\sigma} \rangle X^{\lambda_1}_{q_1 \sigma} X^{\lambda_2}_{q_1 \sigma} a^{+}_{\lambda_1 q_1 \sigma} a_{\lambda_2 q_1 \sigma} \tag{2.38}$$

The commutator in (2.24) is easy to evaluate and for H_o and H_{add} we have:

$$[H_o, a^{+}_{\lambda q'' \downarrow} a_{\lambda - q'' + q \uparrow}] = (\varepsilon^{\lambda}_{q'' \downarrow} - \varepsilon^{\lambda}_{q'' + q \uparrow}) a^{+}_{\lambda q'' \downarrow} a_{\lambda - q'' + q \uparrow} \tag{2.39}$$

and

$$[H_{add}, a^{+}_{\lambda q'' \downarrow} a_{\lambda - q'' + q \uparrow}] = \sum_{\lambda_1} U \langle n_{d\uparrow} \rangle X^{\lambda_1}_{q'' \downarrow} X^{\lambda}_{q'' \downarrow} a^{+}_{\lambda_1 q'' \downarrow} a_{\lambda - q'' + q \uparrow}$$

$$- \sum_{\lambda_2} U \langle n_{d\downarrow} \rangle X^{\lambda_1}_{q'' + q \uparrow} X^{\lambda_2}_{q'' + q \uparrow} a^{+}_{\lambda q'' \downarrow} a_{\lambda_2 q'' + q \uparrow} \tag{2.40}$$

The commutator with H_{dd} is more complicated and requires a little more care. From (2.37) we can see that we need to evaluate the following commutator:

$$\{a^{+}_{\lambda_1}(\xi_4-\xi_5+\ a_{\lambda_2}(\xi_3-\xi_5+a^{+}_{\lambda_3}(\xi_3+\ a_{\lambda_4}(\xi_4+\ a^{+}_{\lambda'}(\xi''+\xi+\}$$

$$= a^{+}_{\lambda_1}(\xi_4-\xi_5+\ a_{\lambda_2}(\xi_3-\xi_5+a^{+}_{\lambda_3}(\xi_3+\ a_{\lambda'}(\xi''+\xi+\ \delta_{\lambda\lambda_4}\ \delta(\xi_4,\xi''$$

$$-\ a^{+}_{\lambda}(\xi''+\ a_{\lambda_2}(\xi_3-\xi_5+a^{+}_{\lambda_3}(\xi_3+\ a_{\lambda_4}(\xi_4+\ \delta_{\lambda_1\lambda'}\ \delta(\xi_4-\xi_5,\xi''+\xi$$

(2.41)

We now use the random phase approximation (RPA) to simplify (2.41) and this is equivalent to making the following replacements:

$$a^{+}_{\lambda_1}(\xi_4-\xi_5+\ a_{\lambda_2}(\xi_3-\xi_5+a^{+}_{\lambda_3}(\xi_3+\ a_{\lambda'}(\xi''+\xi+$$

$$= \langle a^{+}_{\lambda_1}(\xi_4-\xi_5+a_{\lambda_2}(\xi_3-\xi_5+\rangle a^{+}_{\lambda_3}(\xi_3+\ a_{\lambda'}(\xi''+\xi+$$

$$+\ \langle a^{+}_{\lambda_1}(\xi_4-\xi_5+\ a_{\lambda'}(\xi''+\xi+\rangle\ a_{\lambda_2}(\xi_3-\xi_5+\ a^{+}_{\lambda_3}(\xi_3+$$

$$+\ \delta_{\lambda_3\lambda_2}\ \delta(\xi_3,\xi_4\ \langle a^{+}_{\lambda_1}(\xi_4-\xi_5+\ a_{\lambda_1}(\xi_4-\xi_5+\rangle\ a^{+}_{\lambda_3}(\xi_3+\ a_{\lambda'}(\xi''+\xi+$$

$$-\ \delta_{\lambda_3\lambda'}\ \delta(\xi_4-\xi_5,\xi''+\xi\ \langle a^{+}_{\lambda'}(\xi''-\xi+\ a_{\lambda'}(\xi''+\xi+\rangle\ a^{+}_{\lambda_3}(\xi_3+\ a_{\lambda_2}(\xi_3-\xi_5+$$

$$= \delta_{\lambda_3\lambda_2}\ \delta(\xi_3,\xi_4\ f(\varepsilon^{\lambda}_{\xi_4}-\xi_5+)\ a^{+}_{\lambda_3}(\xi_3+\ a_{\lambda'}(\xi''+\xi+$$

$$-\ \delta_{\lambda_3\lambda'}\ \delta(\xi_4-\xi_5,\xi''+\xi\ f(\varepsilon^{\lambda'}_{\xi''+\xi+})\ a^{+}_{\lambda_3}(\xi_3+\ a_{\lambda_2}(\xi_3-\xi_5+$$

(2.42)

where we have replaced the average values by Fermi functions. Similarly we find

$$a^{+}_{\lambda}\,q''\uparrow\; a_{\lambda_2}\,q_3-q_3\uparrow\; a^{+}_{\lambda_3}\,q_3\uparrow\; a_{\lambda_4}\,q_4\uparrow$$

$$= \delta_{\lambda_3\lambda_4}\,\delta_{q_3,q_4}\,f(\varepsilon^{\lambda_3}_{q_3\uparrow})\; a^{+}_{\lambda}\,q''\uparrow\; a_{\lambda_2}\,q_3-q_3\uparrow$$

$$- \delta_{\lambda\lambda_4}\,\delta_{q'',q_4}\,f(\varepsilon^{\lambda}_{q''\uparrow})\; a^{+}_{\lambda_3}\,q_3\uparrow\; a_{\lambda_2}\,q_3-q_3\uparrow \qquad (2.43)$$

From (2.37), (2.41), (2.42) and (2.43) we get

$$[H_{dd}, a^{+}_{\lambda}\,q''\uparrow\; a_{\lambda'}\,q''\uparrow\; q\uparrow]$$

$$= -\frac{U}{N}\sum_{\substack{q_3\\ \lambda_2\lambda_3}} X^{\lambda_2}_{q''-q_3\uparrow}\, X^{\lambda_3}_{q''-q_3\uparrow}\, X^{\lambda}_{q''\uparrow}\, X^{\lambda'}_{q''\uparrow}\; f(\varepsilon^{\lambda_2}_{q''-q_3\uparrow})\; a^{+}_{\lambda_3}\,q''\uparrow\; a_{\lambda'}\,q''\uparrow\; q\uparrow$$

$$-\frac{U}{N}\sum_{q_3,\lambda_2,\lambda_3} X^{\lambda'}_{q''+q\uparrow}\, X^{\lambda_2}_{q_3+q\uparrow}\, X^{\lambda_3}_{q_3\downarrow}\, X^{\lambda}_{q''\uparrow}\; f(\varepsilon^{\lambda}_{q''+q\uparrow})\; a^{+}_{\lambda_2}\,q_3\downarrow\; a_{\lambda_3}\,q_3+q\uparrow$$

$$-\frac{U}{N}\sum_{q_3,\lambda_2,\lambda_3} X^{\lambda'}_{q''+q\uparrow}\, X^{\lambda_2}_{q''+q\uparrow}\, X^{\lambda_3}_{q_3\downarrow}\, X^{\lambda_3}_{q_3\downarrow}\; f(\varepsilon^{\lambda_3}_{q_3\downarrow})\; a^{+}_{\lambda}\,q''\downarrow\; a_{\lambda_3}\,q''+q\uparrow$$

$$+\frac{U}{N}\sum_{q_3,\lambda_2,\lambda_3} X^{\lambda'}_{q''+q\uparrow}\, X^{\lambda_2}_{q_3+q\uparrow}\, X^{\lambda_3}_{q_3\downarrow}\, X^{\lambda}_{q''\downarrow}\; f(\varepsilon^{\lambda}_{q''\downarrow})\; a^{+}_{\lambda_3}\,q_3\downarrow\; a_{\lambda_2}\,q_3+q\uparrow$$

$$-U\langle n_{d\uparrow}\rangle\sum_{\lambda_3} X^{\lambda_3}_{q''\downarrow}\, X^{\lambda}_{q''\downarrow}\; a^{+}_{\lambda_3}\,q''\downarrow\; a_{\lambda'}\,q''+q\uparrow$$

$$-U\langle n_{d\downarrow}\rangle\sum_{\lambda_3} X^{\lambda'}_{q''+q\uparrow}\, X^{\lambda_3}_{q''+q\uparrow}\; a^{+}_{\lambda}\,q''\downarrow\; a_{\lambda_3}\,q''+q\uparrow$$

$$+ U X^{\lambda}_{\underline{q}''\downarrow} X^{\lambda'}_{\underline{q}''+\underline{q}\uparrow} \left(f(\varepsilon^{\lambda}_{\underline{q}''\downarrow}) - f(\varepsilon^{\lambda'}_{\underline{q}''+\underline{q}\uparrow})\right) \frac{1}{N} \sum_{\underline{q}_2\lambda_2\lambda_3} X^{\lambda_2\lambda_3}_{\underline{q}_2\downarrow} X^{\lambda_3}_{\underline{q}_2+\underline{q}\uparrow}$$

$$a^{+}_{\lambda_2\underline{q}_2\downarrow}\, a_{\lambda_2\underline{q}_2'+\underline{q}\uparrow} \tag{2.44}$$

where we have used the fact that

$$\langle n_{d\sigma}\rangle = \frac{1}{N} \sum_{\underline{q}\lambda} Z^{\lambda}_{\underline{q}\sigma}\, f(\varepsilon^{\lambda}_{\underline{q}\sigma}) \tag{2.45}$$

The first two terms of (2.44) exactly cancel (2.40). Hence (2.24) gives

$$\sum_{\underline{q}'\lambda\lambda'} \alpha^{\lambda\lambda'}_{\underline{q}'} \Big\{ \left(\varepsilon^{\lambda}_{\underline{q}''\downarrow} - \varepsilon^{\lambda'}_{\underline{q}''+\underline{q}\uparrow}\right) a^{+}_{\lambda\underline{q}''\downarrow}\, a_{\lambda'\underline{q}''+\underline{q}\uparrow} + U X^{\lambda}_{\underline{q}''\downarrow} X^{\lambda'}_{\underline{q}''+\underline{q}\uparrow} \Big(f(\varepsilon^{\lambda}_{\underline{q}''\downarrow}) - f(\varepsilon^{\lambda'}_{\underline{q}''+\underline{q}\uparrow}) \Big) \frac{1}{N} \sum_{\underline{q}_2\lambda_2\lambda_3} X^{\lambda_2\lambda_3}_{\underline{q}_2\downarrow} X^{\lambda_3}_{\underline{q}_2+\underline{q}\uparrow}\, a^{+}_{\lambda_2\underline{q}_2\downarrow}\, a_{\lambda_2\underline{q}_2+\underline{q}\uparrow} \Big\}$$

$$= \sum_{\underline{q}''\lambda\lambda'} \omega^{sw}_{\underline{q}}\, \alpha^{\lambda\lambda'}_{\underline{q}''}\, a^{+}_{\lambda\underline{q}''\downarrow}\, a_{\lambda'\underline{q}''+\underline{q}\uparrow} .$$

In the second term on the LHS we interchange the summation labels λ_2 and λ, λ_2 and λ', and $\underline{q}_2$ and $\underline{q}''$. This enables us to equate the coefficients of $a^{+}_{\lambda\underline{q}''\downarrow}\, a_{\lambda'\underline{q}''+\underline{q}\uparrow}$ on both sides of the equation which gives:

$$\left[\omega^{sw}_{\underline{q}} - \left(\varepsilon^{\lambda}_{\underline{q}''\downarrow} - \varepsilon^{\lambda'}_{\underline{q}''+\underline{q}\uparrow}\right)\right] \alpha^{\lambda\lambda'}_{\underline{q}''}$$

$$= U X^{\lambda}_{\underline{q}''\downarrow} X^{\lambda'}_{\underline{q}''+\underline{q}\uparrow} \frac{1}{N} \sum_{\underline{q}_2\lambda_2\lambda_3} \alpha^{\lambda_2\lambda_3}_{\underline{q}_2} X^{\lambda_3}_{\underline{q}_2\downarrow} X^{\lambda_2}_{\underline{q}_2+\underline{q}\uparrow} \left(f(\varepsilon^{\lambda_3}_{\underline{q}_2\downarrow}) - f(\varepsilon^{\lambda_2}_{\underline{q}_2+\underline{q}\uparrow}) \right) \tag{2.46}$$

Denoting the sum on the RHS by A', we get

$$\alpha_{q''}^{\lambda\lambda'} = \frac{U X_{q''\downarrow}^{\lambda} X_{q''+q\uparrow}^{\lambda} A'}{\omega_q^{sw} - \left(\varepsilon_{q''\downarrow}^{\lambda} - \varepsilon_{q''+q\uparrow}^{\lambda'}\right)} \tag{2.47}$$

Substituting this back in (2.46) gives:

$$1 = \frac{U}{N} \sum_{q,\lambda_2\lambda_2} Z_{q,\downarrow}^{\lambda_2} Z_{q,+q\uparrow}^{\lambda_2} \frac{\left(f(\varepsilon_{q,\downarrow}^{\lambda_1}) - f(\varepsilon_{q,+q\uparrow}^{\lambda_2})\right)}{\omega_q^{sw} - \left(\varepsilon_{q,\downarrow}^{\lambda_1} - \varepsilon_{q,+q\uparrow}^{\lambda_2}\right)} \tag{2.48}$$

This implicit equation for ω_q^{sw} is the most important result of this chapter. We note that we would have obtained the same expression if we had set the denominator of the dynamic susceptibility (equation (A44) in appendix A) to zero.*

Since we are interested in long-wavelength spin waves we can expand equation (2.48). To do this we first rearrange it as follows:

$$1 = \frac{U}{N} \sum_{Q\lambda\lambda'} \frac{Z_{Q\uparrow}^{\lambda} f(\varepsilon_{Q\uparrow}^{\lambda}) Z_{Q-q\downarrow}^{\lambda'}}{-\omega_q^{sw} - \left(\varepsilon_{Q\uparrow}^{\lambda} - \varepsilon_{Q-q\downarrow}^{\lambda'}\right)} - \frac{Z_{Q\downarrow}^{\lambda'} f(\varepsilon_{Q\downarrow}^{\lambda'}) Z_{Q+q\uparrow}^{\lambda}}{-\omega_q^{sw} - \left(\varepsilon_{Q+q\uparrow}^{\lambda} - \varepsilon_{Q\downarrow}^{\lambda'}\right)} \tag{2.49}$$

Using the Taylor expansion

$$F_{Q+q} = F_Q + (q\cdot\nabla_Q)F_Q + \tfrac{1}{2}(q\cdot\nabla_Q)F_Q + \ldots \tag{2.50}$$

*This result was also obtained by Manohar (1971) from the dynamic susceptibility.

we have

$$\varepsilon^{\lambda}_{\underline{Q}\uparrow} - \varepsilon^{\lambda'}_{\underline{Q}-\underline{q}\downarrow} = \varepsilon^{\lambda}_{\underline{Q}\uparrow} - \varepsilon^{\lambda'}_{\underline{Q}\downarrow} + (\underline{q}\cdot\underline{\nabla}_{\underline{Q}})\varepsilon^{\lambda'}_{\underline{Q}\downarrow} - \tfrac{1}{2}(\underline{q}\cdot\underline{\nabla}_{\underline{Q}})^2\varepsilon^{\lambda'}_{\underline{Q}\downarrow}$$

(2.51)

From inversion symmetry any sum over $\underline{Q}$ which involves $\underline{v}_{\underline{Q}}$ only is zero and therefore, to order q^2 (assuming that the leading term in $\omega^{SW}_{\underline{q}}$ is q^2, see below) we find that:

$$\frac{Z^{\lambda'}_{\underline{Q}-\underline{q}\downarrow}}{-\omega^{SW}_{\underline{q}} - (\varepsilon^{\lambda}_{\underline{Q}\uparrow} - \varepsilon^{\lambda'}_{\underline{Q}-\underline{q}\downarrow})} = \frac{1}{-\Delta_{\underline{Q}\lambda\lambda'}}\left[Z^{\lambda'}_{\underline{Q}\downarrow}\left(1 + \frac{\frac{1}{2}(\underline{q}\cdot\underline{\nabla}_{\underline{Q}})^2\varepsilon^{\lambda'}_{\underline{Q}\downarrow} - \omega^{SW}_{\underline{q}}}{\Delta_{\underline{Q}\lambda\lambda'}} + \left(\frac{\underline{q}\cdot\underline{\nabla}_{\underline{Q}}\varepsilon^{\lambda'}_{\underline{Q}\downarrow}}{\Delta_{\underline{Q}\lambda\lambda'}}\right)^2\right) + \frac{(\underline{q}\cdot\underline{\nabla}_{\underline{Q}}Z^{\lambda'}_{\underline{Q}\downarrow})(\underline{q}\cdot\underline{\nabla}_{\underline{Q}}\varepsilon^{\lambda'}_{\underline{Q}\downarrow})}{\Delta_{\underline{Q}\lambda\lambda'}} + \tfrac{1}{2}(\underline{q}\cdot\underline{\nabla}_{\underline{Q}})^2 Z^{\lambda'}_{\underline{Q}\downarrow}\right]$$

(2.52)

where $$\Delta_{\underline{Q}\lambda\lambda'} = \varepsilon^{\lambda}_{\underline{Q}\uparrow} - \varepsilon^{\lambda'}_{\underline{Q}\downarrow} \qquad (2.53a)$$

Similarly

$$\frac{Z^{\lambda}_{\underline{Q}+\underline{q}\uparrow}}{-\omega^{SW}_{\underline{q}} - (\varepsilon^{\lambda}_{\underline{Q}+\underline{q}\uparrow} - \varepsilon^{\lambda'}_{\underline{Q}\downarrow})} = \frac{1}{-\Delta_{\underline{Q}\lambda\lambda'}}\left[Z^{\lambda}_{\underline{Q}\uparrow}\left(1 + \frac{-\frac{1}{2}(\underline{q}\cdot\underline{\nabla}_{\underline{Q}})^2\varepsilon^{\lambda}_{\underline{Q}\uparrow} - \omega^{SW}_{\underline{q}}}{\Delta_{\underline{Q}\lambda\lambda'}} + \left(\frac{\underline{q}\cdot\underline{\nabla}_{\underline{Q}}\varepsilon^{\lambda}_{\underline{Q}\uparrow}}{\Delta_{\underline{Q}\lambda\lambda'}}\right)^2\right) - \frac{(\underline{q}\cdot\underline{\nabla}_{\underline{Q}}Z^{\lambda}_{\underline{Q}\uparrow})(\underline{q}\cdot\underline{\nabla}_{\underline{Q}}\varepsilon^{\lambda}_{\underline{Q}\uparrow})}{\Delta_{\underline{Q}\lambda\lambda'}} + \tfrac{1}{2}(\underline{q}\cdot\underline{\nabla}_{\underline{Q}})^2 Z^{\lambda}_{\underline{Q}\uparrow}\right]$$

(2.53b)

Hence, from (2.49) we have

$$1 = a + b\,\omega^{SW}_{\underline{q}} - c\,q^2 \qquad (2.54)$$

where

$$a = \frac{U}{N} \sum_{\underline{q}\lambda\lambda'} \frac{Z^{\lambda}_{\underline{q}\uparrow} f(\varepsilon^{\lambda}_{\underline{q}\uparrow}) Z^{\lambda'}_{\underline{q}\downarrow} - Z^{\lambda'}_{\underline{q}\downarrow} f(\varepsilon^{\lambda'}_{\underline{q}\downarrow}) Z^{\lambda}_{\underline{q}\uparrow}}{-\Delta_{\underline{q}\lambda\lambda'}} \tag{2.55}$$

$$b = \frac{U}{N} \sum_{\underline{q}\lambda\lambda'} \frac{Z^{\lambda}_{\underline{q}\uparrow} f(\varepsilon^{\lambda}_{\underline{q}\uparrow}) Z^{\lambda'}_{\underline{q}\downarrow} - Z^{\lambda'}_{\underline{q}\downarrow} f(\varepsilon^{\lambda'}_{\underline{q}\downarrow}) Z^{\lambda}_{\underline{q}\uparrow}}{-\Delta^2_{\underline{q}\lambda\lambda'}} \tag{2.56}$$

and

$$c = \frac{U}{3N} \sum_{\underline{q}\lambda\lambda'} \left\{ \frac{Z^{\lambda}_{\underline{q}\uparrow} f(\varepsilon^{\lambda}_{\underline{q}\uparrow}) \tfrac{1}{2}\nabla^2 Z^{\lambda'}_{\underline{q}\downarrow} - Z^{\lambda'}_{\underline{q}\downarrow} f(\varepsilon^{\lambda'}_{\underline{q}\downarrow}) \tfrac{1}{2}\nabla^2 Z^{\lambda}_{\underline{q}\uparrow}}{\Delta_{\underline{q}\lambda\lambda'}} \right.$$

$$+ \frac{Z^{\lambda}_{\underline{q}\uparrow} f(\varepsilon^{\lambda}_{\underline{q}\uparrow}) \left(Z^{\lambda'}_{\underline{q}\downarrow} \tfrac{1}{2}\nabla^2 \varepsilon^{\lambda'}_{\underline{q}\downarrow} + \nabla Z^{\lambda'}_{\underline{q}\downarrow} \cdot \nabla \varepsilon^{\lambda'}_{\underline{q}\downarrow} \right) + Z^{\lambda'}_{\underline{q}\downarrow} f(\varepsilon^{\lambda'}_{\underline{q}\downarrow}) \left(Z^{\lambda}_{\underline{q}\uparrow} \tfrac{1}{2}\nabla^2 \varepsilon^{\lambda}_{\underline{q}\uparrow} + \nabla Z^{\lambda}_{\underline{q}\uparrow} \cdot \nabla \varepsilon^{\lambda}_{\underline{q}\uparrow} \right)}{\Delta^2_{\underline{q}\lambda\lambda'}}$$

$$\left. + \frac{Z^{\lambda}_{\underline{q}\uparrow} f(\varepsilon^{\lambda}_{\underline{q}\uparrow}) Z^{\lambda'}_{\underline{q}\downarrow} (\nabla \varepsilon^{\lambda'}_{\underline{q}\downarrow})^2 - Z^{\lambda'}_{\underline{q}\downarrow} f(\varepsilon^{\lambda'}_{\underline{q}\downarrow}) Z^{\lambda}_{\underline{q}\uparrow} (\nabla \varepsilon^{\lambda}_{\underline{q}\uparrow})^2}{\Delta^3_{\underline{q}\lambda\lambda'}} \right\} \tag{2.57}$$

and all derivatives are taken with respect to $\underline{q}$. In the above we have averaged over all directions of $\underline{q}$, using the following relations:

$$\sum_{\underline{q}} F_{\underline{q}} (\underline{q}\cdot\nabla)^2 H_{\underline{q}} = \tfrac{1}{3} q^2 \sum_{\underline{q}} F_{\underline{q}} \nabla^2 H_{\underline{q}}$$

and

$$\sum_{\underline{q}} F_{\underline{q}} (\underline{q}\cdot\nabla H_{\underline{q}})(\underline{q}\cdot\nabla G_{\underline{q}}) = \tfrac{1}{3} q^2 \sum_{\underline{q}} F_{\underline{q}} (\nabla H_{\underline{q}} \cdot \nabla G_{\underline{q}})$$

Now, it is straightforward to show that

$$\sum_{\lambda} \frac{Z^{\lambda}_{q\uparrow}}{\Delta_{q\lambda\lambda'}} - \sum_{\lambda'} \frac{Z^{\lambda'}_{q\downarrow}}{\Delta_{q\lambda\lambda'}} = -\frac{1}{UM_d}$$

where M_d is the d-part of the magnetization and is given by (1.53a).

Hence

$$a = \frac{1}{M_d}\left[\sum_{q\lambda} Z^{\lambda}_{q\uparrow} f(\varepsilon^{\lambda}_{q\uparrow}) - \sum_{q\lambda'} Z^{\lambda'}_{q\downarrow} f(\varepsilon^{\lambda'}_{q\downarrow})\right]$$

$$= 1 \text{ from (2.45)}$$

Similarly, it can be shown that

$$b = \frac{M_d + M_c}{UM_d^2}$$

where M_c is the conduction part of the magnetization given by (1.53b).

Hence from (2.54) we have

$$\omega_q^{SW} = Dq^2 \qquad (2.58)$$

with

$$D = \frac{cUM_d^2}{M_d + M_c} \qquad (2.59)$$

Thus the dispersion for long-wavelength spin wave is of the form Dq^2 (Figure 2.4b) in the narrow band model as in the

localized and itinerant models described previously. We have evaluated D for the model calculations of chapter I and the results are shown in Figure 2.5a where D is plotted as a function of U. The magnetization M_d is also plotted for comparision. In Figure 2.5b we plot D as a function of the magnetization M_d and we note that for small M_d the stiffness coefficient is proportional to M_d.

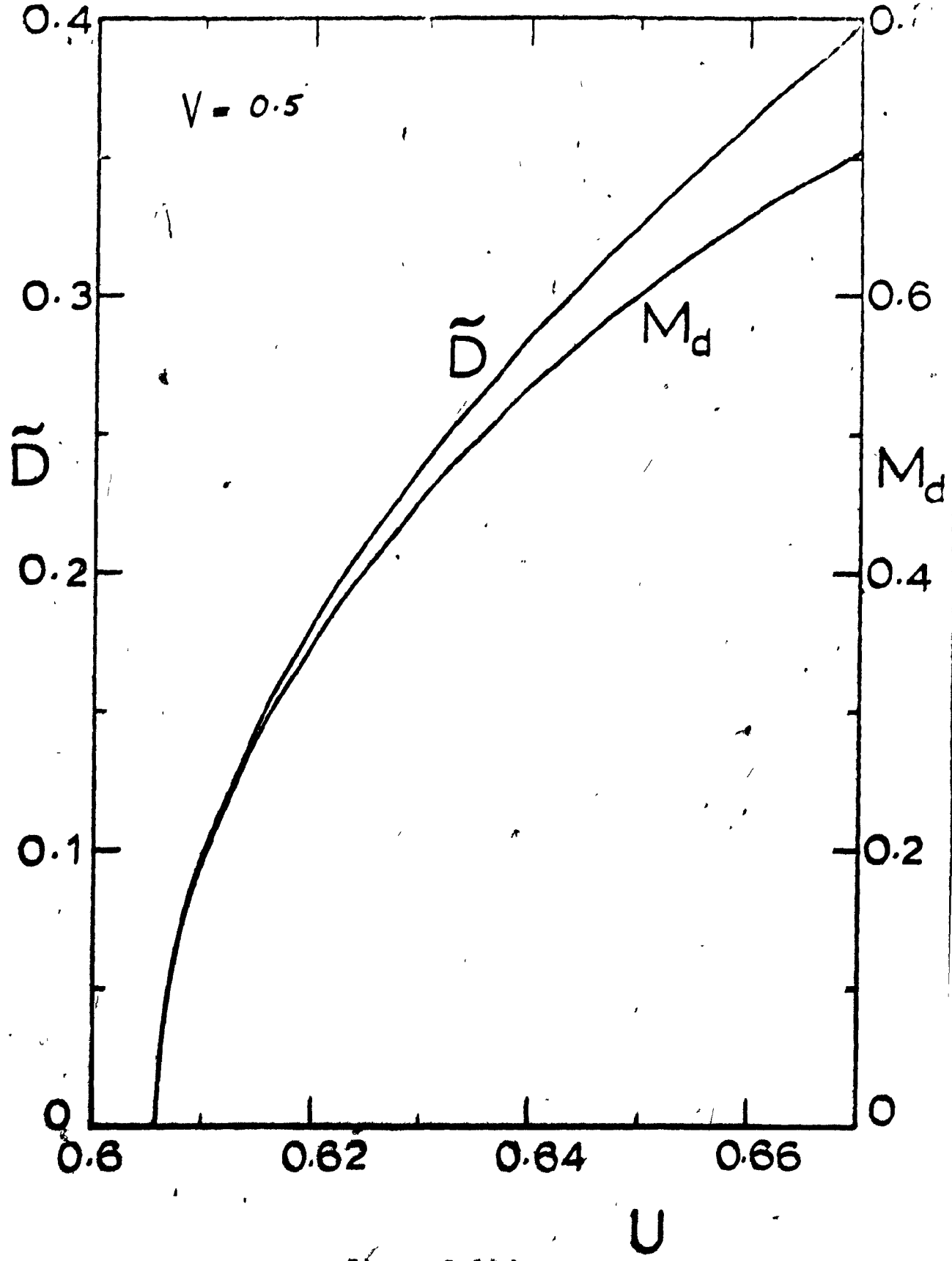

Figure 2.5(a)
Stiffness coefficient $\tilde{D}$ (= $D/\hbar^2/2m$) and magnetization M_d (equation (1.53a)) as a function of U in the narrow band model. All energies are normalised to ϵ_0 (equation (1.43)).

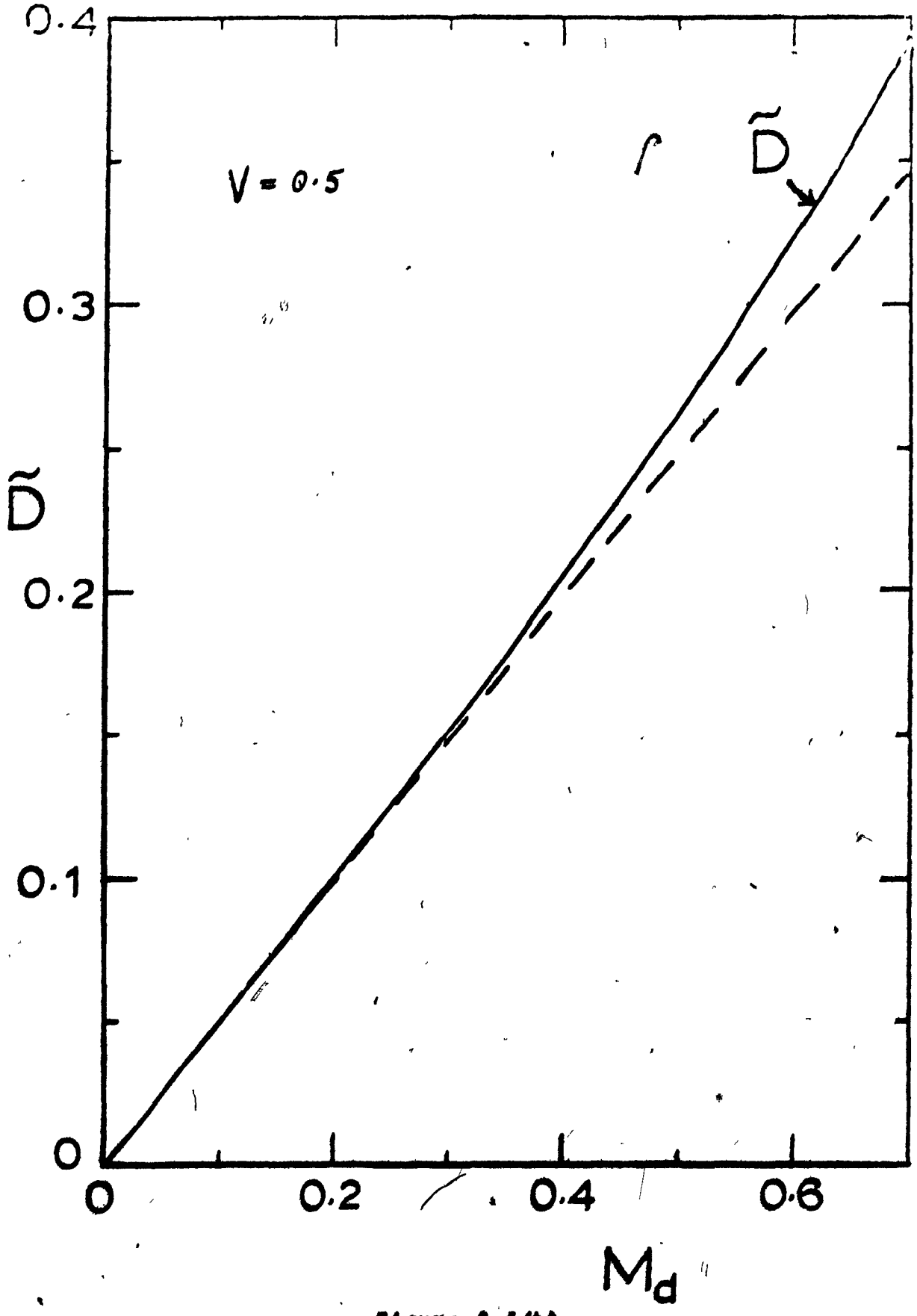

Figure 2.5(b)
Stiffness coefficient $\tilde{D}$ (= $D/\hbar^2/2m$) as a function of magnetization M_d (equation (1.53a)) in the narrow band model. The broken line is the extrapolation of the linear form at low magnetization.

Chapter III

Spin fluctuations in the narrow band model

The magnetic susceptibility of nearly ferromagnetic metals such as Pd is enhanced by strong interactions between opposite spin electrons in the d-band. The average occupation of both spin bands is the same, but the interactions induce transient parallel spin alignments over microscopic regions of the crystal. These fluctuations are known as spin fluctuations. The nearer the metal is to the ferromagnetic instability, the greater is the spatial and temporal persistence of these spin fluctuations. The effect of spin fluctuations is seen in several properties of nearly ferromagnetic metals. Doniach and Engelsberg (1966) showed that spin fluctuations produce a large renormalization of the d-hole mass in Pd, leading to an enhancement of the electronic specific heat for example. Figure 3.1 shows the enhancement of the susceptibility and the specific heat constant towards the end of the 4d and 5d series. Also shown is the suppression of the superconducting critical temperature as the enhancement increases. Following an initial suggestion by Doniach, Bork and Schrieffer (1966) showed that the tendency towards parallel alignment represented by spin fluctuations opposes the superconductive pairing of opposite spin electrons, thereby suppressing the superconducting critical temperature.

One of the most interesting effects of spin fluctuations

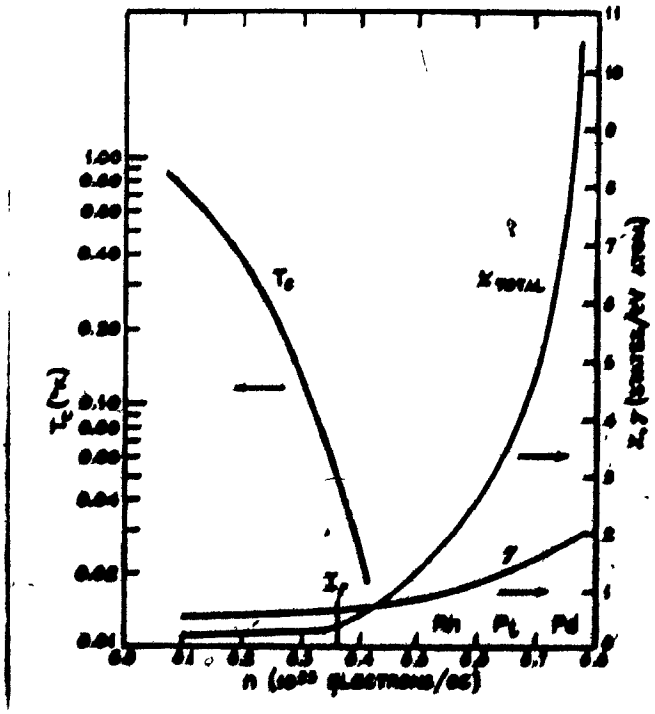

Figure 3.1

Susceptibility (X), electronic specific heat constant (γ) and superconducting critical temperature (T_c) for metals and alloys towards the end of the 4d and 5d series (after Andres and Jensen (1968))

is in the transport properties of solids. It is now generally accepted that the T^2 term in the low temperature resistivity of Pd, Pd-Ni, Ir-Fe and other transition metal alloys is due to the scattering of conduction electrons from spin fluctuations. In section 3.1 we review briefly spin fluctuations and spin fluctuation resistivity in the itinerant model. Then, in section 3.2, we examine spin fluctuations in the narrow band model.

3.1 Spin fluctuations in the itinerant model

Because of the dynamic character of spin fluctuations their properties must be examined by looking at the dynamic susceptibility of the system. The dynamic susceptibility $\chi(\underline{r},t)$ is the response function for the magnetization $M(\underline{r},t)$ arising from an applied magnetic field $H(\underline{r},t)$:

$$M(x,t) = \int \chi(x-x', t-t')\, H(x', t')\, dx'\, dt' \qquad (3.1)$$

The linear response theory of Kubo (1957) shows that for a transverse field the response function is given by the retarded Green's function:

$$\chi(x,t) = -i\,\theta(t)\left\langle \left[S^{+}(x,t),\, S^{-}(0,0) \right] \right\rangle \qquad (3.2)$$

where $\underline{S}(r)$ is the spin density operator. Izuyama, Kim and

Kubo (1963) have evaluated the dynamic susceptibility, in the random phase approximation (RPA), for interacting itinerant electrons described by the Hubbard Hamiltonian (equation (2.17)). They find that the Fourier transform of the dynamic susceptibility has the form

$$\chi(\underline{q},\omega) = \frac{\chi^{\circ}(\underline{q},\omega)}{1 - I\,\chi^{\circ}(\underline{q},\omega)} \qquad (3.3)$$

where

$$\chi^{\circ}(\underline{q},\omega) = \frac{1}{N}\sum_{\underline{k}} \frac{f(\varepsilon_{\underline{k}\uparrow}) - f(\varepsilon_{\underline{k}+\underline{q}\downarrow})}{\varepsilon_{\underline{k}+\underline{q}\downarrow} - \varepsilon_{\underline{k}\uparrow} - \omega} \qquad (3.4)$$

and $\varepsilon_{\underline{k}\sigma}$ is given by (2.21). We note from (3.3) that the static susceptibility $\chi(0,0)$ is enhanced above the non-interacting Pauli susceptibility $\chi^{\circ}(0,0)$ by the Stoner enhancement factor S. In the paramagnetic phase $\chi^{\circ}(0,0)$ is equal to the density of states at the Fermi level ρ_d. Thus

$$S = \frac{1}{1 - I\rho_d} \qquad (3.5)$$

The static susceptibility diverges for $I\rho_d = 1$ and this indicates a phase transition from a paramagnetic state to a ferromagnetic state. If $I\rho_d < 1$ then the system is paramagnetic while the ferromagnetic state is stable for $I\rho_d > 1$.

The poles of the dynamic susceptibility $X(\underline{q},\omega)$ represent the excited states of the system and its imaginary part gives the frequency distribution, or spectral density, of these excitations. Figure 3.2 shows Im $X(\underline{q},\omega)$ for a few values of the Stoner enhancement factor in the paramagnetic phase. The position of the peak in the spectral density, $\omega_{SF}(\underline{q})$, is given by the pole of $X(\underline{q},\omega)$. For small ω, this pole is given by (Doniach (1967):

$$\omega = \pm i\, \omega_{SF}(\underline{q}) \qquad (3.6)$$

where

$$\omega_{SF}(\underline{q}) = \frac{2\,\varepsilon_F (1 - I\rho_d)\, q}{\pi\, I\rho_d\, k_F} \qquad (3.7)$$

Thus we have poles of $X(\underline{q},\omega)$ on the imaginary axis which give rise to peaks in the spectral density. The excitations represented by such a spectral density are therefore critically damped and are the spin fluctuations mentioned earlier. Equation (3.7) is the dispersion relation for spin fluctuations and ω_{SF} is in fact the inverse of the life-time of these fluctuations. We note from (3.7) that the life-time tends to infinity as $I\rho_d \to 1$ i.e. as the ferromagnetic instability is approached the persistence of the spin fluctuations increases.

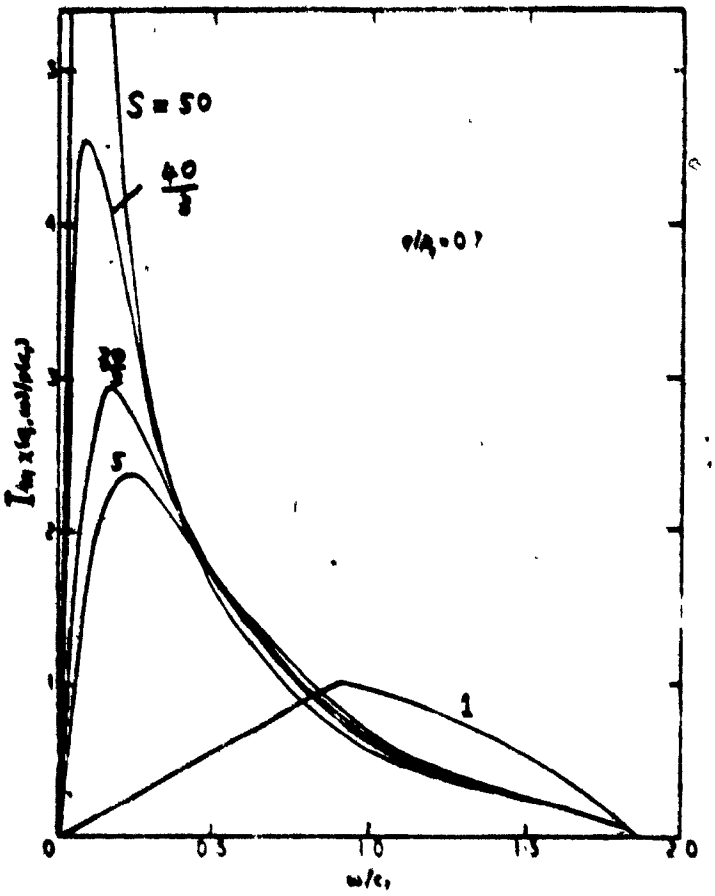

Figure 3.2

Spectral density for spin fluctuations in the itinerant model. The peak becomes sharper as the Stoner enhancement factor S (equation (3.5)) increases (after Doniach (1967)).

The scattering of s electrons off d-band spin fluctuations has been discussed by Mills and Lederer (1960). A simple two-band model is used, one representing the s-like portion of the Fermi surface and the other the d-like portion. The conductivity of the metal is assumed to arise solely from the s-band, which has a nearly free electron character, while the effective electron mass in the narrow d-band is much larger. The d-band, on the other hand, is assumed to dominate the magnetic properties. The s-electrons can then scatter off d-band spin fluctuations via an s-d exchange ipteraction of the form

$$H_{ex} = v J \int \underline{s}(\underline{r}) . \underline{S}(\underline{r}) \, d\underline{r} \qquad (3.8)$$

where v is the volume of the unit cell, J the coupling constant, $\underline{s}(\underline{r})$ the spin density of the s-electrons and $S(\underline{r})$ the spin density of the d-band. Treating the interaction H_{ex} as a perturbation, Mills and Lederer (1966) have calculated the spin-flip scattering rate $P(\underline{k} \rightarrow \underline{k}')$ of s-electrons from the state $\underline{k}$ to $\underline{k}'$ using the Fermi Golden rule and find that it is given by:

$$P(\underline{k} \rightarrow \underline{k}') = \frac{\pi J^2}{N} f_{\underline{k}} (1 - f_{\underline{k}'}) (1 + n(\Omega)) |F(\underline{q})|^2 A(\underline{q}, \Omega) \qquad (3.9)$$

Here N is the total number of atoms, $f_{\underline{k}}$ is the distribution

function for the conduction state k, $n(\Omega)$ is the Bose function, $F(\underline{q})$ is the form factor for the d-orbitals and $A(\underline{q},\Omega)$ is the spectral density of the spin fluctuations given by

$$A(\underline{q},\Omega) = i\left(\chi(\underline{q},\Omega+i\delta) - \chi(\underline{q},\Omega-i\delta)\right) \quad (3.10)$$

where $\underline{q} = \underline{k}-\underline{k}'$ is the electron wave vector change on scattering and $\Omega = \varepsilon_{\underline{k}}-\varepsilon_{\underline{k}'}$ is the energy change.

In equilibrium, the detailed balance condition $P(\underline{k}\to\underline{k}') = P(\underline{k}'\to\underline{k})$ is satisfied and one can then use the variational method (Ziman (1960)) to evaluate the resistivity ρ. This is given by

$$\rho = \frac{1}{2k_BT}\,\frac{\left(\frac{V}{(2\pi)^3}\right)^2 \frac{1}{3}\iint d\underline{k}\,d\underline{k}'\,|\underline{k}-\underline{k}'|^2 P_0(\underline{k}\to\underline{k}')}{V\left(e k_F^3/3\pi^2\right)^2} \quad (3.11)$$

where e is the electronic charge and k_F the Fermi vector of the conduction electrons. $P_0(\underline{k}\to\underline{k}')$ is the equilibrium value of the scattering rate. Equation (3.11) can be simplified using (3.9) to give

$$\rho = \frac{3\pi J^2}{16 k_B T n_a e^2}\iint d\underline{k}\,d\underline{k}'\, f_{\underline{k}}^0\left(1-f_{\underline{k}'}^0\right)\left(1+n(\Omega)\right) \times \int_0^2 |F(k_F\eta)|^2 A(k_F\eta,\Omega)\eta^3 d\eta \quad (3.12)$$

where $f_{\underline{k}}$ is the equilibrium distribution and n_a is the number of atoms per unit volume. Mills and Lederer were the first to point out that equation (3.12) gives a T^2 dependence for the resistivity and would explain the large T^2 term in the resistivity of Pd and Pt at low temperatures. Later we will discuss how in general a T^2 dependence can be obtained.

The addition of Ni impurities to Pd greatly enhances the T^2 term in the resistivity. But for such alloys a localized spin fluctuation model is needed. To compute the spin fluctuation spectral density in dilute Pd-Ni alloys Lederer and Mills (1968) used a simple extension of the Hubbard model. Localized spin fluctuations arise because the Coulomb interaction is increased to a value $I + \Delta I$ in the Ni impurity cell, I being the value in the Pd host cells. The Hamiltonian is then:

$$H = H_0 + \Delta I \sum_j n_{dj\uparrow} n_{dj\downarrow} \qquad (3.13)$$

where H_0 is the Hubbard Hamiltonian (equation (2.17)) and the sum over j in the second term is taken over the impurity cells. Lederer and Mills (1968) investigated the response of this system to a time and spatially varying magnetic field using a dynamic molecular field approximation equivalent to the RPA. Since the impurities destroy the translational invariance of the system, the definition of the magnetic response function is generalized. The susceptibility X is now a function of

both $\underline{r}$ and $\underline{r}'$, and not simply of $\underline{r}-\underline{r}'$ as was the case in the pure metal. The Fourier transform of the dynamic susceptibility then has the form $\chi(\underline{q},\underline{q}',\omega)$ and Lederer and Mills show that

$$\chi(\underline{q},\underline{q}',\omega) = \chi(\underline{q},\omega)\delta_{\underline{q}\underline{q}'} + \frac{c\Delta I\,\chi(\underline{q},\omega)\,\chi(\underline{q}',\omega)}{1-\Delta I\,\bar{\chi}(\omega)} \qquad (3.13)$$

where $\chi(\underline{q},\omega)$ is the enhanced host susceptibility (3.3), c is the impurity concentration and $\bar{\chi}(\omega)$ is given by

$$\bar{\chi}(\omega) = \frac{1}{N}\sum_{\underline{q}} \chi(\underline{q},\omega) \qquad (3.15)$$

The spectral density is now a sum of a host and an impurity spectral density given by the first and second terms of (3.14) respectively. Lederer and Mills have shown that the localized spin fluctuations due to the impurities also lead to a T^2 term in the resistivity.

This calculation by Lederer and Mills of the resistivity due to scattering of conduction electrons from localized spin fluctuations has been extended by Kaiser and Doniach (1970) to higher temperatures. These authors rewrite equation (3.14) as:

$$\rho = \rho_0\beta\int_0^\infty \frac{d\omega\;\omega\;\bar{A}(\omega)}{(e^{\beta\omega}-1)(1-e^{-\beta\omega})} \qquad (3.16)$$

where

$$\bar{A}(\omega) = \frac{1}{k_F} \int_0^{2k_F} |F(q)|^2 A(q,\omega) q^3 dq \qquad (3.17)$$

and

$$\rho_0 = \left(\frac{J\rho_c}{4}\right)^2 \left(\frac{n_a}{n}\right) \frac{m}{ne^2\tau_F} \qquad (3.18)$$

Here $\tau_F = 1/\epsilon_F$, ρ_c is the density of states per atom at the Fermi level for the conduction electrons, m is their effective mass and n is their density. Equation (3.16) shows the general form of the resistivity due to scattering from Bose excitations.

The averaged spectral density for the localized spin fluctuations is given by (Kaiser and Doniach (1970)):

$$\bar{A}(\omega) = B \frac{\omega}{\omega_{SF}^2 + \omega^2} \qquad (3.19)$$

where ω_{SF} is a characteristic paramagnon frequency:

$$\omega_{SF} = \left(\frac{\alpha \Delta I \bar{\chi}_I}{\omega}\right)^{-1} \qquad (3.20)$$

α is the local enhancement factor given by

$$\alpha = \frac{1}{1 - \Delta I \, \bar{\chi}_R} \tag{3.21}$$

and $\bar{\chi}_R$ and $\bar{\chi}_I$ are the real and imaginary parts of $\bar{\chi}(\omega)$ i.e.

$$\bar{\chi}(\omega) = \bar{\chi}_R + i \, \bar{\chi}_I \tag{3.22}$$

For small ω, $\bar{\chi}_I$ is proportional to ω and hence ω_{SF} is independent of ω. The spectral density $\bar{A}(\omega)$ increases linearly with energy ω at low energies, peaks at ω_{SF} and falls off approximately as $1/\omega$ at high energies as shown in Figure 3.3. Defining a characteristic paramagnon temperature T_{SF} and a characteristic resistivity ρ_{SF} by

$$K_B T_{SF} = \omega_{SF} \tag{3.23}$$

$$\rho_{SF} = B \rho_0 \tag{3.24}$$

and introducing a normalized resistivity $\tilde{\rho}$ and a normalized temperature $\tilde{T}$

$$\tilde{\rho} = \rho / \rho_{SF} \tag{3.25}$$

$$\tilde{T} = T / T_{SF} \tag{3.26}$$

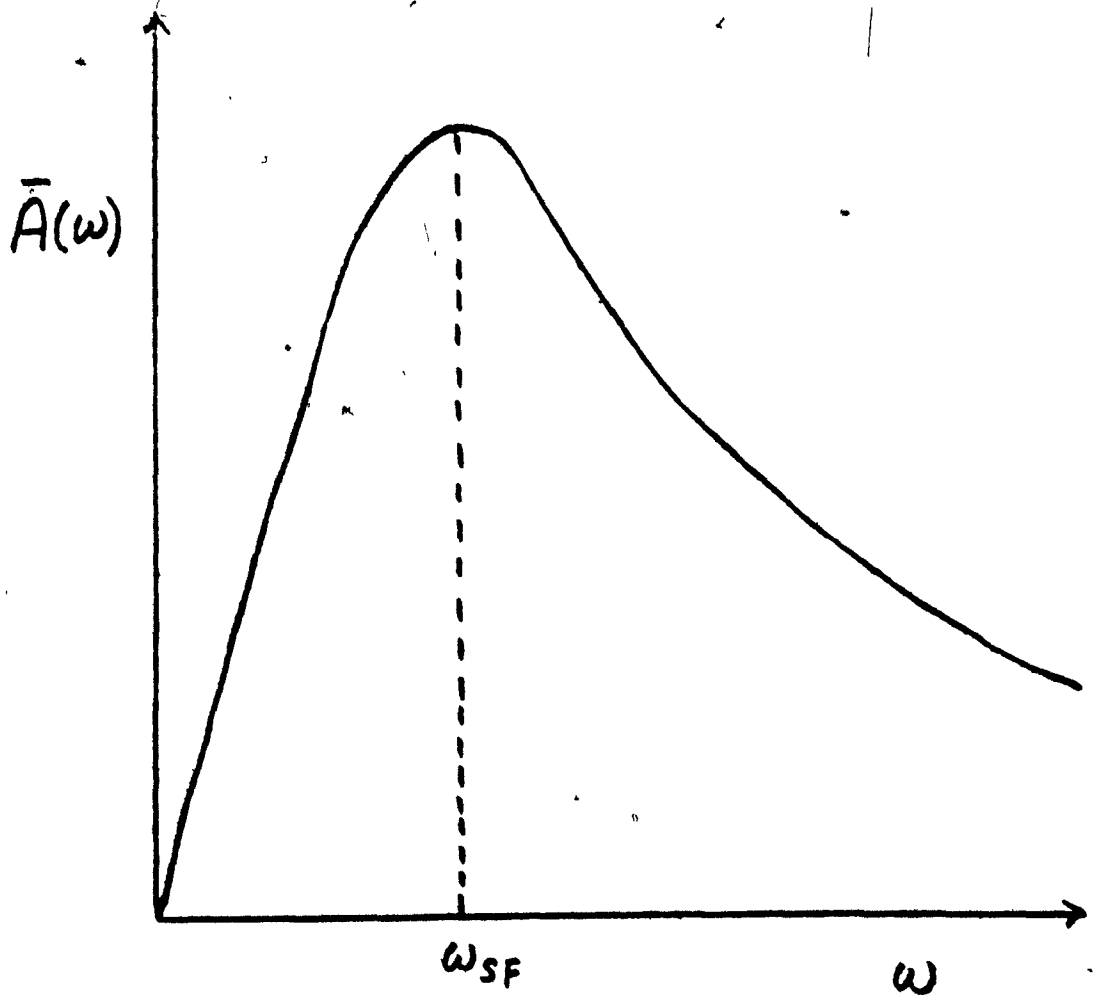

Figure 3.3

The averaged spectral density (equation (3.19)) for localized spin fluctuations (schematic)

the resistivity expression (3.16) can be written as

$$\tilde{\rho} = \frac{1}{\tilde{T}} \int_0^\infty d\tilde{\omega} \, \frac{\tilde{\omega}^2}{(1+\tilde{\omega}^2)(e^{\tilde{\omega}/\tilde{T}}-1)(1-e^{-\tilde{\omega}/\tilde{T}})} \qquad (3.27)$$

Equation (3.27) is a universal expression for the resistivity in terms of the dimensionless quantities $\tilde{\rho}$ and $\tilde{T}$ and all parameters of the host metal and impurity atoms are included in the normalization factors in (3.25) and (3.26). Figure 3.4 shows a plot of $\tilde{\rho}$ versus $\tilde{T}$. At low temperatures the $\tilde{\omega}^2$ term in the denominator of (3.27) can be neglected and this is equivalent to taking the spectral density to be linear in energy. Putting $x = \tilde{\omega}/\tilde{T}$ we then find that

$$\tilde{\rho}(T \to 0) = \int_0^\infty dx \, \frac{x^2}{(e^x-1)(1-e^{-x})} \cdot \tilde{T}^2$$

$$= \frac{\pi^2}{3} \left(T/T_{SF}\right)^2 \qquad (3.28)$$

This is the low temperature T^2 law obtained by Lederer and Mills. At high temperatures equation (3.27) gives

$$\tilde{\rho}(T \to \infty) = \frac{\pi}{2} \left(T/T_{SF}\right) \qquad (3.29)$$

The resistivity ρ as a function of temperature T will have the same form as the universal curve in Figure 3.4 only if the scaling factors in (3.25) and (3.26) are temperature independent.

At high temperatures, the variation of the susceptibility with temperature will affect these scaling factors. The temperature variation of $\bar{\chi}_R$ and $\bar{\chi}_I$ is very small, but it can be seen from (3.21) that a small change in $\bar{\chi}_R$ produces a large change in α when α is large. To illustrate this effect, Kaiser and Doniach (1970) calculated the temperature dependence of α for an unenhanced host metal (Fig. 3.5). For α large the variation of B, and hence ρ_{SF}, with temperature can be neglected but the decrease in α with temperature will change the scaling factor T_{SF} according to (3.23) and (3.20). Figure 3.6 shows the decrease below the linear law produced by the variation of α with temperature.

Kaiser and Doniach have shown that the above theory describes fairly well the observed behaviour of the impurity resistivity in dilute Ir-Fe alloys over an extended temperature range (Figure 3.7).

3.2 Spin fluctuations in the narrow band model

We now examine spin fluctuations in the narrow band model described in section 1.2. Since the main magnetic effects are expected to occur in the d-band we look at the d-part of the dynamic susceptibility:

$$\chi_{ij}(t-t') = i\theta(t-t')\left\langle \left[S_i^-(t), S_j^+(t') \right] \right\rangle \qquad (3.30)$$

where

$$S_i^- = C_{di\downarrow}^\dagger C_{di\uparrow} \qquad (3.31a)$$

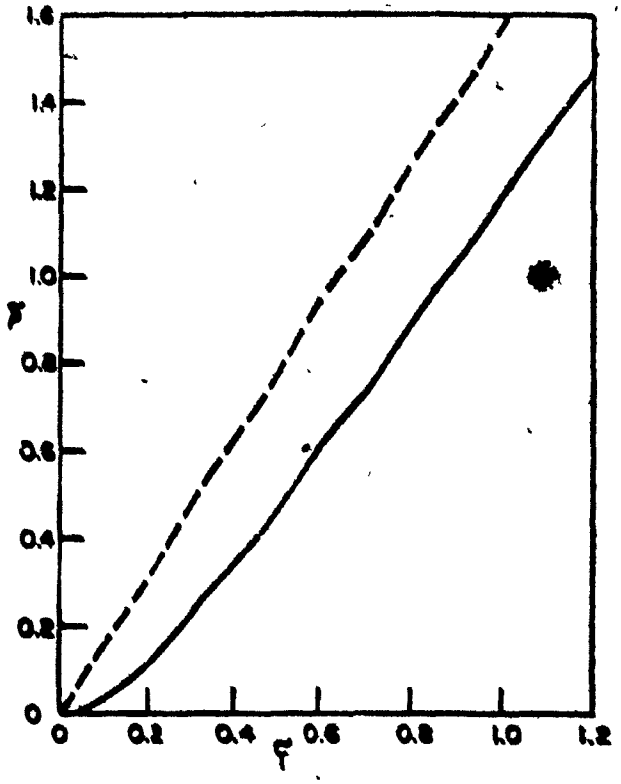

Figure 3.4

Universal curve for spin fluctuation resistivity calculated from (3.27). The dotted line is the high temperature limit (after Kaiser and Donaich (1970)).

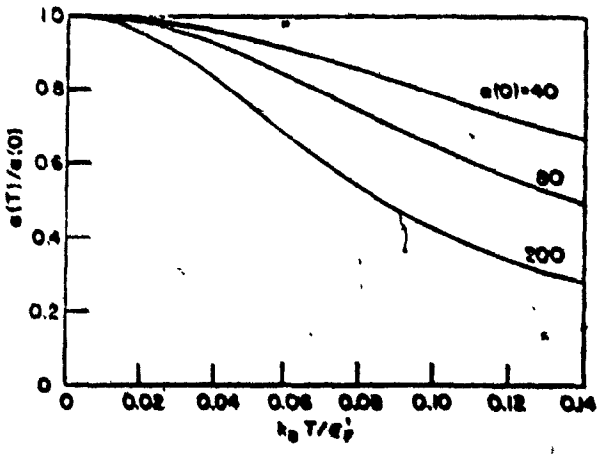

Figure 3.5

Decrease of the local enhancement factor (α) (equation (3.21)) as the temperature (T) increases. ϵ_F^* is the Fermi energy of the host d-band(after Kaiser and Doniach (1970)).

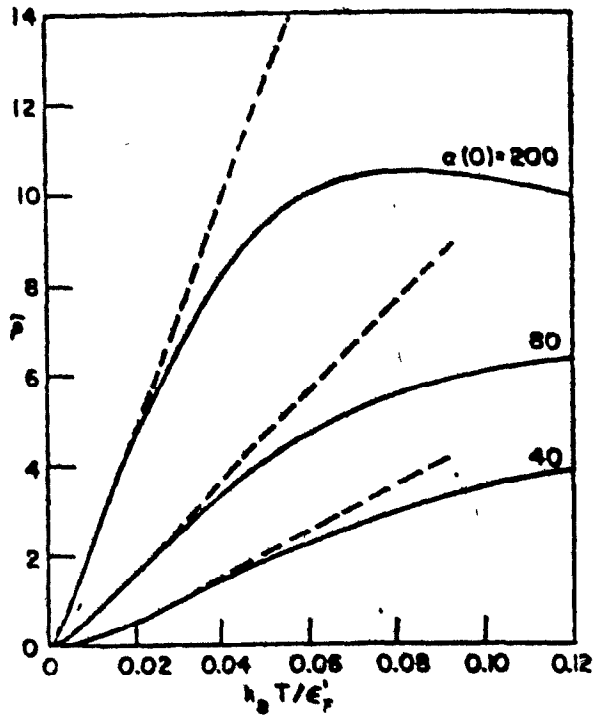

Figure 3.6
The effect on the spin fluctuation resistivity of the temperature dependence of α shown in Figure 3.5 (after Kaiser and Doniach (1970)).

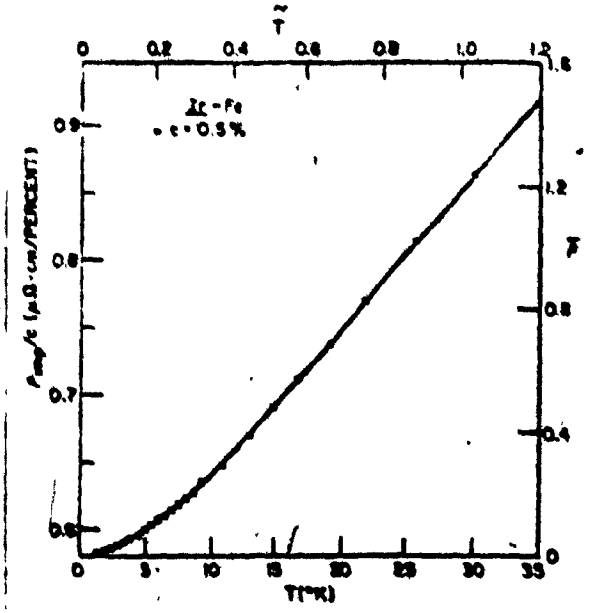

Figure 3.7(a)

Resistivity date of Sarachik (1968) for Ir-Fe. The full line is the universal curve of Figure 3.4 (after Kaiser and Doniach (1970)).

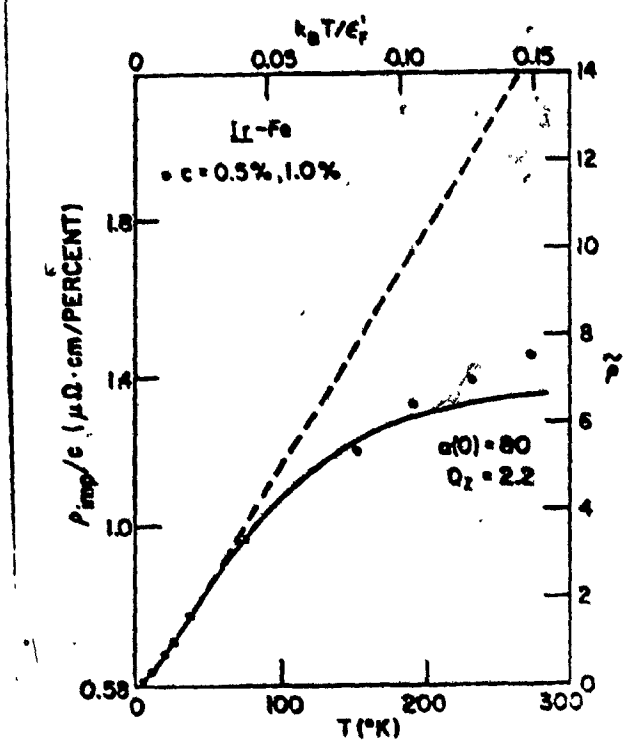

Figure 3.7(b)
Resistivity data of Sarachik (1968) for Ir-Fe. The full line is a theoretical curve from Figure 3.6 (after Kaiser and Doniach (1970

$$S_i^+ = C_{di\uparrow}^\dagger C_{di\downarrow} \qquad (3.31b)$$

The Green's function (3.30) is evaluated in Appendix A using diagrammatic techniques. In RPA the Fourier transform of the dynamic susceptibility is given by

$$\chi(\underline{q},\omega) = \frac{\chi^0(\underline{q},\omega)}{1 - U\chi^0(\underline{q},\omega)} \qquad (3.32)$$

where

$$\chi^0(\underline{q},\omega) = \frac{1}{N}\sum_{\underline{Q}\lambda\lambda'} Z^{\lambda}_{\underline{Q}+\underline{q}\uparrow} Z^{\lambda'}_{\underline{Q}\downarrow} \frac{\left(f(\varepsilon^{\lambda}_{\underline{Q}+\underline{q}\uparrow}) - f(\varepsilon^{\lambda'}_{\underline{Q}\downarrow})\right)}{\omega + \left(\varepsilon^{\lambda}_{\underline{Q}+\underline{q}\uparrow} - \varepsilon^{\lambda'}_{\underline{Q}\downarrow}\right) + i\delta} \qquad (3.33)$$

where $\varepsilon^{\lambda}_{\underline{q}\sigma}$ and $Z^{\lambda}_{\underline{q}\sigma}$ are as defined in Chapter I (equations (1.28) and (1.29)). As we are interested in the paramagnetic phase we will drop all spin indices in (3.33). Replacing the sum over $\underline{Q}$ by an integral over a sphere of radius q_s, as discussed in Chapter I (see equation (1.40)), we find

$$\chi^0(\underline{q},\omega) = \frac{3}{4\varepsilon_s^{3/2}} \sum_{\lambda\lambda'} \int_0^{\varepsilon_s} \varepsilon_Q^{1/2}\, d\varepsilon_Q\, Z^{\lambda}_{\underline{Q}} f(\varepsilon^{\lambda}_{\underline{Q}}) \qquad (3.34)$$

$$\times \int_{-1}^{+1} d\mu \left\{ \frac{Z^{\lambda'}_{\underline{Q}-\underline{q}}}{\omega - \left(\varepsilon^{\lambda}_{\underline{Q}} - \varepsilon^{\lambda'}_{\underline{Q}-\underline{q}}\right) + i\delta} - \frac{Z^{\lambda'}_{\underline{Q}+\underline{q}}}{\omega - \left(\varepsilon^{\lambda'}_{\underline{Q}+\underline{q}} - \varepsilon^{\lambda}_{\underline{Q}}\right) + i\delta} \right\}$$

where $\mu = \cos\theta$ and θ is the angle between $\underline{Q}$ and $\underline{q}$.

For a parabolic band, we have:

$$\varepsilon_{\underline{Q}\pm\underline{q}} = \varepsilon_Q + \varepsilon_q \pm 2(\varepsilon_Q \varepsilon_q)^{1/2}\mu \qquad (3.35)$$

Substituting (3.35) into (3.34) and again normalizing all energies to ε_s (equation (1.43)) we find:

$$\chi^0(q,\omega) = -\frac{3}{4}\sum_{\substack{\lambda\lambda' \\ \nu=\pm}} \int_0^1 \varepsilon_Q^{1/2} d\varepsilon_Q \, Z_Q^{\lambda'} f(\varepsilon_Q^{\lambda'}) J^\nu \qquad (3.36)$$

where

$$J^\nu = \int_{-1}^{+1} d\mu \, \frac{\frac{1}{2}\left(1 + \lambda \frac{(\eta - \nu\zeta\mu)}{((\eta-\nu\zeta\mu)^2+\gamma)^{1/2}}\right)}{\beta^\nu - \varepsilon^\lambda(\nu\zeta\mu) + i\nu\delta} \qquad (3.37)$$

$$\eta = E_{dc} - \varepsilon_Q - \varepsilon_q \qquad (3.38)$$

$$\zeta = 2(\varepsilon_Q \varepsilon_q)^{1/2} \qquad (3.39)$$

$$\beta^\nu = \nu\omega - \varepsilon_Q - \varepsilon_q - \varepsilon_Q^{\lambda'} \qquad (3.40)$$

$$\gamma = 4V^2$$

and

$$\varepsilon^\lambda(x) = \frac{1}{2}\left(\eta + x + \lambda\left((\eta - x)^2 + \gamma\right)^{1/2}\right) \qquad (3.41)$$

In (3.36) we have also normalized $X^{\circ}(q,\omega)$ by multiplying it by ϵ_s. We note from (3.37) and (3.40) that

$$Re\ \chi^{\circ}(q,-\omega) = Re\ \chi^{\circ}(q,\omega) \tag{3.42}$$

and

$$Im\ \chi^{\circ}(q,-\omega) = -Im\ \chi^{\circ}(q,\omega) \tag{3.43}$$

i.e. the real part of $X^{\circ}(q,\omega)$ is even in ω while its imaginary part is odd. The spectral density is

$$A(q,\omega) = 2\, Im\, \chi(q,\omega)$$

$$= \frac{2\, Im\, \chi^{\circ}(q,\omega)}{\left(1-U Re\chi^{\circ}(q,\omega)\right)^2+\left(U Im\chi^{\circ}(q,\omega)\right)^2} \tag{3.44}$$

Hence, from (3.42) and (3.43), the spectral density is odd in ω. We can simplify the expression for $X^{\circ}(q,\omega)$ by making the substitution

$$y = \varepsilon^{\lambda}(\nu\zeta\mu) \tag{3.45}$$

in (3.37) Thus we find:

$$J^{\nu} = \frac{\gamma}{4\nu\zeta} \int_{\varepsilon^{\lambda}(-\nu\zeta)}^{\varepsilon^{\lambda}(\nu\zeta)} dy\, \frac{1}{(y-\eta)^2(\beta^{\nu}-y+i\nu\delta)} \tag{3.46}$$

Evaluating the real and imaginary parts of J^ν and substituting them into (3.36) we obtain, after some algebra:

$$Im\,\chi^\circ(q,\omega) = \sum_{\lambda'} \int_0^1 I_Q^{\lambda'} f(\varepsilon_Q^{\lambda'})\, d\varepsilon_Q \tag{3.47}$$

$$Re\,\chi^\circ(q,\omega) = \sum_{\lambda'} \int_0^1 R_Q^{\lambda'} f(\varepsilon_Q^{\lambda'})\, d\varepsilon_Q \tag{3.48}$$

where

$$I_Q^{\lambda'} = \frac{3\pi\gamma Z_Q^{\lambda'}}{32 q} \sum_\nu \frac{\nu\,\theta^\nu}{(\beta^\nu-\eta)^2} \tag{3.49}$$

with

$$\theta^\nu = 1 \quad for \prod_{\nu'\lambda'} (\beta^\nu - \varepsilon^{\lambda'}(\nu'\zeta)) < 0$$

$$= 0 \quad otherwise \tag{3.50}$$

and

$$R_Q^{\lambda'} = \frac{-3\gamma Z_Q^{\lambda'}}{32 q} \sum_\nu \phi^\nu \tag{3.51}$$

with

$$\phi^\nu = \frac{8\zeta}{\gamma(\beta^\nu-\eta)} + \frac{1}{(\beta^\nu-\eta)^2} \ln \left| \frac{(\varepsilon^+(-\zeta)-\beta^\nu)(\varepsilon^-(-\zeta)-\beta^\nu)}{(\varepsilon^+(\zeta)-\beta^\nu)(\varepsilon^-(\zeta)-\beta^\nu)} \right| \tag{3.52}$$

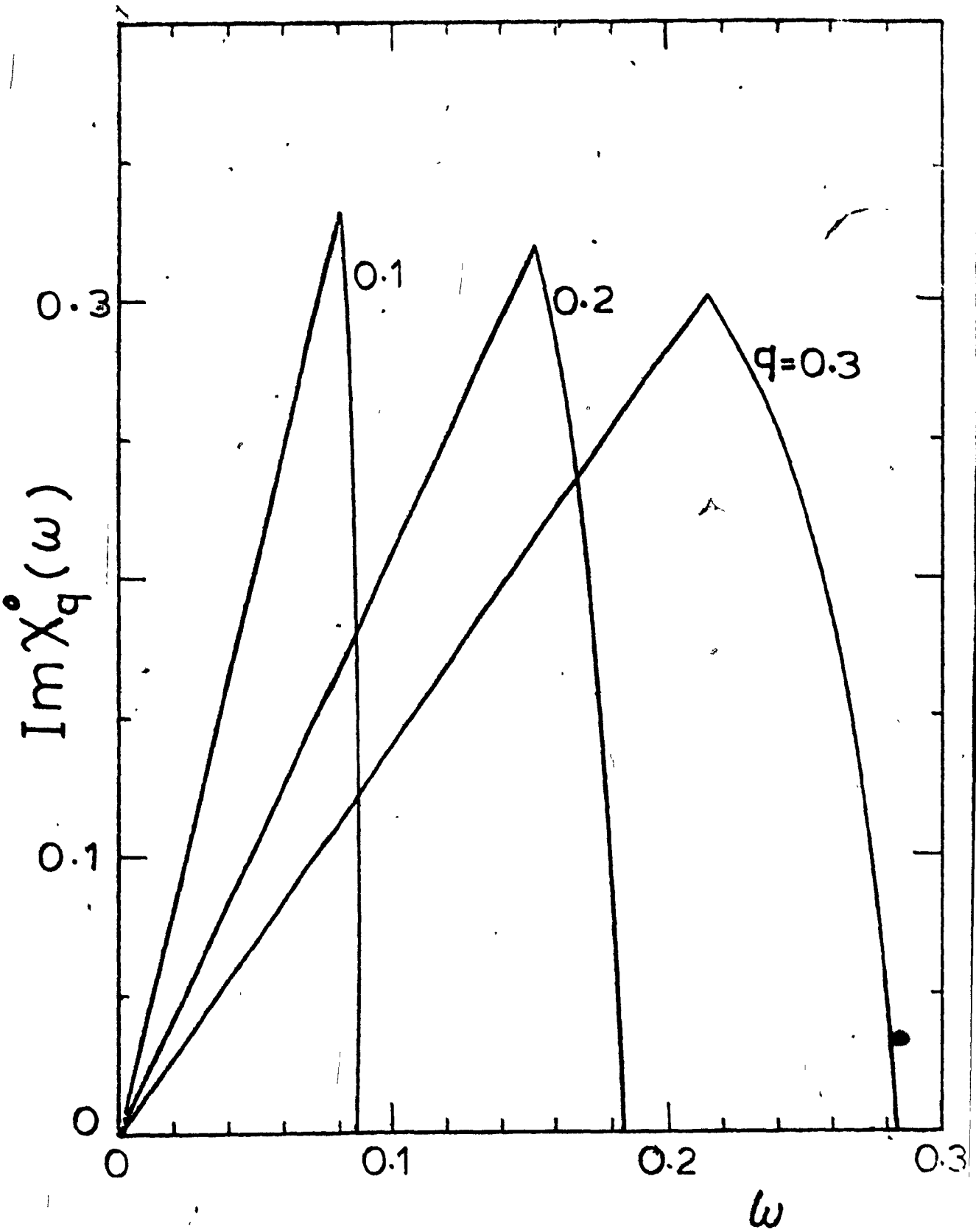

Figure 3.8
The imaginary part of the unenhanced susceptibility in the narrow band model for V=1.0, U=2.7 and $\epsilon=E_{dg} - \epsilon_F = 1.3$. All energies are normalized to ϵ_s (equation (1.45)).

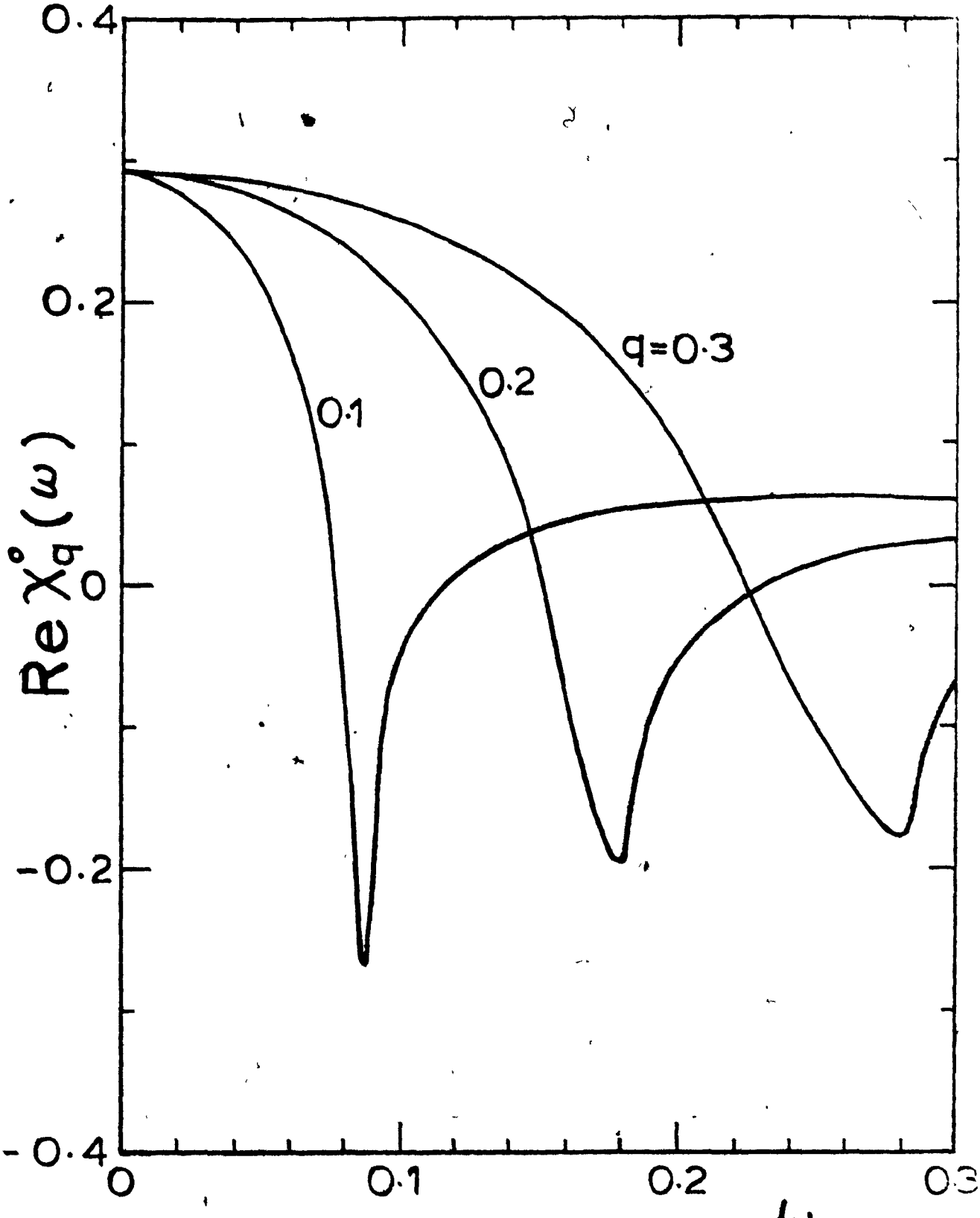

Figure 3.9
The real part of the unenhanced susceptibility in the narrow band model for V = 1.0, U = 2.7 and $\epsilon = E_{d\sigma} - \epsilon_F = 1.3$. All energies are normalized to ϵ_s (equation (1.43)).

Figure 3.10

The spectral density for spin fluctuations in the narrow band model for $V = 1.0$, $U = 2.7$ and $\epsilon = E_{d\sigma} - \epsilon_F = 1.3$. All energies are normalized to ϵ_s (equation (1.43)).

Figure 3.10

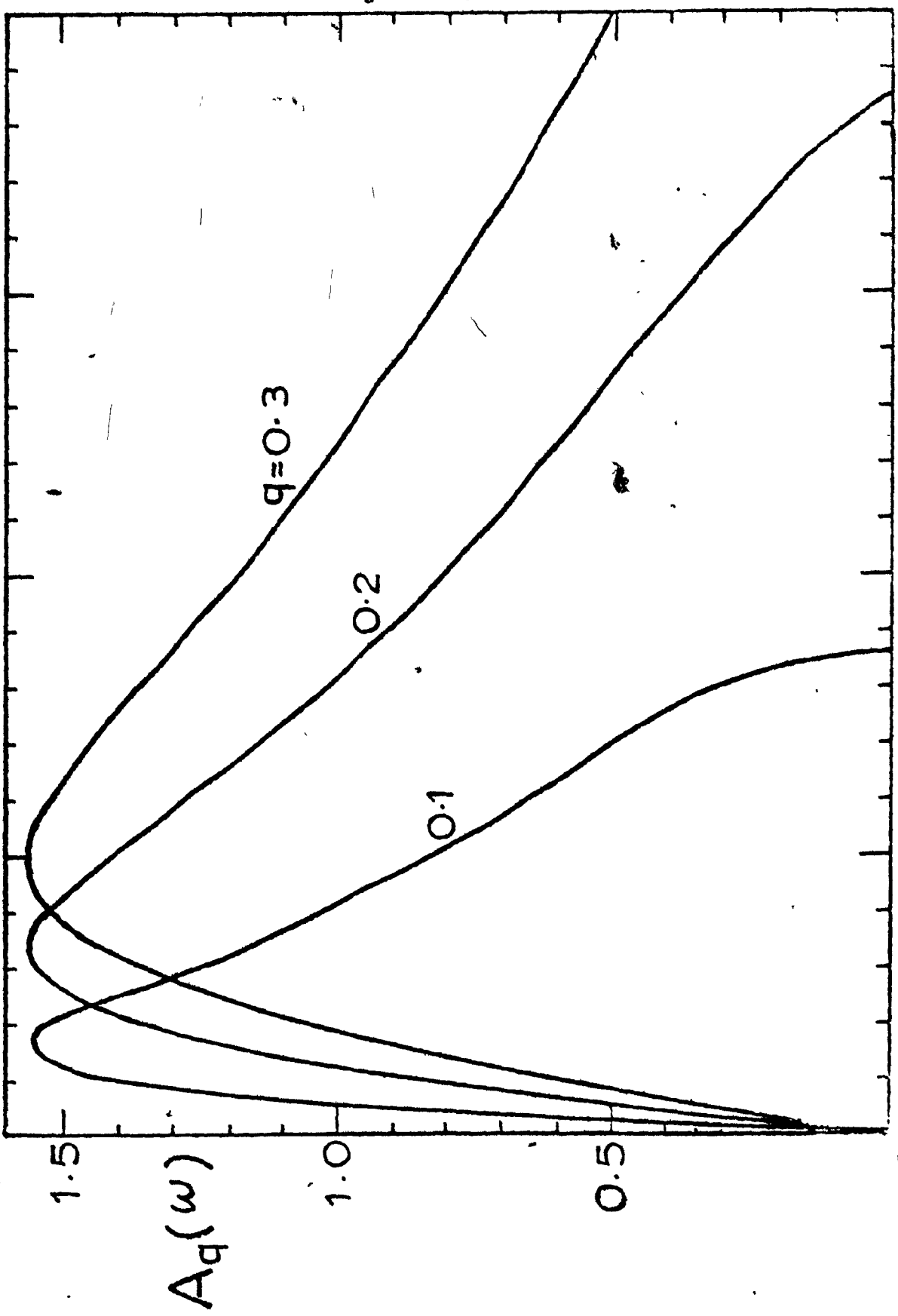

To see the behaviour of the dynamic susceptibility and the spectral density we have again performed model calculations and as an illustration we give here the results of one set of such calculations. The parameters we chose were V=1.0 and U=2.7 (all energies normalized to ϵ_s). Another important parameter is the separation of the d-level from the Fermi level. We label this ϵ and we have

$$\epsilon = E_{d\sigma} - \epsilon_F \qquad (3.53)$$

The results for ϵ=1.3 are shown in Figure 3.8 to Figure 3.10. In Figure 3.8 we have plotted the imaginary part of $X^\circ(q,\omega)$ as a function of ω for various values of q. For each q, Im $X^\circ(q,\omega)$ starts off linearly with ω and then drops off sharply to zero. Figure 3.9 shows the real part of $X^\circ(q,\omega)$ as a function of ω. We note that for very small values of ω, Re $X^\circ(q,\omega)$ varies slowly with ω. Finally in Figure 3.10 we plot the spectral density $A(q,\omega)$ as a function of ω. As in the case of the itinerant model, $A(q,\omega)$ rises very sharply to a peak and then drops off to zero.

For small ω, the imaginary part of $X^\circ(q,\omega)$ has the following form:

$$Im\ \chi^\circ(q,\omega) = \xi \frac{\omega}{q} \qquad (3.54)$$

where ξ is a real constant. Also, for small ω, we may use the following approximation for the real part of $\chi^\circ(q,\omega)$

$$Re\ \chi^\circ(q,\omega) = \chi^\circ_s \qquad (3.55)$$

where $\chi^\circ_s = \chi^\circ(0,0)$ is the static susceptibility. Under these conditions the poles of the dynamic susceptibility are given by

$$\omega = \pm i\, \omega_{SF}(q) \qquad (3.56)$$

From (3.55), (3.54) and (3.32) we have

$$\omega_{SF}(q) = \frac{(1 - U\chi^\circ_s)}{U\xi}\, q \qquad (3.57)$$

Again, from equation (3.56) we note that the excitations are critically damped spin fluctuations and the dispersion relation for these excitations is given by (3.57).

With the above approximations the spectral density becomes

$$A(q,\omega) = \frac{2\xi_s^2\, q}{U^2 \xi\, q_s} \cdot \frac{\omega}{\omega_{SF}^2(q) + \omega^2} \qquad (3.58)$$

Hence the average spectral density that appears in the expression for the resistivity (equation (3.16)) is

$$\bar{A}(\omega) \simeq \frac{2\xi_s^2 \omega}{U^2 \Xi q_s k_F^4} \int_0^{2k_F} dq \, \frac{|F(q)|^2 q^4}{\omega_{SF}^2(q) + \omega^2} \qquad (3.59)$$

The main q-dependence of the integrand in (3.59) comes from the q^4 term and we therefore make the simplifying assumption of replacing $\omega_{SF}(q)$ by an appropriate average value. We take its value at q_s and introduce a characteristic spin fluctuation frequency ω_{SF}:

$$\omega_{SF} = \omega_{SF}(q_s) \qquad (3.60)$$

Substituting this into (3.59) we find

$$\bar{A}(\omega) = B \frac{\omega}{\omega_{SF}^2 + \omega^2} \qquad (3.61)$$

where

$$B = \frac{2\xi_s^2}{U^2 \Xi q_s k_F^4} \int_0^{2k_F} dq \, |F(q)|^2 q^4 \qquad (3.62)$$

Thus the averaged spectral density has the same form as in the localized spin fluctuation model of Kaiser and Doniach. Hence the universal curve given by equation (3.27) and shown

in Figure 3.4 applies in the narrow band model too. The scaling factors for $\tilde{\rho}$ and $\tilde{T}$ in the narrow band model are, however, given by different expressions. From (3.57) and (3.60), and defining T_{SF} as before (equation (3.25)), we have for this model

$$K_B T_{SF} = \frac{\xi_s^2}{U \xi S} \qquad (3.63)$$

where S is the Stoner enhancement factor

$$S = \frac{1}{1 - U \chi_s^0} \qquad (3.64)$$

As the temperature increases S decreases and hence (neglecting the temperature dependence of ξ) T_{SF} increases and ρ_{SF} remains unchanged. This behaviour is similar to the localized spin fluctuation model and thus we expect the resistivity in the narrow band model to deviate from the universal curve in a manner similar to Figure 3.6.

Chapter IV

Applications of the narrow band model

We now examine possible applications of the narrow band model described in the previous chapters. Because of the idealized nature of the model we can only make qualitative comparison of the basic features of the model with experiment. In particular, we will discuss two cases: magnetic properties of Heusler alloys and the effects of pressure on the magnetic properties of α-Ce.

4.1 Heusler alloys

The magnetic moment on Mn atoms in the non-cobalt Heusler alloys is of the order of 4 Bohr magnetons. Because we assumed in our model that the localized level is non-degenerate the maximum magnetization that can result from the spin splitting of such a level is 1. Thus, in order to compare experiment with the results of the model calculations of Chapter I we take 1/5 of the magnetic moment (the degeneracy of the d-level of Mn is 5) i.e. 0.8 Bohr magnetons. From Figure 1.8 we see that for a magnetization of 0.8 we need a value of U of the order of 0.65. With this value of U the Curie temperature given in Figure 1.9 is of the order of 0.054. These are given in units of energy that are normalized to ε_s i.e. if T_c is the Curie temperature in degree K then

$$k_B T_c = 0.054\, \varepsilon_s \qquad (4.1)$$

where k_B is the Boltzmann constant. Since ϵ_s is of the order of 4eV we find that T_c is of the order of 2500K. This value of T_c is at least 4 times greater than any of the non-cobalt alloys listed on page 6 . To obtain an improvement in these results we must perform more realistic calculations. Such calculations have to take into account the band structure of these alloys, the degeneracy of the d-level and the exchange effects on the Mn atoms. This is a complex problem and we do not attempt it here. Instead, we discuss in Chapter V, a different model which gives good fits to both the magnetization and Curie temperature in the Heusler alloys.

Finally, it is interesting to examine the results of the spin wave calculations of Chapter II. From Figure 2.5b we see that for a magnetization of 0.25, $(D/\hbar^2/2m) \sim 0.12$. Putting in values of $\hbar$ and m we find D ~450 meV Å ^{2}. Evidence of spin waves in the Heusler alloys is found indirectly in nuclear magnetic resonance experiments and directly from inelastic neutron scattering experiments. Sugibuchi and Endo[1](1964) report that the nuclear magnetic resonance lines and magnetization follow a $T^{3/2}$ law in Cu_2MnAl. They find the following relationship for the NMR frequency:

$$\omega(T) = \omega(0)\left(1 - AT^{3/2}\right) \qquad (4.2)$$

with

$$A \approx 2 \times 10^{-5}\ K^{-3/2}$$

Since $\omega(T)$ is directly proportional to the magnetization, this is the same constant A that appears in the Bloch $T^{3/2}$ law. Equation (2.16) can be rewritten as

$$M(T) = M(0)\left(1 - \tilde{A}\left(\frac{k_B T}{D}\right)^{3/2}\right) \qquad (4.3)$$

with

$$\tilde{A} = \frac{g\mu_B \zeta(3/2)}{M(0)\,(4\pi)^{3/2}} = \frac{0.0587}{(NS/V)}$$

Hence

$$A = \frac{0.0587}{(NS/V)}\left(\frac{k_B}{D}\right)^{3/2}$$

and

$$D = \left(\frac{0.0587V}{NSA}\right)^{2/3} k_B$$

For Cu_2MnAl, $(V/N) = 2a_0^3$ where $2a_0 = 5.95$ and $S \sim 4$ giving

$$D \sim 100\ meV\ \mathring{A}^2$$

The dispersion relation for spin waves in Pd_2MnSn was studied by Ishikawa and Noda (1973) by the neutron inelastic scattering method. These authors also find a value of D of about 100 meV $\mathring{A}^2$ for this alloy. The order of magnitude of the results of the narrow band model are thus consistent with experimental values.

4.2 Pressure effects in α-Ce

The localized f-level in the rare-earth metal cerium also hybridizes with the conduction band. Hence the narrow

band model is appropriate here too. The position of the f-level in cerium changes with pressure leading to dramatic changes in its magnetic properties. The most striking feature is the change in the spin fluctuation resistivity with pressure in the paramagnetic phase of cerium. In this section we show that these results can be explained in the narrow band model by extending the calculations of Chapter III and investigating the effect of a shift in the position of the localized level on spin fluctuations. Before we do this we give a brief description of the main experimental results.

The change in the magnetic properties of cerium with pressure is illustrated by its pressure-temperature phase-diagram shown in Figure 4.1. The β and γ phases have net magnetic moments but we concentrate here only on the paramagnetic α-phase. In the α-phase Cerium is a Pauli paramagnet with a strong local exchange enhancement which decreases with increasing pressure (MacPherson et al (1971)). Furthermore, the resistivity data of Katzman and Mydosh (1972) shows a spin fluctuation contribution which decreases with pressure as shown in Figure 4.2. Apart from a residual value which is non-spin fluctuation in origin, the resistivity curves of Figure 4.2a strongly resemble those of Figures 3.4 and 3.6. For all pressures, the resistivity varies as T^2 at low temperatures and changes to a linear law at higher temperatures. As the temperature increases further, the resistivity deviates below the linear law. We also note that as the pressure increases the resistivity decreases.

The T^2 law is more clearly seen in Figure 4.2b, where the

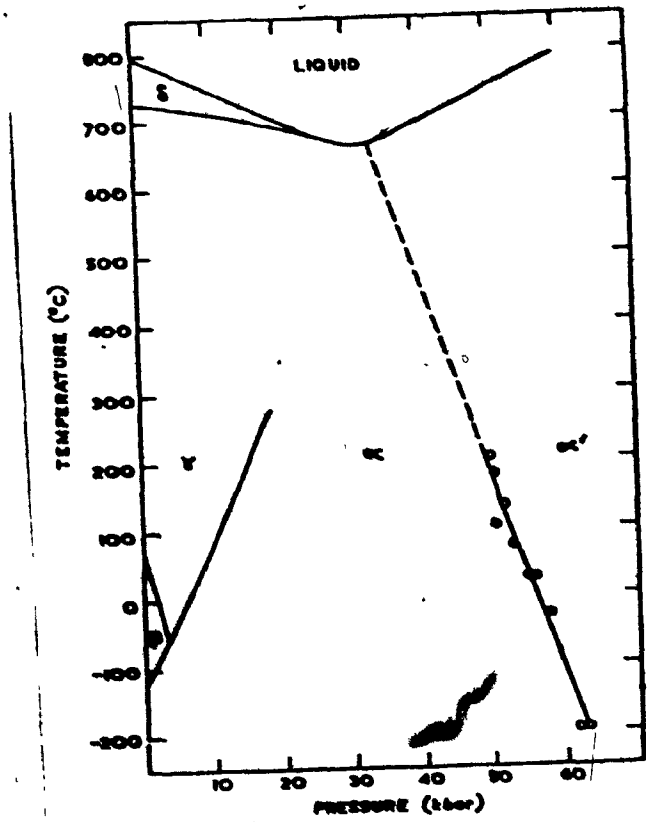

Figure 4.1

Phase diagram for cerium (after King et al (1970)).

resistivity is plotted as a function of T^2 . Thus the low temperature resistivity has the form

$$\rho(T) = \rho_0 + a T^2 \qquad (4.4)$$

where ρ_0 is the residual resistivity. The coefficient a as a function of pressure is shown in Figure 4.3. Also shown in this figure is the experimentally determined spin fluctuation temperature T_{SF} as a function of pressure (from equations (3.28) and (3.29) $T_{SF} = \frac{2}{3}\pi b/a$ where b is the slope of the linear part of the resistivity curve). We see that as the pressure increases a decreases while T_{SF} increases.

In the virtual bound state model the pressure effects in α-Ce can be explained in terms of an upward shift of the f-level away from the Fermi level as pressure increases (Coqblin (1971)). However, this model is oversimplified since the Ce atoms are treated as independent of each other. In this respect the narrow band model is more suitable. However, following Coqblin, we must also assume in the narrow band model that as pressure increases the f-level moves upwards away from the Fermi level i.e. ε(given by (3.53)) increases. To simulate pressure effects we have evaluated the dynamic susceptibility for various values of ε and these are shown in Figures 4.4 to 4.6. As seen in Figure 4.6 the spin fluctuation spectral function increases as ε decreases i.e. as pressure decreases and this will result in an increase in spin fluctuation resistivity as

is found experimentally. To investigate this further we plot in Figure 4.7 T_{SF} given by (3.63) and the coefficient a of the T^2 term given by (3.28) as a function of ϵ. The qualitative features of these plots are in agreement with the experimental curves of Figure 4.3. Also shown in Figure 4.7 is the Stoner enhancement factor S which decreases with ϵ or pressure in agreement with the susceptibility measurements of MacPherson et al (1971). We conclude that the narrow band model gives a fairly good qualitative description of the pressure effects in α-Ce (Bahurmuz and Zuckermann (1974)).

The model described in section 1.2 has been used by a number of authors. Ratto et al (1969)incorporated this model in a theory to explain the pressure dependence of the superconducting transition temperature of lanthanum and the presence of a superconducting high pressure phase in cerium. Kishore and Joshi (1970) obtained the conditions for ferromagnetism, for zero and finite width of the d-band, as a function of the widths of both the conduction and d-bands. This was extended by Jullien and Coqblin (1973), who included a variable hybridization, to explain the magnetism of actinide metals. Daniel (1971) used this model to discuss spin polarization and hyperfine fields in Heusler alloys.

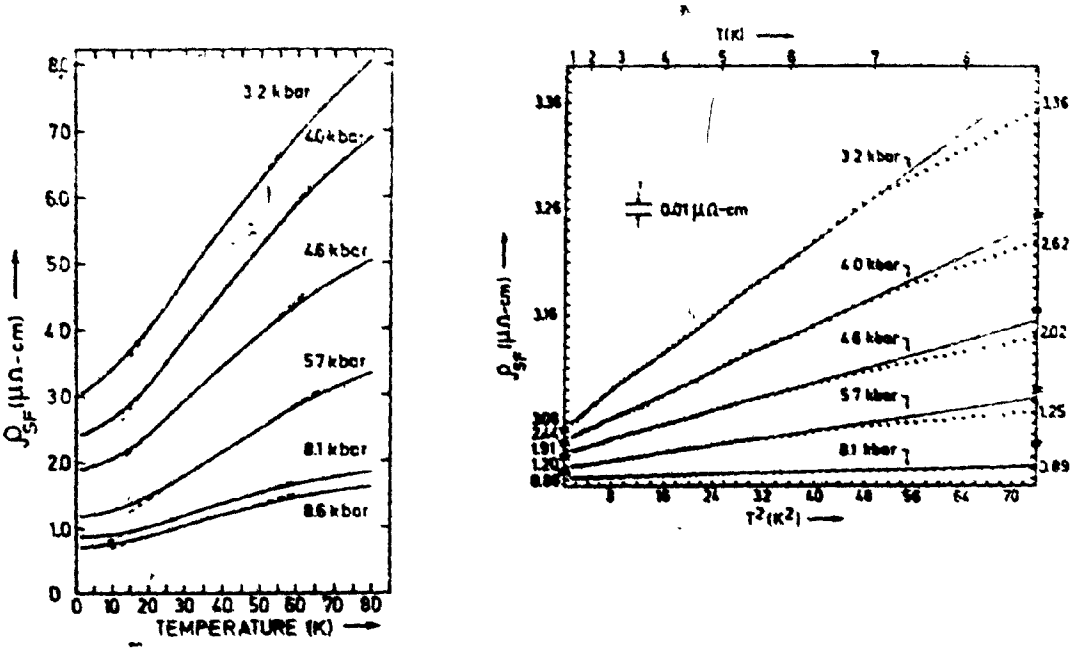

Figure 4.2

Spin fluctuation resistivity in α-Ce as a function of temperature and pressure (after Katzman and Mydosh (1972)).

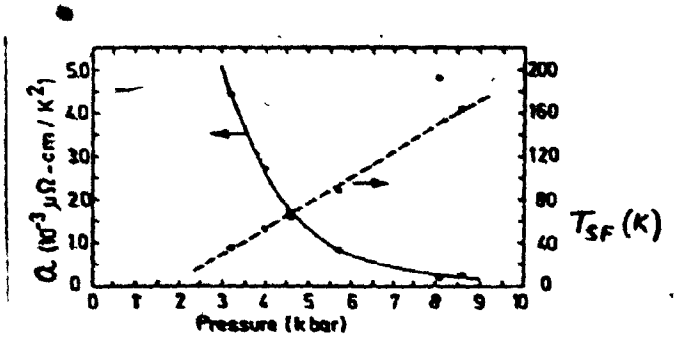

Figure 4.3

The T^2 coefficient (a) and the spin fluctuation temperature (T_{SF}) versus pressure in α-Ce (after Katzman and Mydosh).

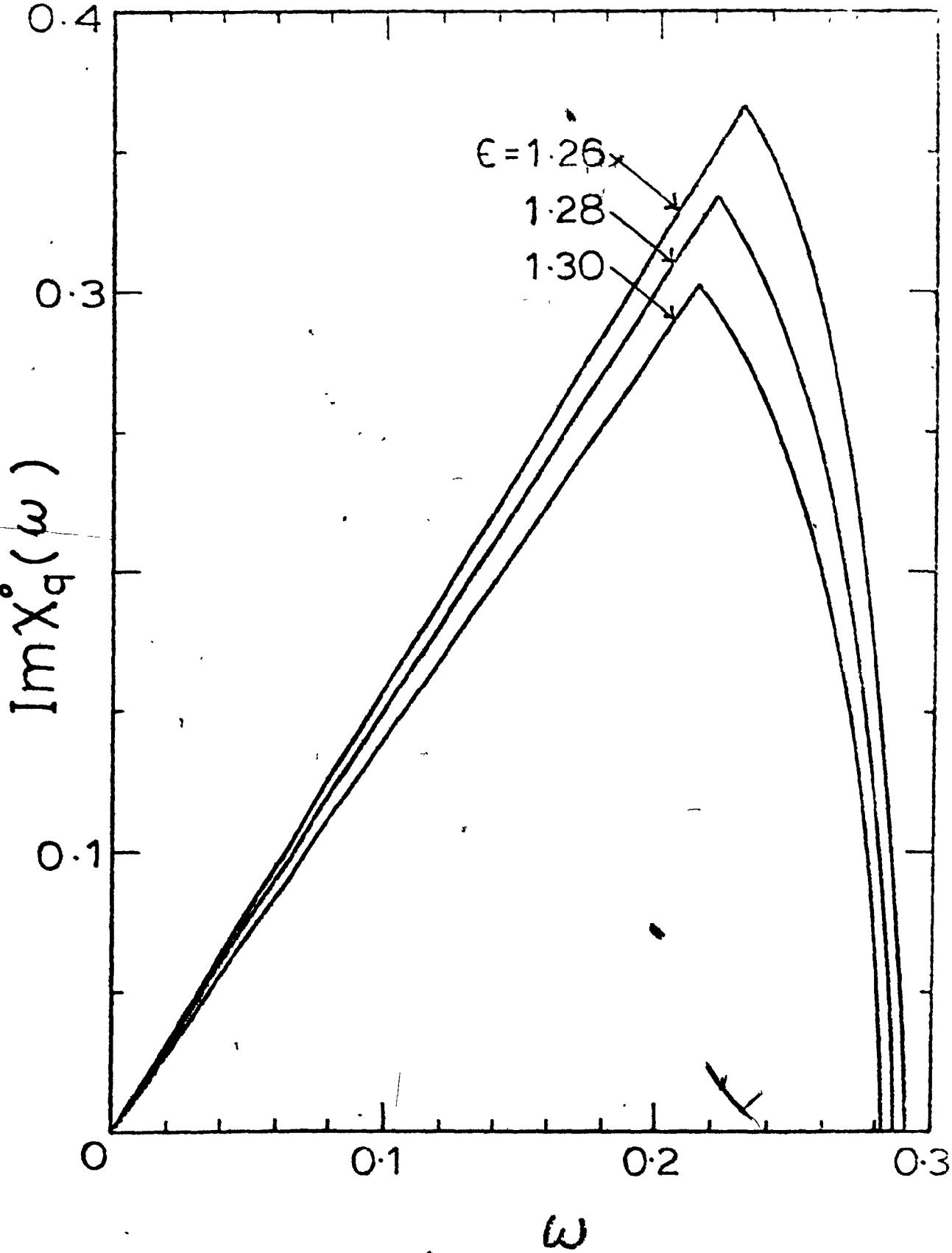

Figure 4.4

Imaginary part of the unenhanced susceptibility for V = 1.0, U = 2.7 and 3 values of $\epsilon = E_{d\sigma} - \epsilon_F$. All energies are normalized to ϵ_s (equation (1.43)).

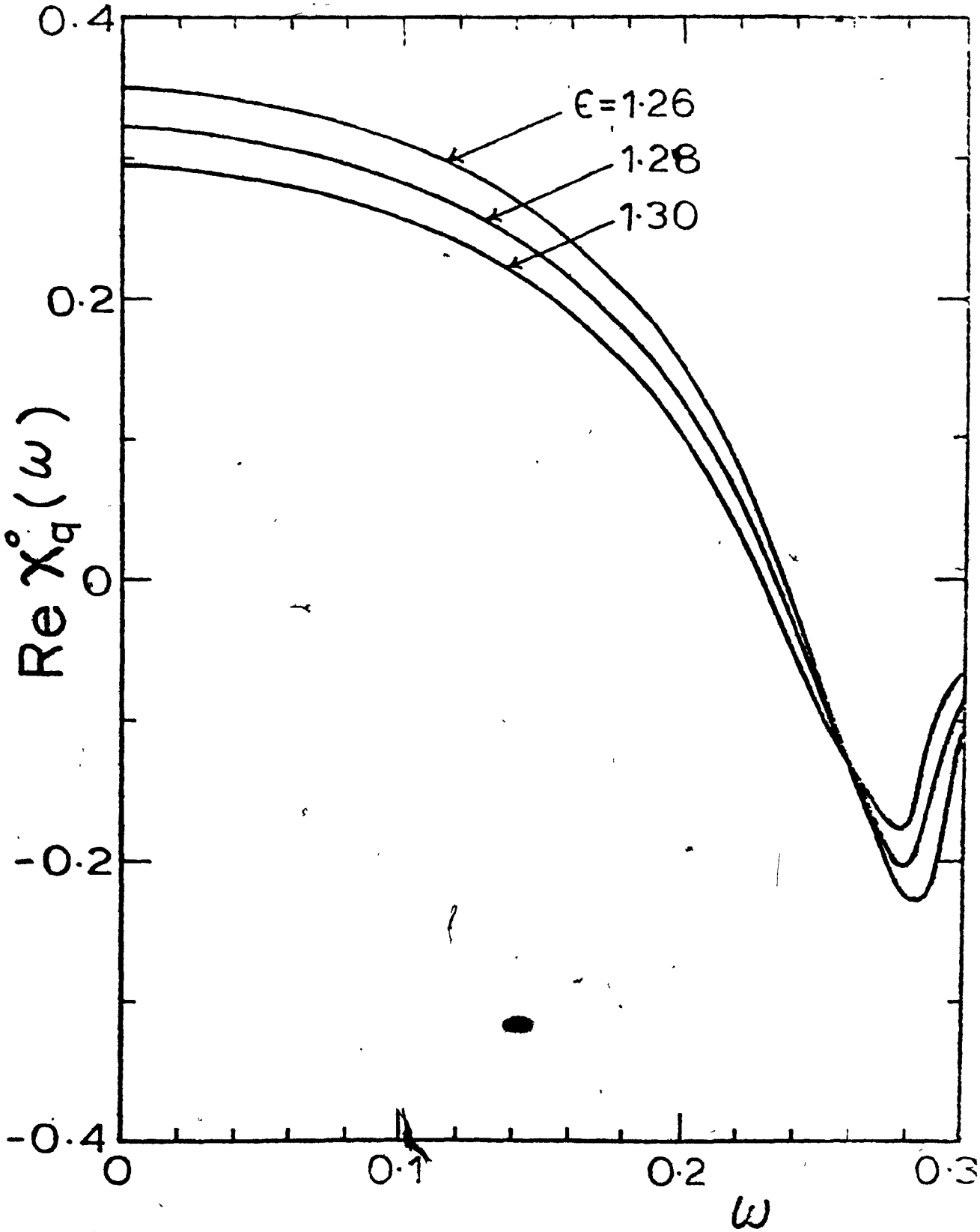

Figure 4.5
Real part of the unenhanced susceptibility for V=1.0, U=2.7 and 3 values of $\varepsilon = E_{d\sigma} - \varepsilon_F$. All energies are normalized to ε_s (equation (1.43)).

Figure 4.6

The spectral density for spin fluctuations for V = 1.0, U = 2.7 and $\varepsilon = E_{d\sigma} - \varepsilon_F$. All energies are normalized to ε_s (equation (1.43)).

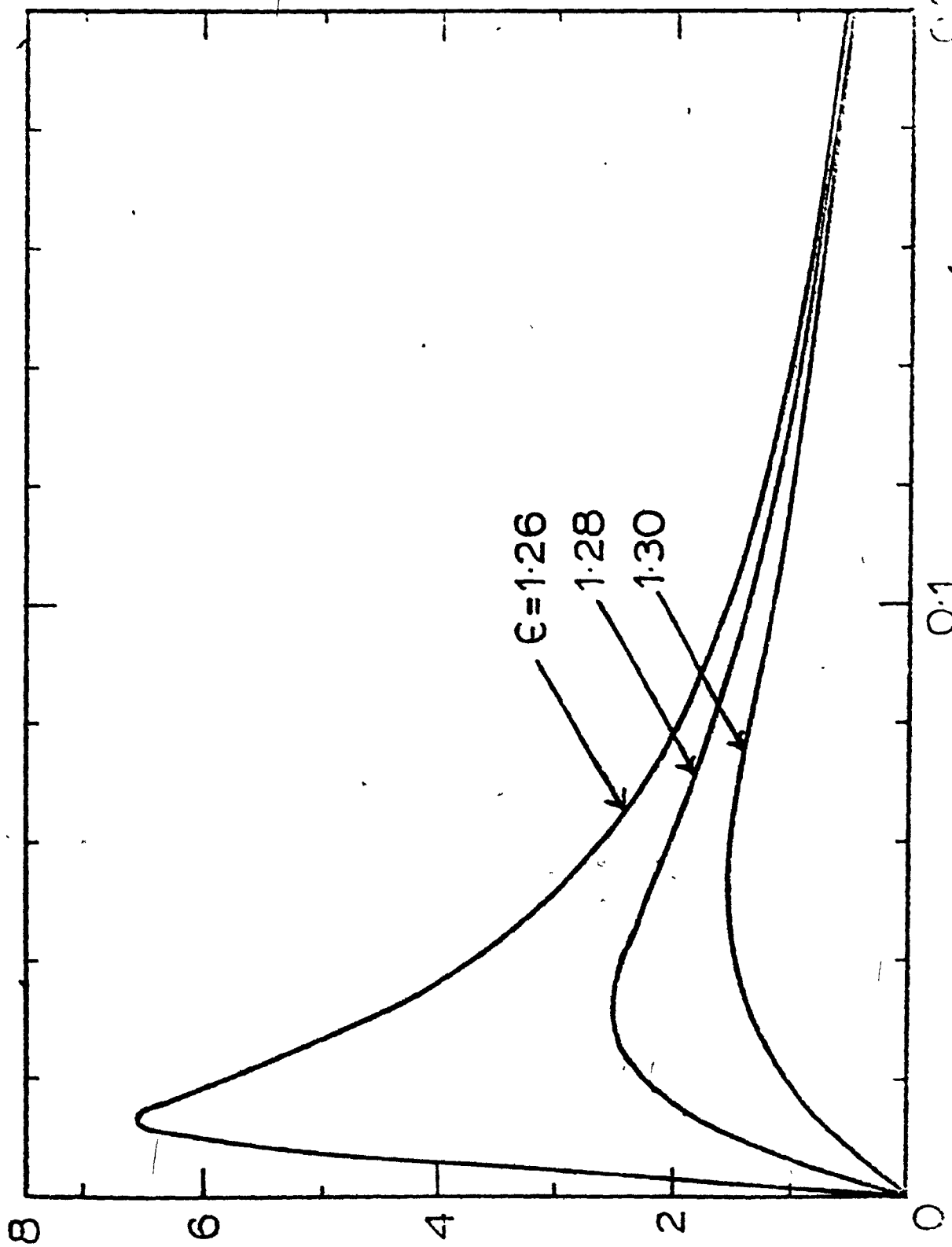

Figure 4.6

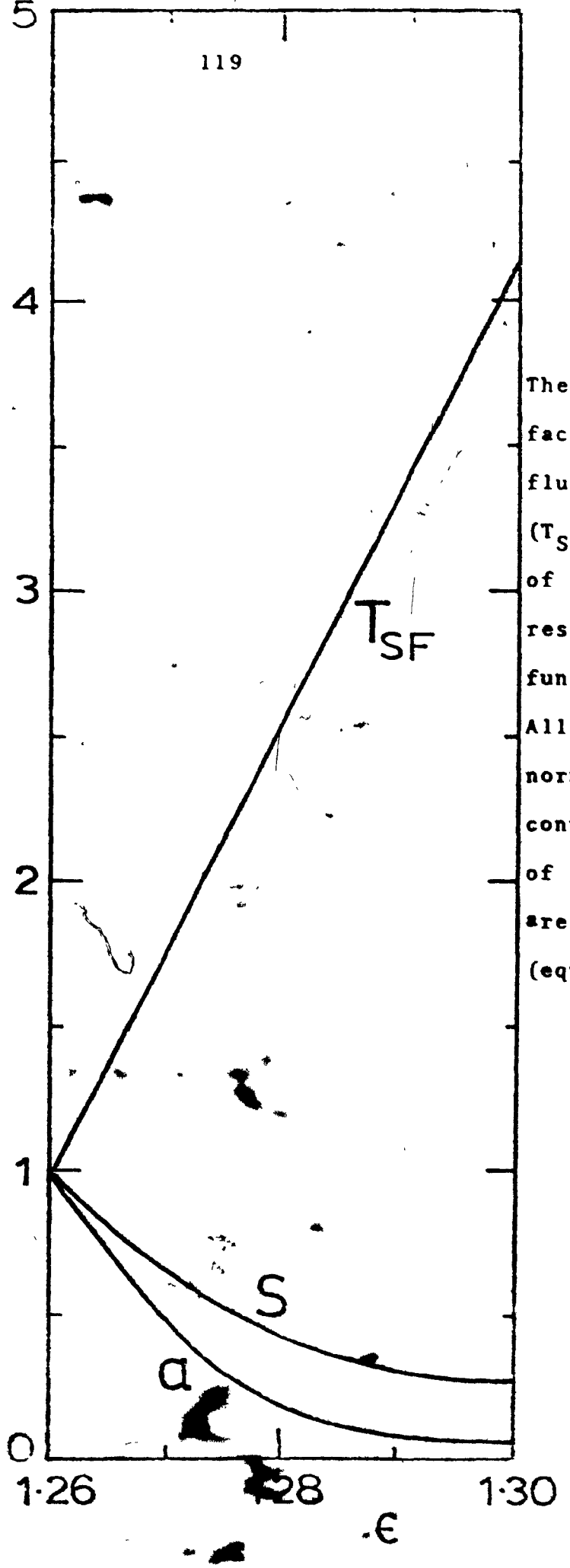

Figure 4.7

The Stoner enhancement factor (S), the spin fluctuation temperature (T_{SF}) and the coefficient of the T^2 term in the resistivity (a) as a function of $\varepsilon = E_{d\sigma} - \varepsilon_F$ All values are normalized, for convenience, to those of $\varepsilon = 1.26$. All energies are normalized to ε_s (equation (1.43)).

Chapter V

The double resonance theory

The Curie temperatures for the Heusler alloys predicted by the narrow band model of Chapter I were found to be too high compared to the experimental values. Hence, in this chapter we examine an alternative model for the Heusler alloys which gives a better fit to their Curie temperatures.

One of the more successful theories for the Heusler alloys is the double resonance theory of Caroli (1967). In this theory the interaction between the magnetic moments of two transition atoms, e.g. Mn, dissolved in a normal metal such as Cu is considered. However, the interaction energy in this model is derived in the limit of very large separation of the two impurities and this is not a good approximation for concentrated alloys or intermetallic compounds such as the Heusler alloys. In the limit of large separation, the interaction energy in this model varies as $1/R^3$ where R is the distance between the magnetic atoms. In this chapter we derive the next correction term to the interaction energy which is of the order $1/R^4$ and show that it gives a better fit to the Heusler alloys than the first approximation of Caroli. In section 5.1 we examine briefly the Caroli model and then in section 5.2 discuss the extension of this model and investigate its consequences.

5.1 The Caroli model

Caroli (1967) has discussed the problem of interaction between two impurity atoms in the framework of the Anderson model. The Hamiltonian considered is a generalization of (1.1) to the case of 2 impurities:

$$H = \sum_{\underline{k}\sigma} \varepsilon_{\underline{k}} C^{\dagger}_{\underline{k}\sigma} C_{\underline{k}\sigma} + \sum_{i\sigma} E_{di} C^{\dagger}_{di\sigma} C_{di\sigma} + \sum_{i} U n_{di\uparrow} n_{di\downarrow} + \sum_{\underline{k}i\sigma} \left(V_{\underline{k}di} C^{\dagger}_{\underline{k}\sigma} C_{di\sigma} + V_{di\underline{k}} C^{\dagger}_{di\sigma} C_{\underline{k}\sigma} \right) \quad (5.1)$$

where i refers to impurities 1 and 2. The mechanism of interaction can be qualitatively explained as follows: the first impurity scatters an electron of spin σ and wavevector $\underline{k}$ and thus the wavefunction for large r is :

$$\psi_{\underline{k}\sigma}(\underline{r}) \simeq e^{i\underline{k}\cdot\underline{r}} + \frac{e^{ikr}}{kr} e^{i\delta^{\sigma}} \sin\delta^{\sigma}$$

where δ^{σ} is the phase shift. The electron is then scattered by the second impurity and the problem can be treated in the original Anderson fashion by replacing the matrix element $V_{\underline{k}d_2}$ by:

$$\langle \psi_{\underline{k}\sigma} | V_2 | d \rangle = V_{\underline{k}d_2} \left(e^{i\underline{k}\cdot\underline{r}} + \frac{e^{ikr}}{kr} e^{i\delta^{\sigma}} \sin\delta^{\sigma} \right)$$

where R is the distance between the two impurities. The Green's function for the second impurity is thus modified and Caroli finds that

$$G_{d_2\sigma}(\omega) = \frac{1}{\pi} \cdot \frac{1}{\omega - E_{d_2\sigma} - (\Gamma_2' - i\Delta_2')}$$

where

$$\Gamma_2' - i\Delta_2' = \Gamma_2 - i\Delta_2 - \Delta_2 \sin\delta^{\sigma} \frac{e^{i(2kR+\delta^{\sigma})}}{(kR)^2}$$

with Γ_2 and Δ_2 being respectively the shift and width of the isolated second impurity. Due to the presence of the first impurity, the effective shift Γ_2' and width Δ_2' of the second impurity are modified. This creates a variation of the number of electrons on the second impurity and consequently to a coupling between the two impurities. It is obvious that the problem has to be treated self-consistently but it exhibits clearly the mechanisms of interaction. Caroli has shown that for two magnetic impurities, the interaction energy can be written in terms of a coupling between their moments just as in the Heisenberg Hamiltonian. Thus, if $\underline{S}_1$ and $\underline{S}_2$ are the spins of the two impurities, then the interaction Hamiltonian has the form

$$H = \frac{J(R)}{S^2} \; \underline{S}_1 \cdot \underline{S}_2 \qquad (5.2)$$

where

$$J(R) = \sum_{\sigma\sigma'} \frac{1}{2} \sigma\sigma' E^{\sigma\sigma'}(R) \qquad (5.3)$$

and $E^{\sigma\sigma'}(R)$ is given, in the limit of large separation, by the following expression

$$E^{\sigma\sigma'}(R) = \frac{25\,\epsilon_F \sin\delta^{\sigma} \sin\delta^{\sigma'}}{\pi} \frac{\cos(2k_F R + \delta^{\sigma} + \delta^{\sigma'})}{(k_F R)^3} \qquad (5.4)$$

where the phase shift δ^{σ} is given in terms of $N_{d\sigma}$, the number of electrons of spin σ in the d-states, by Friedel's theorem:

$$\delta^{\sigma} = \frac{\pi}{5} \cdot N_{d\sigma} \qquad (5.5)$$

Before we apply these results to the Heusler alloys we note that the interaction energy J(R) in this model has a form similar to the RKKY interaction (equation (4.1)).

In the molecular-field approximation the paramagnetic Curie temperature resulting from (5.2) is

$$T_c = -\frac{1}{3k_B} \sum_R J(R) \qquad (5.6)$$

We consider first the alloy Cu_2MnAl: the number of sp electrons contributed to the conduction band by each Cu and Al atom is 1 and 3 respectively. Mn has 7 electrons in its outer s and d shells and if $N_{d\uparrow}$ and $N_{d\downarrow}$ are the number of spin up and spin down electrons in the d-state then the number contributed to the conduction band is $7-N_{d\uparrow}-N_{d\downarrow}$. Thus the number of conduction electrons per Mn atom is $12-N_{d\uparrow}-N_{d\downarrow}$ and knowing the volume per Mn atom the conduction electron concentration, and consequently ϵ_F and k_F, can be found. Also

knowing $N_{d\uparrow}$ and $N_{d\downarrow}$ fixes the magnetization i.e. we have

$$M_d = N_{d\uparrow} - N_{d\downarrow} \qquad (5.7)$$

where M_d is the magnetic moment in Bohr magnetons. Because of the oscillatory nature of J(R) the sum in (5.6) converges very slowly and we needed to sum over 300 shells to obtain good convergence. The resultant Curie temperatures are shown in Figure 5.1 as a function of magnetization for various values of $N_{d\uparrow}$. For a given value of $N_{d\uparrow}$ the Curie temperature is very sensitive to the value of the magnetization because of the phase factors in (5.4). We note that for the value of the magnetization given in the table on page 6 (M_d=3.8) the maximum value of T_c is $\sim$ 500K and this is in good agreement with the experimental value of 600K. However, for the other alloys the agreement is poor e.g. for the ferromagnetic alloys Pd_2MnSn and Pd_2MnSb the Caroli theory predicts negative Curie temperatures.

5.2 Extension of the Caroli model

The expression for the interaction energy (equation (5.4)) is only valid in the limit $R\to\infty$. This is expected to be a good approximation for dilute alloys but in concentrated alloys like the Heusler alloys it is a poor approximation. We need to consider the next term in (5.4) which will be of order $1/R^4$. To do this we start with the following expression for the

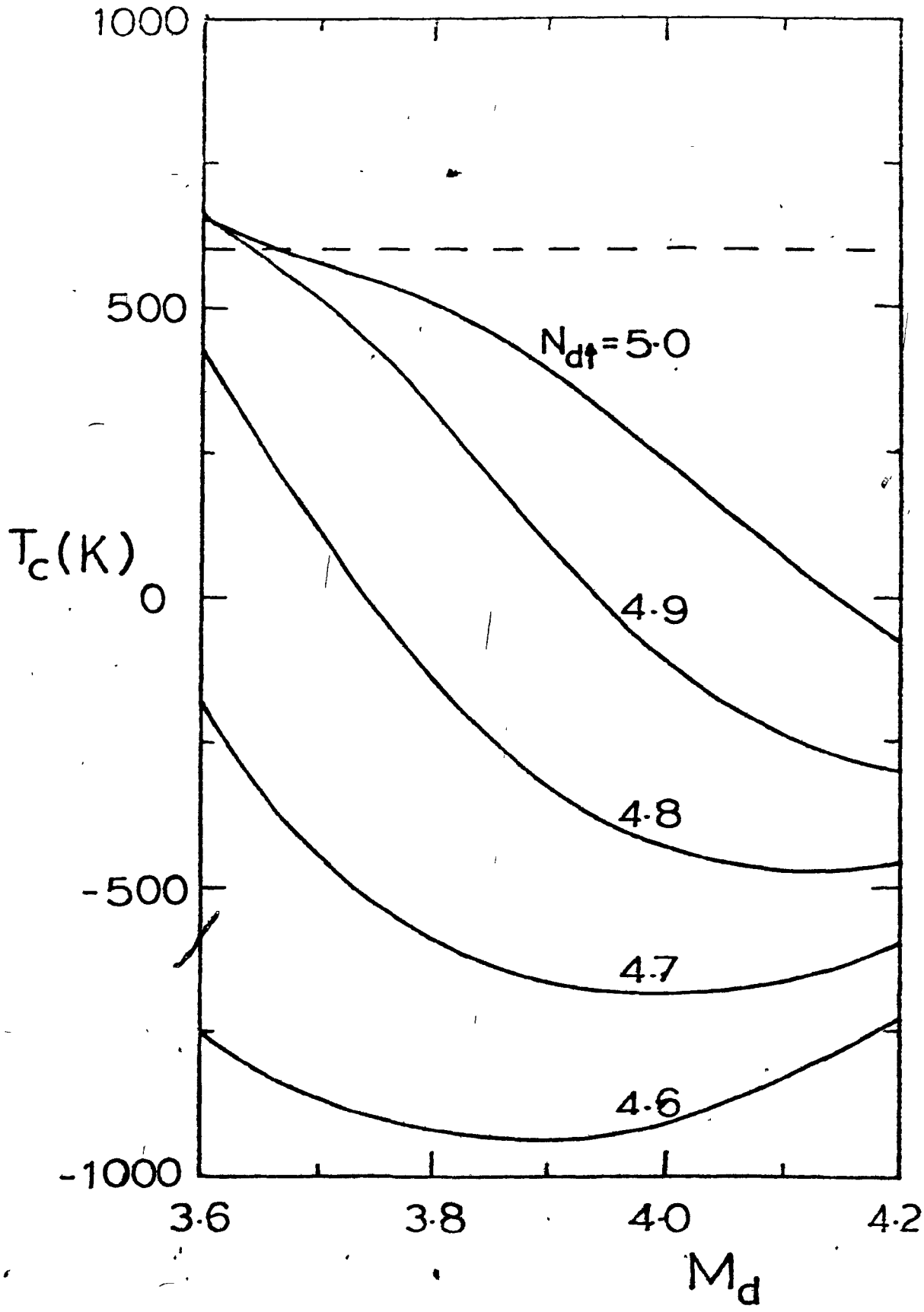

Figure 5.1
Theoretical curves of the Curie temperature in the Caroli model (equations (5.6) and (5.4)) for Cu_2MnAl. The broken horizontal line is the experimental value of the Curie temperature.

interaction energy (Caroli (1967)):

$$E^{\sigma\sigma'}(R) = \frac{1}{\pi} \mathrm{Im} \int_0^{\varepsilon_F} G^{\sigma}_{od}(\varepsilon)\, F(\varepsilon,R)\, G^{\sigma'}_{od}(\varepsilon)\, d\varepsilon \qquad (5.8)$$

where $G^{\sigma}_{od}(\varepsilon)$ is the isolated impurity Green's function

$$G^{\sigma}_{od}(\varepsilon) = \frac{1}{\varepsilon - E_{d\sigma} + i\Delta} \qquad (5.9)$$

and $F(\varepsilon,R)$ is given by

$$F(\varepsilon,R) = \sum_{\underline{k}} \frac{V_{\underline{k}d_2} V_{d_1\underline{k}}}{\varepsilon - \varepsilon_{\underline{k}} + i\delta} \sum_{\underline{k}} \frac{V_{\underline{k}d_1} V_{d_2\underline{k}}}{\varepsilon - \varepsilon_{\underline{k}} + i\delta}$$

It is shown in appendix B that for a five-fold degenerate d-orbital F is given by

$$F(\varepsilon,R) = 25\, \Delta^2(\varepsilon)\, \frac{e^{i2kR}}{(kR)^2}\, A(kR). \qquad (5.10)$$

where

$$\Delta(\varepsilon) = \Delta \left[\frac{(q_{sc}+\lambda)^2 + k_F^2}{(q_{sc}+\lambda)^2 + k^2} \right]^6 \left(\frac{k}{k_F} \right)^5 \qquad (5.11)$$

and

$$A(x) = \left(1 + \frac{2i}{x} - \frac{102}{x^2} - \frac{576i}{x^3} + \frac{2232}{x^4} + \frac{5940i}{x^5} - \frac{10530}{x^6} - \frac{11340i}{x^7} + \frac{5670}{x^8} \right) \qquad (5.12)$$

Substituting (5.10) and (5.9) into (5.8) and integrating by parts, keeping only terms to order $1/R^3$, we find after some algebra

$$E^{\sigma\sigma'}(R) = \frac{25\,\varepsilon_F \sin\delta^\sigma \sin\delta^{\sigma'}}{\pi\,(k_F R)^3} \mathrm{Re}\, e^{i(2k_F R + \delta^\sigma + \delta^{\sigma'})} \times \left(1 - \frac{T^{\sigma\sigma'}}{k_F R} + i\,\frac{U^{\sigma\sigma'}}{k_F R}\right) \tag{5.13}$$

where

$$T^{\sigma\sigma'} = \frac{\sin^2\delta^\sigma + \sin^2\delta^{\sigma'}}{B} \tag{5.14}$$

$$U^{\sigma\sigma'} = 16.5 - \frac{12\,k_F^2}{\left(k_F^2 + (q_{sc}+\lambda)^2\right)} + \frac{\sin 2\delta^\sigma + \sin 2\delta^{\sigma'}}{2B} \tag{5.15}$$

$$B = \Delta/\varepsilon_F \tag{5.16}$$

q_{sc} and λ are defined in appendix B. In deriving (5.13) we have expressed (5.9) in terms of the phase shifts δ^σ as (Caroli (1967))

$$G_{od}^\sigma(\varepsilon) = -\frac{\sin\delta^\sigma}{\Delta}\, e^{i\delta^\sigma} \tag{5.17}$$

Δ being the width of an isolated impurity. The value of Δ (and hence of B) is not known for the Heusler alloys and may be considered an adjustable parameter. However, for transition metal impurities in normal metals $\Delta \sim$ leV and since ε_F is one

order of magnitude greater we have taken B = 0.1 in our subsequent calculations.

We note that (5.13) can be written as a sum of two terms:

$$E^{\sigma\sigma'}(R) = E_0^{\sigma\sigma'}(R) + E_1^{\sigma\sigma'}(R) \qquad (5.18)$$

where $E_0^{\sigma\sigma'}(R)$ is Caroli's expression (equation (5.4) and $E_1^{\sigma\sigma'}(R)$ the leading correction term:

$$E_1^{\sigma\sigma'}(R) = \frac{-25\,\varepsilon_F \sin\delta^{\sigma}\sin\delta^{\sigma'}}{\pi\,(k_F R)^4}\left(T^{\sigma\sigma'}\cos(2k_F R+\delta^{\sigma}+\delta^{\sigma'}) + U^{\sigma\sigma'}\sin(2k_F R+\delta^{\sigma}+\delta^{\sigma'})\right) \qquad (5.19)$$

Substituting for $E^{\sigma\sigma'}(R)$ in (5.3) we can also write the exchange coupling J(R) as a sum of two corresponding terms

$$\bar{J}(R) = \bar{J}_0(R) + \bar{J}_1(R) \qquad (5.20)$$

$J_0(R)$ is the Caroli term (equation (5.3)) and $J_1(R)$ is the correction term

$$\bar{J}_1(R) = \sum_{\sigma\sigma'} \frac{1}{2}\sigma\sigma' E_1^{\sigma\sigma'}(R) \qquad (5.21)$$

Although $J_1(R) \sim 1/R^4$ compared to $1/R^3$ for $J_0(R)$, the combination of sine and cosine factors that appear in (5.4) and (5.19) can

make $J_1(R)$ larger than $J_o(R)$. This is illustrated in Figure 5.2a for Cu_2MnAl which shows that the interaction energy is substantially changed by the correction term. For example, the first neighbour interaction changes from a small positive value to a large negative value. This is illustrated further in Figure 5.2b where we plot the ratio J_1/J_o for the nearest neighbour distance as a function of $N_{d\uparrow}$ for Cu_2MnAl.

This figure shows that $J_1/J_o < -1$ for all possible values of $N_{d\uparrow}$ which means that the correction term changes the sign of the nearest neighbour interaction. Thus we expect the Curie temperature to be changed substantially by the new term in the interaction energy and indeed this is what is found.

In Figure 5.3 we plot the Curie temperature T_c of Cu_2MnAl resulting from the interaction energy $J(R)$ (equation (5.20)). Also shown, for comparison, is the Curie temperature T_{co} given by the Caroli term $J_o(R)$. As mentioned earlier, for Cu_2MnAl with magnetization $M_d=3.8$, the Caroli expression gives a Curie temperature which is slightly smaller than the experimental value ($\sim$500K compared with 600K found experimentally). With the correction term we are able to fit exactly the Curie temperature of Cu_2MnAl as shown in Figure 5.3 where the broken horizontal line represents the experimental value of the Curie temperature.

Figures 5.4 and 5.5 show the results for Cu_2MnIn and Cu_2MnSn respectively and again we see that we need the

correction term $J_1(R)$ to give the right Curie temperatures. Finally, Figure 5.6 shows the results for Pd_2MnSn and Pd_2MnSb. In these two alloys Caroli's expression gives negative values for T_c for all possible values of $N_{d\uparrow}$ but again with the correction term $J_1(R)$ we can obtain the right Curie temperatures as shown.

Figure 5.2(a)

Interaction energy for Cu_2MnAl. $J(R) = J_o(R) + J_1(R)$ where J_o is the Caroli term and J_1 is the correction term. The parameters used are $M_d = 3.8$, $N_{d\uparrow} = 5.0$ and $B = 0.1$. The normalization constant $eo = 100\varepsilon_F/\pi = 266.6$ eV and R_o is the Mn-Mn nearest neighbour distance.

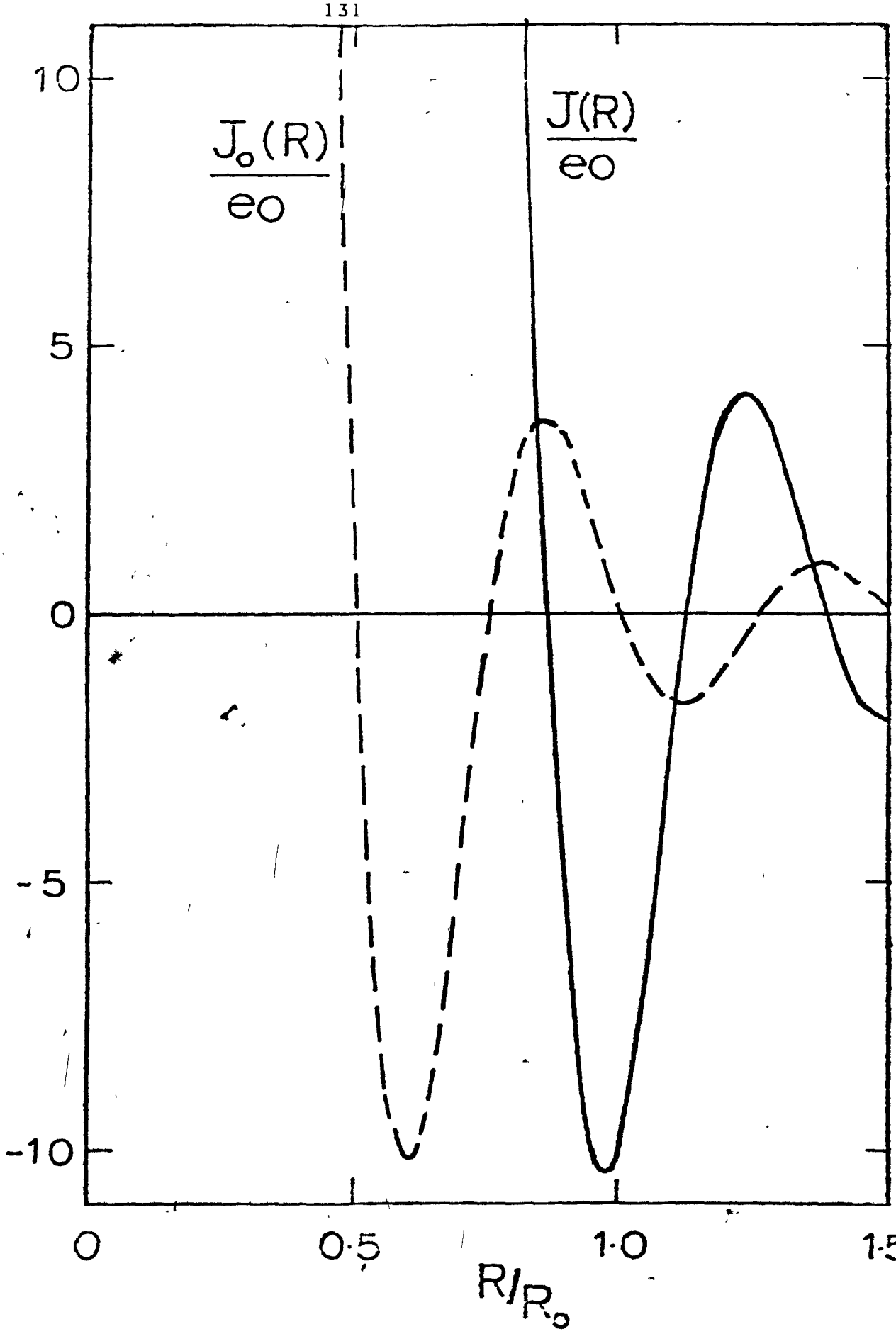

Figure 5.2(a)

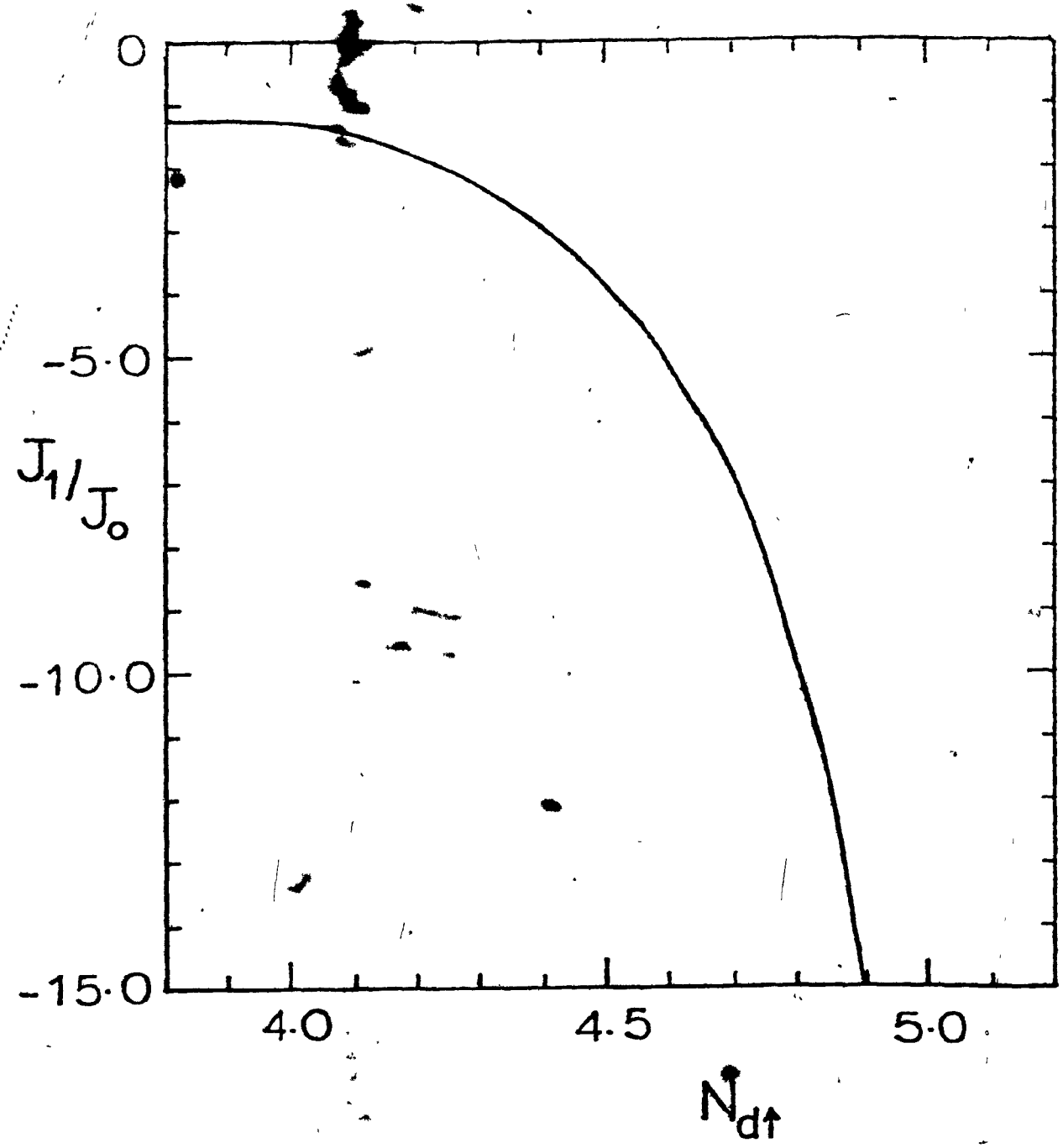

Figure 5.2(b)

J_1/J_0 for nearest neighbour distance as a function of $N_{d\uparrow}$ for Cu_2MnAl. The parameters used are M_d=3.8 and B=0.1.

Figure 5.3

Curie temperature of Cu_2MnAl as a function of $N_{d\uparrow}$. T_{co} is evaluated using Caroli's expression for the interaction energy (equation (5.4)) and T_c is obtained by including the correction term (equation (5.8)). The broken horizontal line is the experimental value. The parameters used are $M_d = 3.8$ and $B = 0.1$.

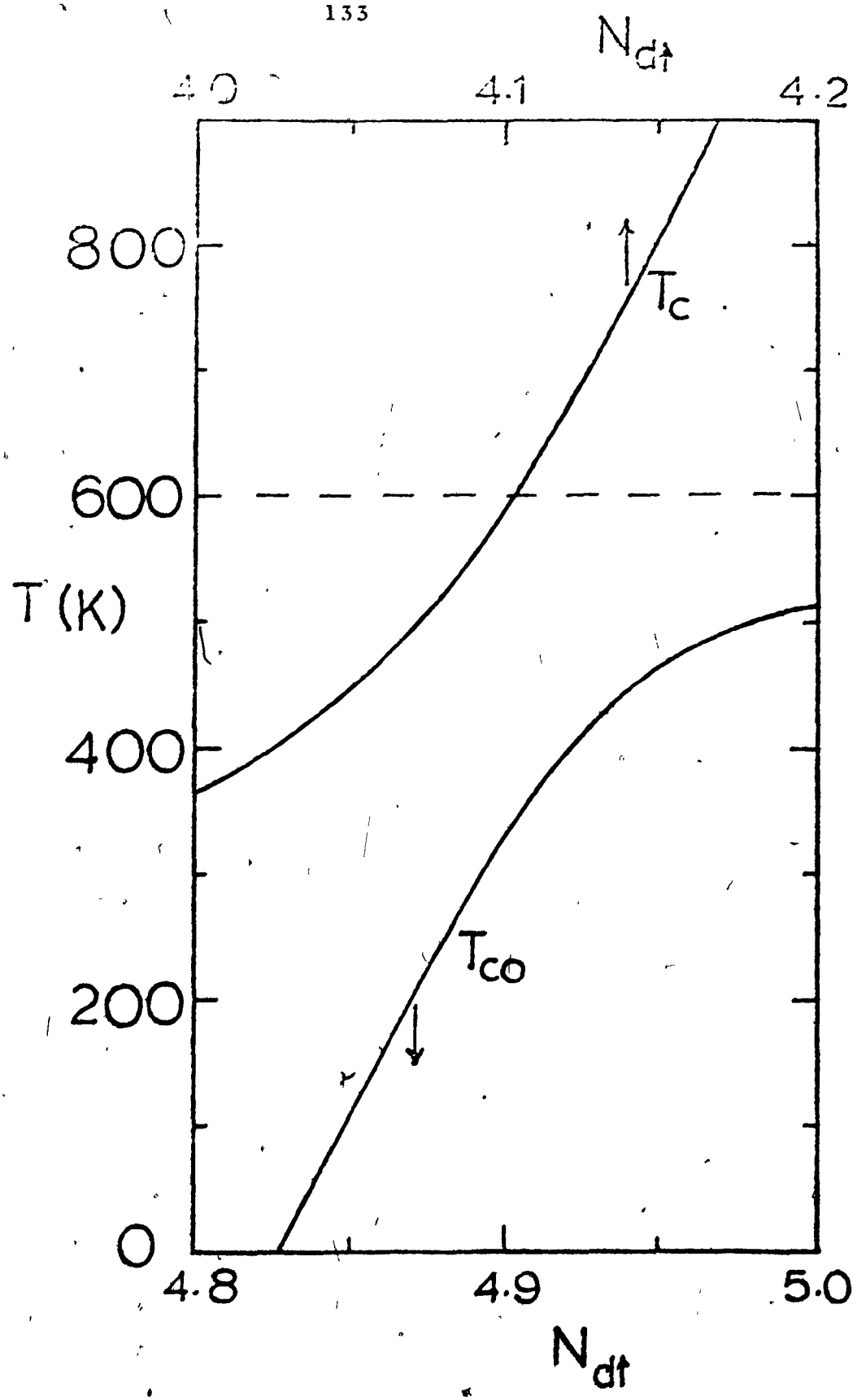

Figure 5.3

Figure 5.4

Curie temperature of Cu_2MnIn as a function of $N_{d\uparrow}$. T_{co} is evaluated using Caroli's expression for the interaction energy (equation (5.4)) and T_c is obtained by including the correction term (equation (5.8)). The broken horizontal line is the experimental value. The parameters used are $M_d = 4.0$ and $B = 0.1$.

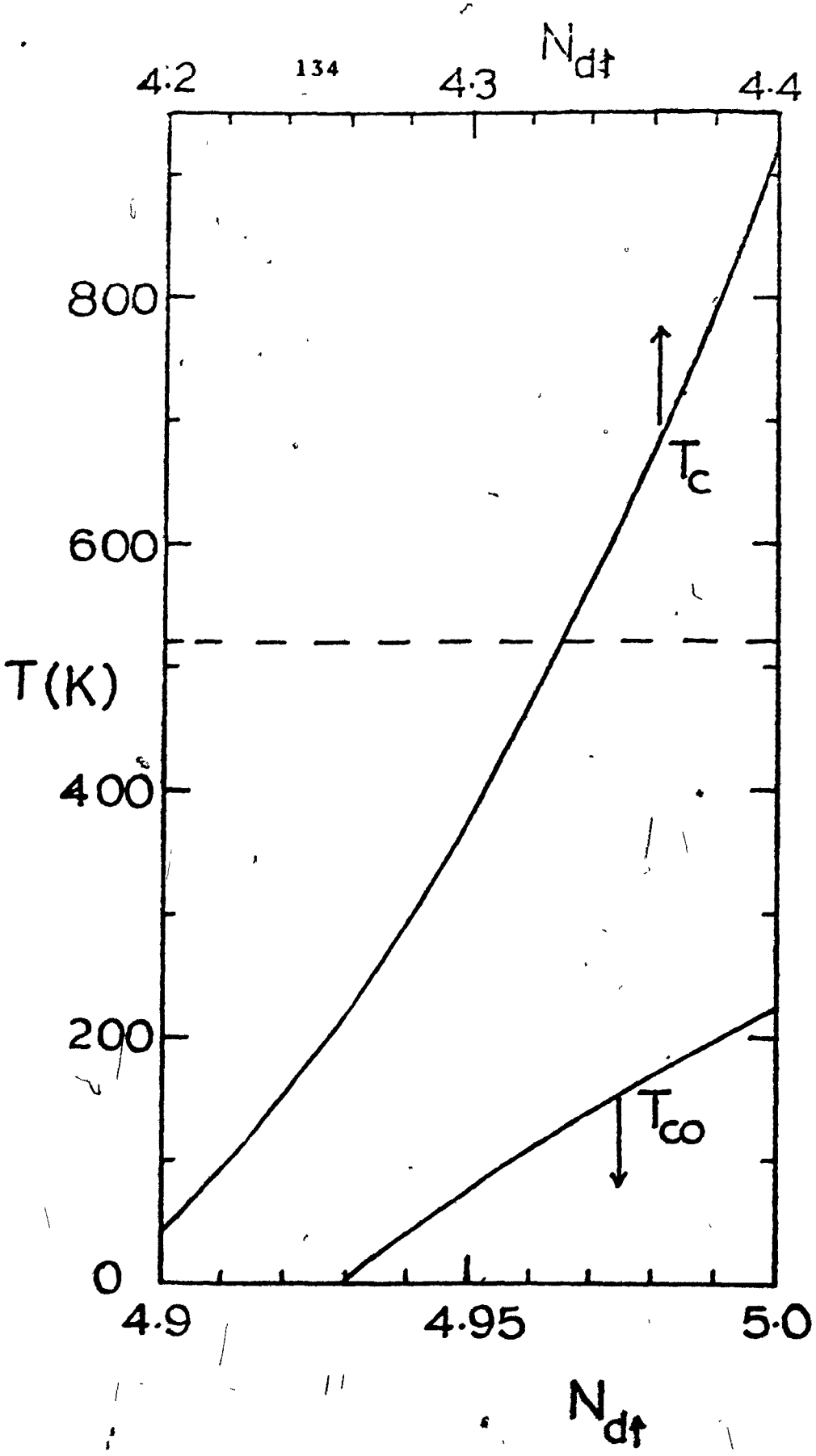
4·2
4·3
$N_{d\uparrow}$
4·4
800
600
400
200
0
T(K)
T_c
T_{co}
4·9
4·95
5·0
$N_{d\uparrow}$

Figure 5.4

Figure 5.5

Curie temperature of Cu_2MnSn as a function of $N_{d\uparrow}$. T_{co} is evaluated using Caroli's expression for the interaction energy (equation (5.4)) and T_c is obtained by including the correction term (equation (5.8)). The broken horizontal line is the experimental value. The parameters used are $M_d = 4.1$ and $B = 0.1$.

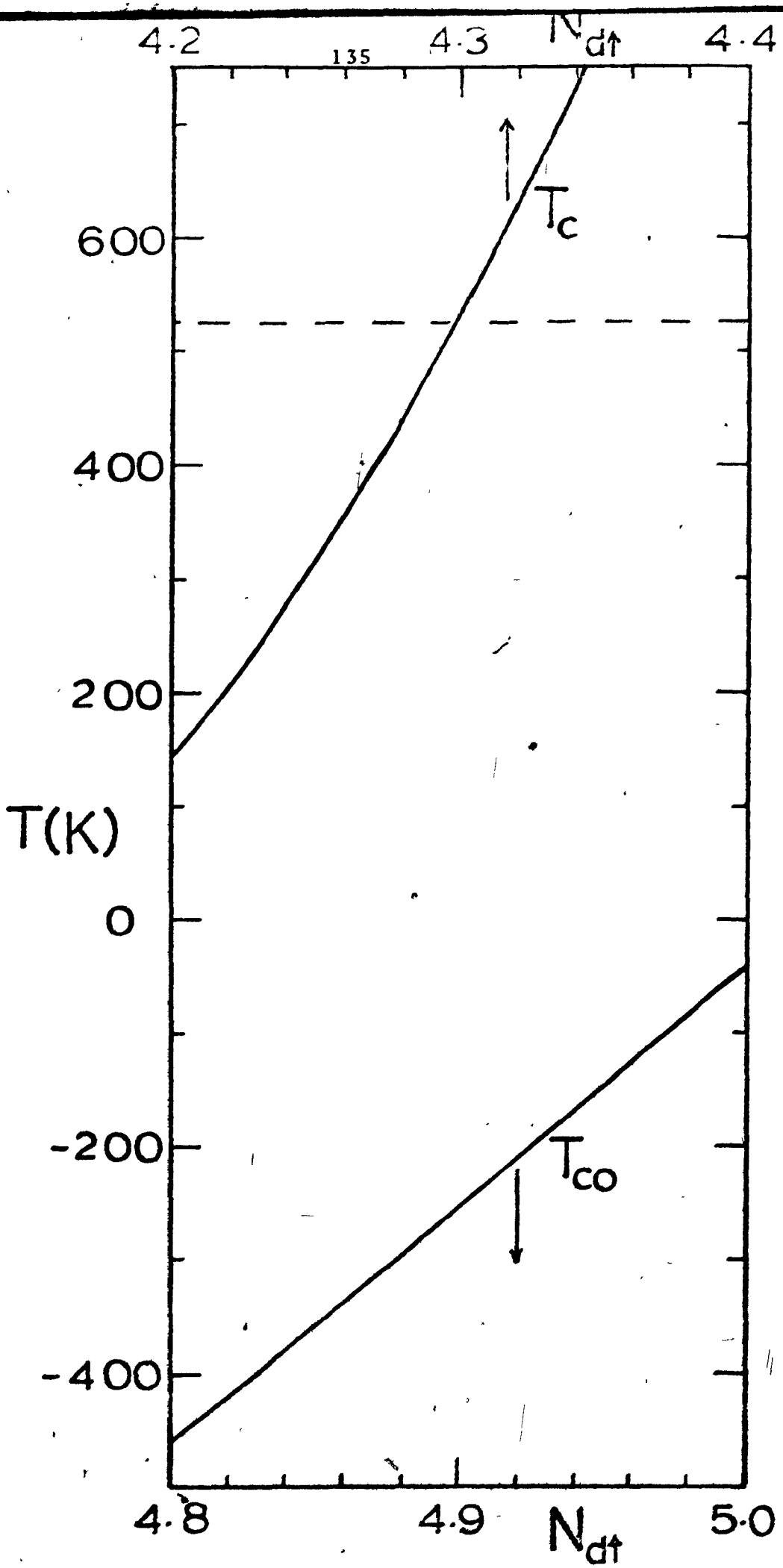
4·2
4·3
$N_{d\uparrow}$
4·4
T_c
600
400
200
T(K)
0
-200
T_{co}
-400
4·8
4·9
$N_{d\uparrow}$
5·0

Figure 5.5

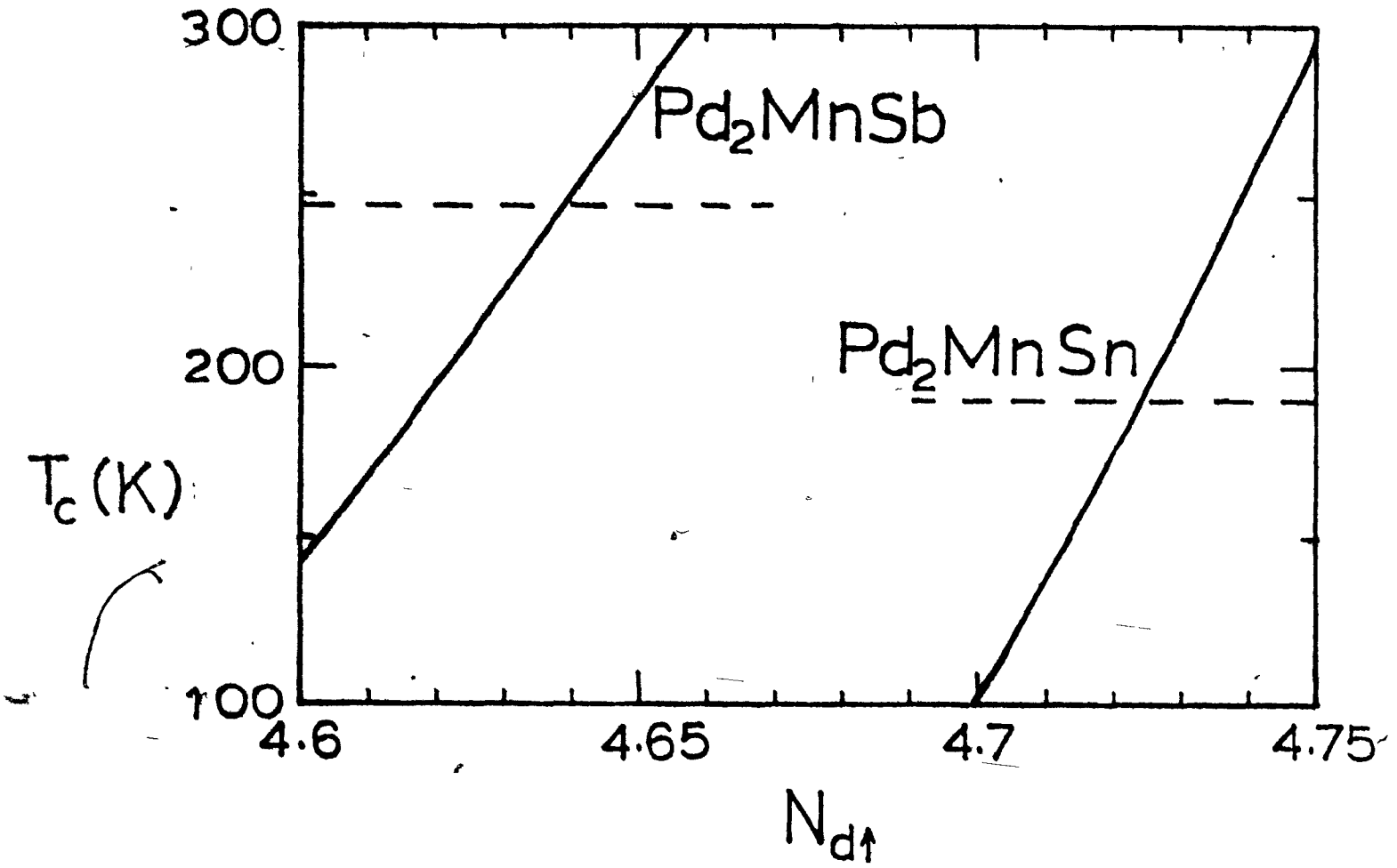

Figure 5.6

Curie temperatures for Pd_2MnSn and Pd_2MnSb in the double resonance model including the correction term to the interaction energy (equation (5.18)). The Curie temperatures obtained using Caroli's expression for the interaction energy (equation (5.4)) are negative and are not shown. The dashed lines are the experimental values of the Curie temperatures. The parameters used are B=1.0 and M_d=4.23 for Pd_2MnSn and 4.4 for Pd_2MnSb.

Appendix A

In this appendix, we give a brief sketch of the derivation of the dynamic susceptibility. The d-part of the susceptibility is defined as:

$$\chi_{ij}(t,t') = i\,\theta(t-t')\left\langle \left[S_i^-(t),\, S_j^+(t') \right] \right\rangle \qquad (A.1)$$

where

$$S_i^- = C_{di\downarrow}^+ C_{di\uparrow} \qquad (A.2a)$$

and

$$S_i^+ = C_{di\uparrow}^+ C_{di\downarrow} \qquad (A.2b)$$

The Green's function in (A.1) will be evaluated using diagramatic methods. The Hamiltonian of the system (equation (1.7)) is written as a sum of a non-interacting part H_o and the interaction term H_{int}:

$$H = H_o + H_{int} \qquad (A.3)$$

where

$$H_o = H_s + H_d + H_{sd}$$

and

$$H_{int} = H_{dd}$$

with H_s, H_d, H_{sd} and H_{dd} given in (1.7). The diagrams are then developed by expanding in a perturbation series in H_{int}. Following Matsubara (1955), we introduce the so-called "temperature Green's function", which depends on a fictitious imaginary time $\tau = it$:

$$\chi_{ij}(\tau,\tau') = \left\langle T_\tau \left(C^+_{di\downarrow}(\tau) C_{di\uparrow}(\tau) C^+_{dj\uparrow}(\tau') C_{dj\downarrow}(\tau') \right) \right\rangle \tag{A.4}$$

where the Heisenberg operators $C_{di\sigma}(\tau)$ are defined by

$$C_{di\sigma}(\tau) = e^{(H-\mu N)\tau} C_{di\sigma} e^{-(H-\mu N)\tau} \tag{A.5}$$

μ is the chemical potential, N the number operator and T_τ is the ordering operator for τ. Going over into the interaction representation, equation (A.4) becomes (Abrikosov et al (1963)):

$$\chi_{ij}(\tau,\tau') = \frac{\left\langle T_\tau \left(C^+_{di\downarrow}(\tau) C_{di\uparrow}(\tau) C^+_{dj\uparrow}(\tau') C_{dj\downarrow}(\tau') S \right) \right\rangle_0}{\langle S \rangle_0} \tag{A.6}$$

where $C_{di\sigma}(\tau)$ are now in the interaction representation

$$C_{di\sigma}(\tau) = e^{(H_0-\mu N)\tau} C_{di\sigma} e^{-(H_0-\mu N)\tau} \tag{A.7}$$

$\langle \ldots \rangle_0$ represents the thermal average in the non-interacting

system and S is given by

$$S = T_\tau \exp\left\{-\int_0^{1/T} H_{int}(\tau')\,d\tau'\right\}$$

$$= \sum_{n=0}^{\infty} \frac{(-1)^n}{n!} \int_0^{1/T} \cdots \int_0^{1/T} d\tau_1 \cdots d\tau_n \left(T_\tau \left(H_{int}(\tau_1) \cdots H_{int}(\tau_n)\right)\right) \quad (A.8)$$

Substituting this in the numerator of (A.6) we obtain the perturbation series for the susceptibility

$$\chi_{ij}(\tau,\tau') = \frac{1}{\langle S\rangle_0} \sum_{n=0}^{\infty} \frac{(-1)^n}{n!} \int_0^{1/T} \cdots \int_0^{1/T} d\tau_1 \cdots d\tau_n \cdot$$

$$\times \left\langle T_\tau \left(c^+_{di\downarrow}(\tau)\, c_{di\uparrow}(\tau)\, c^+_{dj\uparrow}(\tau')\, c_{dj\downarrow}(\tau')\, H_{int}(\tau_1) \cdots H_{int}(\tau_n)\right)\right\rangle_0 \quad (A.9)$$

We shall not expand S in the denominator of (A.6) because, as it turns out, the factor $\langle S\rangle_0$ cancels an identical factor in the numerator (in terms of diagrams, this is equivalent to neglecting all disconnected diagrams).

The first term in (A.9) is the zeroth order term

$$\chi^0_{ij}(\tau,\tau') = \left\langle T_\tau \left(c^+_{di\downarrow}(\tau)\, c_{di\uparrow}(\tau)\, c^+_{dj\uparrow}(\tau')\, c_{dj\downarrow}(\tau')\right)\right\rangle_0 \quad (A.10)$$

Using Wick's theorem, this decomposes into

$$\chi^0_{ij}(\tau,\tau') = \left\langle T_\tau \left(c_{di\uparrow}(\tau)\, c^+_{dj\uparrow}(\tau')\right)\right\rangle_0 \left\langle T_\tau \left(c^+_{di\downarrow}(\tau)\, c_{dj\downarrow}(\tau')\right)\right\rangle_0$$

$$= -\,G^0_{ij\uparrow}(\tau,\tau')\, G^0_{ji\downarrow}(\tau',\tau) \quad (A.11)$$

where we have introduced the free-particle Green's function

$$G^{\circ}_{ij\sigma}(\tau,\tau') = -\left\langle T_\tau \left(c_{di\sigma}(\tau)\, c^{\dagger}_{dj\sigma}(\tau') \right) \right\rangle_0 \qquad \text{(A.12)}$$

The second term in (A.9) is the first order term

$$\chi'_{ij}(\tau,\tau') = -\int_0^{1/T} d\tau_1 \left\langle T_\tau \left(c^{\dagger}_{di\downarrow}(\tau)\, c_{di\uparrow}(\tau)\, c^{\dagger}_{dj\uparrow}(\tau')\, c_{dj\downarrow}(\tau')\, H_{int}(\tau_1) \right) \right\rangle_0$$

$$= -U \sum_{\ell} \int_0^{1/T} d\tau_1 \left\langle T_\tau \left(c^{\dagger}_{di\downarrow}(\tau)\, c_{di\uparrow}(\tau)\, c^{\dagger}_{dj\uparrow}(\tau')\, c_{dj\downarrow}(\tau') \right.\right.$$

$$\left.\left. \times\, c^{\dagger}_{d\ell\uparrow}(\tau_1)\, c_{d\ell\uparrow}(\tau_1)\, c^{\dagger}_{d\ell\downarrow}(\tau_1)\, c_{d\ell\downarrow}(\tau_1) \right) \right\rangle_0 \qquad \text{(A.13)}$$

Again, using Wick's theorem, this reduces to

$$\chi'_{ij}(\tau,\tau') = -U \sum_{\ell} \int_0^{1/T} d\tau_1 \Big\{ G^{\circ}_{\ell j\uparrow}(\tau_1,\tau')\, G^{\circ}_{i\ell\uparrow}(\tau,\tau_1)\, G^{\circ}_{j i\downarrow}(\tau',\tau)\, G^{\circ}_{\ell\ell\downarrow}(\tau_1,\tau_1)$$

$$+ G^{\circ}_{ij\uparrow}(\tau,\tau')\, G^{\circ}_{\ell i\downarrow}(\tau_1,\tau)\, G^{\circ}_{j\ell\downarrow}(\tau',\tau_1)\, G^{\circ}_{\ell\ell\uparrow}(\tau_1,\tau_1)$$

$$- G^{\circ}_{\ell j\uparrow}(\tau_1,\tau')\, G^{\circ}_{i\ell\uparrow}(\tau,\tau_1)\, G^{\circ}_{\ell i\downarrow}(\tau_1,\tau)\, G^{\circ}_{j\ell\downarrow}(\tau',\tau_1)$$

$$- G^{\circ}_{ij\uparrow}(\tau,\tau')\, G^{\circ}_{j i\downarrow}(\tau',\tau)\, G^{\circ}_{\ell\ell\uparrow}(\tau_1,\tau_1)\, G^{\circ}_{\ell\ell\downarrow}(\tau_1,\tau_1) \Big\} \qquad \text{(A.14)}$$

To draw diagrams, we represent the free-particle Green's function G° by a straight line and the interaction U by a wavy line:

$G^{\circ}_{ij\sigma}(\tau,\tau') \equiv$ 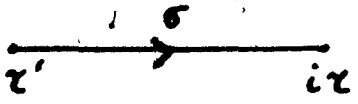

and

$U \equiv$ 

The diagrams corresponding to (A.11) and (A.14) are

$\chi^{o}_{ij}(\tau,\tau') \equiv$ 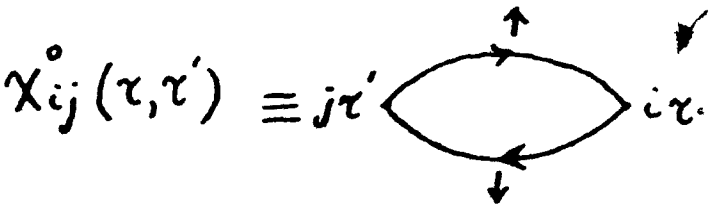

(A.15)

$\chi'_{ij}(\tau,\tau') \equiv$ 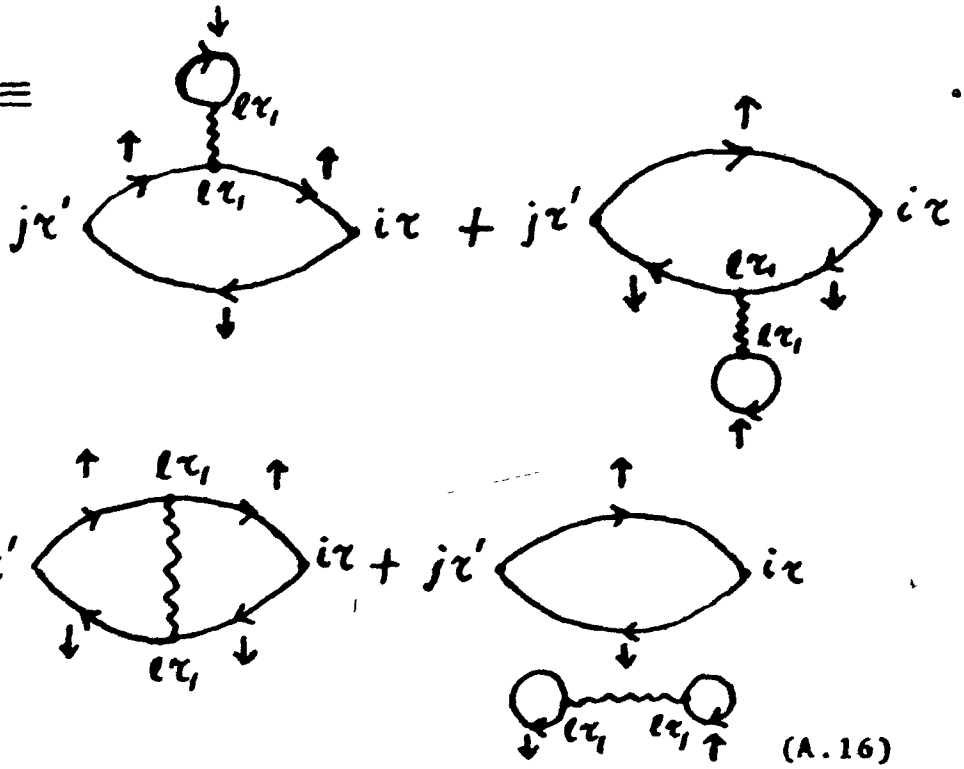

(A.16)

Similarly we can find diagrams corresponding to the higher order terms in (A.9). The number of terms increases very fast with order but, fortunately, we need not consider them all. To begin with, and as mentioned earlier, we can neglect all disconnected diagrams such as the fourth diagram in X^{1}_{ij}. Secondly, for the nth order term, there will be sets of n! "topologically" similar diagrams each giving the same contribution to X^{n}_{ij}. Because of the n! factor in (A.9) we can consider only one diagram in the set if we drop the n! factor in (A.9). Finally, we can neglect any diagram containing the

factor  , provided we replace all the free particle Green's function $G^{\circ}_{ij\sigma}$ by the Hartree-Fock propagators. With these simplifications we have

$\chi_{ij}(\tau,\tau') =$ 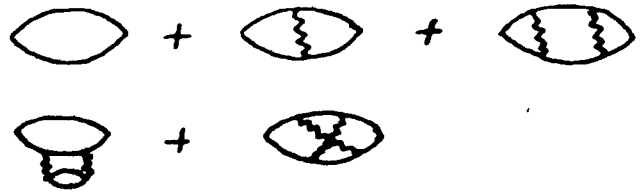

+ third and higher order diagrams (A.17)

Inspite of the above simplifications it is still not possible to evaluate the above sum. However, as we shall show, we can sum a certain subset of these diagrams to infinite order. These are the so-called "bubble" diagrams

$\chi_{ij}(\tau,\tau') =$  (A.18)

This is an approximation equivalent to the random phase approximation. The sum in (A.18) can be easily performed if we Fourier transform it. We first consider the zeroth order term

$\chi^{\circ}_{ij}(\tau,\tau') \equiv$ 

$= - G^{\circ}_{ij\uparrow}(\tau,\tau')\, G^{\circ}_{ji\downarrow}(\tau',\tau)$ (A.19)

Following Abrikosov et al (1963) the Fourier series for G and X are defined as:

$$G^{\circ}_{ij\sigma}(\tau,\tau') = T\sum_{n} G^{\circ}_{ij\sigma}(\omega_n)\, e^{-i\omega_n(\tau-\tau')} \qquad \text{(A.20)}$$

and

$$\chi^{\circ}_{ij}(\tau,\tau') = T\sum_{n} \chi^{\circ}_{ij}(\Omega_n)\, e^{-i\Omega_n(\tau-\tau')} \qquad \text{(A.21)}$$

where

$$\omega_n = (2n+1)\pi T \qquad \text{(A.22a)}$$

$$\Omega_n = 2n\pi T \qquad \text{(A.22b)}$$

and

$$n = 0, \pm 1, \pm 2, \ldots\ldots \qquad \text{(A.22c)}$$

Substituting (A.20) into (A.19) gives

$$\chi^{\circ}_{ij}(\tau,\tau') = -T^2\sum_{nn'} G^{\circ}_{ij\uparrow}(\omega_n)\, G^{\circ}_{ji\downarrow}(\omega_{n'})\, e^{-i(\omega_n-\omega_{n'})(\tau-\tau')}$$

$$= -T^2\sum_{nn'} G^{\circ}_{ij\uparrow}(\Omega_n+\omega_{n'})\, G^{\circ}_{ji\downarrow}(\omega_{n'})\, e^{-i\Omega_n(\tau-\tau')} \qquad \text{(A.23)}$$

where we have put $\omega_n = \Omega_n + \omega_{n'}$. Comparing (A.21) and (A.23) we find

$$\chi^{\circ}_{ij}(\Omega_n) = -T\sum_{n'} G^{\circ}_{ij\uparrow}(\Omega_n+\omega_{n'})\, G^{\circ}_{ji\downarrow}(\omega_{n'}) \qquad \text{(A.24)}$$

We now introduce the spatial Fourier transform for G° and X° as:

$$G^\circ_{ij\sigma}(\omega_n) = \frac{1}{N}\sum_{\underline{q}} G^\circ_{\underline{q}\sigma}(\omega_n)\, e^{i\underline{q}\cdot(\underline{R}_i - \underline{R}_j)} \tag{A.25}$$

and

$$\chi^\circ_{ij}(\Omega_n) = \frac{1}{N}\sum_{\underline{q}} \chi^\circ(\underline{q}, \Omega_n)\, e^{i\underline{q}\cdot(\underline{R}_i - \underline{R}_j)} \tag{A.26}$$

where $\underline{R}_i$ is the position of the ith atom. Substituting (A.25) in (A.24) gives

$$\begin{aligned}\chi^\circ_{ij}(\Omega_n) &= -T\sum_{n'\underline{q}\underline{q}'} G^\circ_{\underline{q}\uparrow}(\Omega_n + i\omega_{n'})\, G^\circ_{\underline{q}'\downarrow}(i\omega_{n'})\, e^{i(\underline{q}-\underline{q}')\cdot(\underline{R}_i - \underline{R}_j)} \\ &= -T\sum_{n'\underline{q}\underline{q}'} G^\circ_{\underline{q}+\underline{q}'\uparrow}(\Omega_n + i\omega_{n'})\, G^\circ_{\underline{q}'\downarrow}(i\omega_{n'})\, e^{i\underline{q}\cdot(\underline{R}_i - \underline{R}_j)}\end{aligned} \tag{A.27}$$

Comparing (A.27) and (A.26) we obtain:

$$\chi^\circ(\underline{q}, \Omega_n) = -\frac{T}{N}\sum_{n'\underline{q}'} G^\circ_{\underline{q}+\underline{q}'\uparrow}(\Omega_n + i\omega_{n'})\, G^\circ_{\underline{q}'\downarrow}(i\omega_{n'}) \tag{A.28}$$

Next we consider the first order term

$$\chi'_{ij}(\tau,\tau') \equiv$$

$$= U\sum_{\ell}\int_0^{1/T} d\tau_1\, G^\circ_{\ell j\uparrow}(\tau_1,\tau')\, G^\circ_{i\ell\uparrow}(\tau,\tau_1)\, G^\circ_{\ell i\downarrow}(\tau_1,\tau)\, G^\circ_{j\ell\downarrow}(\tau',\tau_1)$$

$$= UT^4\sum_{\ell n_1 n_2 n_3 n_4}\int_0^{1/T} d\tau_1\, G^\circ_{\ell j\uparrow}(i\omega_{n_1})\, G^\circ_{i\ell\uparrow}(i\omega_{n_2})\, G^\circ_{\ell i\downarrow}(i\omega_{n_3})\, G^\circ_{j\ell\downarrow}(i\omega_{n_4})$$

$$\times e^{-i[(\omega_{n_1}-\omega_{n_4})(\tau_1-\tau') + (\omega_{n_3}-\omega_{n_2})(\tau-\tau_1)]} \tag{A.29}$$

Using the relation

$$T\int_0^{1/T} d\tau_1\, e^{i(\omega_{n_1}-\omega_{n_2})\tau_1} = \delta_{\omega_{n_1},\omega_{n_2}} \qquad (A.30)$$

we find

$$\chi'_{ij}(\tau,\tau') = UT^3 \sum_{\ell n_1 n_2 n_3} G^0_{\ell j\uparrow}(\omega_{n_1})\, G^0_{i\ell\downarrow}(\omega_{n_2})\, G^0_{\ell i\downarrow}(\omega_{n_3})\, G^0_{j\ell\downarrow}(\omega_{n_1}-\omega_{n_2}+\omega_{n_3})$$
$$\times\, e^{-i(\omega_{n_2}-\omega_{n_3})(\tau-\tau')} \qquad (A.31)$$

Letting $\omega_{n_2} - \omega_{n_3} = \Omega_n$ and $\omega_{n_1} - \omega_{n_2} + \omega_{n_3} = \omega_{n'}$ gives

$$\chi'_{ij}(\tau,\tau') = UT^3 \sum_{\ell n n' n_3} G^0_{\ell j\uparrow}(\Omega_n+\omega_{n'})\, G^0_{i\ell\downarrow}(\Omega_n+\omega_{n_3})\, G^0_{\ell i\downarrow}(\omega_{n_3})$$
$$\times\, G^0_{j\ell\downarrow}(\omega_{n'})\, e^{-i\Omega_n(\tau-\tau')}$$
$$= T\sum_n \chi'_{ij}(\Omega_n)\, e^{-i\Omega_n(\tau-\tau')}\,, \qquad (A.32)$$

Hence

$$\chi'_{ij}(\Omega_n) = UT^2 \sum_{\ell n' n_3} G^0_{\ell j\uparrow}(\Omega_n+\omega_{n'})\, G^0_{i\ell\downarrow}(\Omega_n+\omega_{n_3})\, G^0_{\ell i\downarrow}(\omega_{n_3})\, G^0_{j\ell\downarrow}(\omega_{n'}) \qquad (A.33)$$

Similarly substituting (A.25) into (A.33) gives

$$\chi'_{ij}(\Omega_n) = \frac{UT^2}{N} \sum_{n' n_3 \underline{q}\underline{q}'\underline{q}_3} G^0_{\underline{q}+\underline{q}'\uparrow}(\Omega_n+\omega_{n'})\, G^0_{\underline{q}+\underline{q}_3\uparrow}(\Omega_n+\omega_{n_3})\, G^0_{\underline{q}_3\downarrow}(\omega_{n_3})$$
$$\times\, G^0_{\underline{q}'\downarrow}(\omega_{n'})\, e^{i\underline{q}\cdot(\underline{R}_i-\underline{R}_j)}$$
$$= \frac{1}{N}\sum_{\underline{q}} \chi'(\underline{q},\Omega_n)\, e^{i\underline{q}\cdot(\underline{R}_i-\underline{R}_j)} \qquad (A.34)$$

Hence

$$\chi'(q,\Omega_n) = \frac{UT^2}{N^2}\sum_{n'n_3 q' q_3} G^0_{q+q'\uparrow}(\Omega_n+\omega_{n'})\, G^0_{q+q_3\uparrow}(\Omega_n+\omega_{n_3})\, G^0_{q_3\downarrow}(\omega_{n_3}) \times G^0_{q'\downarrow}(\omega_{n'}) \tag{A.35}$$

Using (A.28), we have

$$\chi'(q,\Omega_n) = \chi^0(q,\Omega_n)\, U\, \chi^0(q,\Omega_n) \tag{A.36}$$

In a similar manner, we find for the second order term

$$\chi^2(q,\Omega_n) = \chi^0(q,\Omega_n)\, U\, \chi^0(q,\Omega_n)\, U\, \chi^0(q,\Omega_n) \tag{A.37}$$

We thus find for X the following geometric series:

$$\begin{aligned}\chi(q,\Omega_n) &= \chi^0(q,\Omega_n) + \chi'(q,\Omega_n) + \chi^2(q,\Omega_n) + \cdots \\ &= \chi^0(q,\Omega_n)\left(1 + U\chi^0(q,\Omega_n) + (U\chi^0(q,\Omega_n))^2 + \cdots\right) \\ &= \chi^0(q,\Omega_n)/\left(1 - U\chi^0(q,\Omega_n)\right)\end{aligned} \tag{A.38}$$

From equation (1.27) of Chapter I we have the Hartree-Fock propagator

$$G^0_{q\sigma}(\omega_n) = \sum_{\lambda=\pm} \frac{Z^\lambda_{q\sigma}}{i\omega_n - \tilde{\varepsilon}^\lambda_{q\sigma}} \tag{A.39}$$

To evaluate $\chi^0(q,\Omega_n)$, we use the following relation

$$T\sum_n F(i\omega_n) = -\frac{1}{2\pi i}\oint_C F(z)f(z)\,dz \qquad (A.40)$$

where

$$f(z) = \frac{1}{e^{\beta z}+1} \qquad (A.41)$$

and $\beta = 1/T$ (using units such that the Boltzmann constant $K_B = 1$). The contour C is shown in Figure A.1. Equation (A.40) is easily proved by noting that the function f(z) has poles on the imaginary axis at $z = \frac{i}{\beta}(2n+1)\pi = i\omega_n$, and that the residue at these poles is $(-\frac{1}{\beta})$. Hence, from (A.28), (A.39) and (A.40) we have

$$\chi^\circ(\underline{q},\Omega_n) = \frac{1}{2\pi i N}\sum_{\lambda\lambda'\underline{q}'}\oint_C \frac{Z^\lambda_{\underline{q}+\underline{q}'\uparrow}}{z+i\Omega_n-\varepsilon^\lambda_{\underline{q}+\underline{q}'\uparrow}}\cdot\frac{Z^{\lambda'}_{\underline{q}'\downarrow}}{z-\varepsilon^{\lambda'}_{\underline{q}'\downarrow}}f(z)\,dz \qquad (A.42)$$

In addition to the poles of f(z), the integrand in (A.42) has poles at $z = \varepsilon^{\lambda'}_{\underline{q}'\downarrow}$ and at $z = -i\Omega_n + \varepsilon^\lambda_{\underline{q}+\underline{q}'\uparrow}$. These poles are shown in Figure A.2 which also shows how one can deform the contour C in Figure A.1 in order to evaluate the integral (A.42). The deformed contour in Figure A.2 encloses two simple poles at $\varepsilon^{\lambda'}_{\underline{q}'\downarrow}$ and $-i\Omega_n + \varepsilon^\lambda_{\underline{q}+\underline{q}'\uparrow}$. Hence

$$\chi^\circ(\underline{q},\Omega_n) = -\frac{1}{N}\sum_{\lambda\lambda'\underline{q}'} Z^\lambda_{\underline{q}+\underline{q}'\uparrow} Z^{\lambda'}_{\underline{q}'\downarrow}\left(\frac{f(\varepsilon^{\lambda'}_{\underline{q}'\downarrow})}{i\Omega_n+\varepsilon^{\lambda'}_{\underline{q}'\downarrow}-\varepsilon^\lambda_{\underline{q}+\underline{q}'\uparrow}}\right.$$

$$\left.-\frac{f(\varepsilon^\lambda_{\underline{q}+\underline{q}'\uparrow}-i\Omega_n)}{-i\Omega_n+\varepsilon^\lambda_{\underline{q}+\underline{q}'\uparrow}-\varepsilon^{\lambda'}_{\underline{q}'\downarrow}}\right) \qquad (A.43)$$

$$= \frac{1}{N} \sum_{\lambda\lambda' q'} Z^{\lambda}_{q+q'\uparrow} Z^{\lambda'}_{q'\downarrow} \frac{\left(f(\varepsilon^{\lambda}_{q+q'\uparrow}) - f(\varepsilon^{\lambda'}_{q'\downarrow})\right)}{i\Omega_n - (\varepsilon^{\lambda}_{q+q'\uparrow} - \varepsilon^{\lambda'}_{q'\downarrow})}$$

where we have used the fact that $f(z - i\Omega_n) = f(z)$ since $\Omega_n = 2n\pi/\beta$.

Finally we obtain the real time Green's function $X(q,\omega)$ from the temperature Green's function $X(q,\Omega_n)$ by replacing $i\Omega_n$ by ω (Abrikosov et al (1963)). Thus

$$X(q,\omega) = \frac{X^{\circ}(q,\omega)}{1 - U X^{\circ}(q,\omega)} \qquad (A.44)$$

where

$$X^{\circ}(q,\omega) = \frac{1}{N} \sum_{\lambda\lambda' q'} Z^{\lambda}_{q+q'\uparrow} Z^{\lambda'}_{q'\downarrow} \frac{\left(f(\varepsilon^{\lambda}_{q+q'\uparrow}) - f(\varepsilon^{\lambda'}_{q'\downarrow})\right)}{\omega - (\varepsilon^{\lambda}_{q+q'\uparrow} - \varepsilon^{\lambda'}_{q'\downarrow})}$$

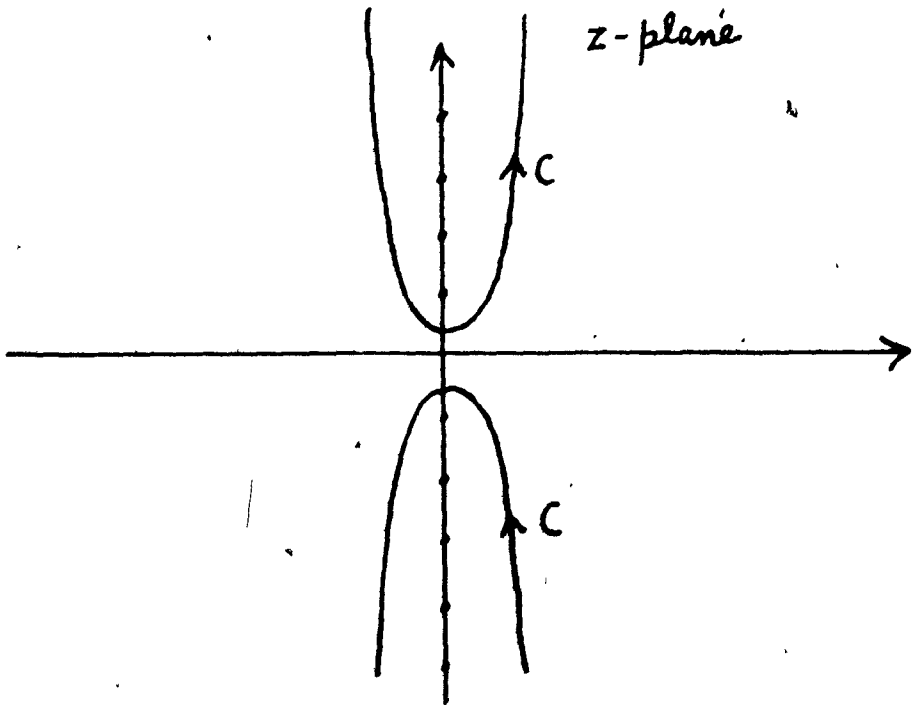

Figure A.1

Contour for the integral in (A.40). The full circles indicate the poles of f(z).

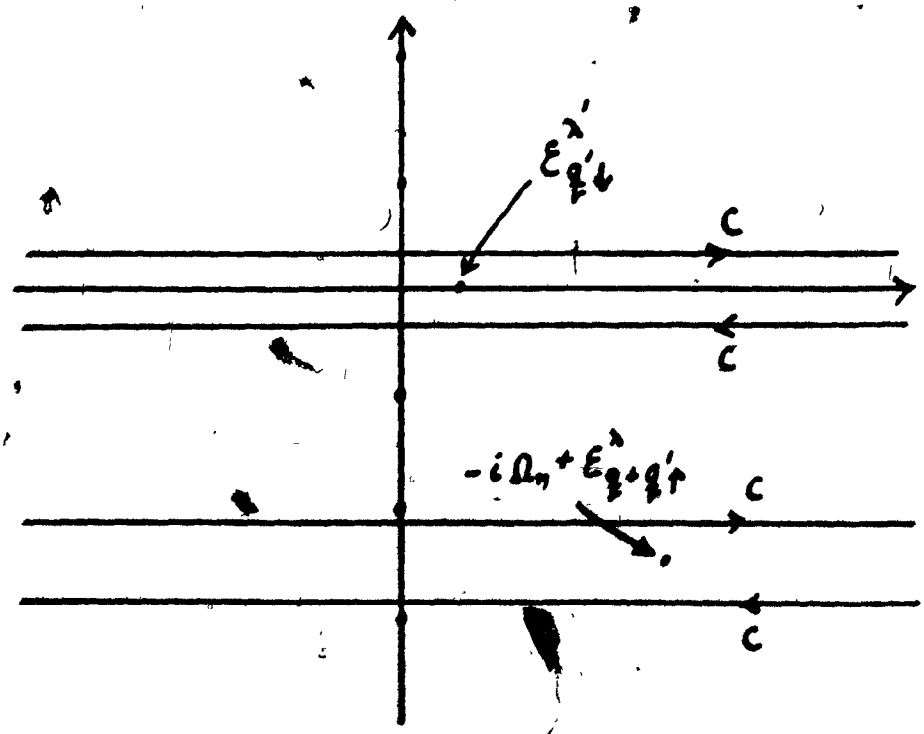

Figure A.2

Deformed contour for the integral in (A.42).

Appendix B

In this appendix we evaluate the function $F(\varepsilon,R)$ that appears in equation (5.8). This derivation is due to D.J.W. Geldart (private communication). Caroli's expression for F (Caroli (1967)) is generalized to the case of a five-fold degenerate $\ell = 2$ orbital to give

$$F(\varepsilon,R) = \sum_{m=-\ell}^{\ell} \left(F_m(\varepsilon,R)\right)^2 \tag{B1}$$

with

$$F_m(\varepsilon,R) = \sum_{\underline{k}} V_{dm\underline{k}} V_{\underline{k}dm} \frac{e^{-i\underline{k}\cdot\underline{R}}}{\varepsilon - \varepsilon_{\underline{k}} + i\delta} \tag{B2}$$

and

$$V_{dm\underline{k}} = \int d\underline{r}\ \phi^*_{dm}(r) V(r) e^{i\underline{k}\cdot\underline{r}} \tag{B3}$$

ϕ_{dm} is the d-orbital wavefunction

$$\phi_{dm}(r) = C r^2 e^{-\lambda r} Y_{dm}(\hat{r}) \tag{B4}$$

where C is a normalization constant, Y_{dm} is a spherical

harmonic and, for a Mn ion, $\lambda = 3.5417$ Å^{-1} (Griffith (1961)). For V, the screened Coulomb potential is used

$$V(r) = V_0 \frac{e^{-q_{sc} r}}{r} \tag{B5}$$

q_{sc} is the inverse of the Thomas-Fermi screening length and is given by

$$q_{sc} = \left(6\pi n e^2/\varepsilon_f\right)^{1/2} \tag{B6}$$

where n is the conduction electron concentration, e the electronic charge and ε_F the Fermi level.

Substituting (B5) and (B4) into (B3) and expanding the plane wave in spherical harmonics the integral is easily evaluated giving

$$V_{dm\underline{k}} = -4\pi I(k) Y^*_{dm}(\hat{\underline{k}}) \tag{B7}$$

where

$$I(k) = \frac{8 V_0 C_m k^2}{\left[(q_{sc}+\lambda)^2 + k^2\right]^3} \tag{B8}$$

Inserting (B7) into (B2) gives

$$F_m(\varepsilon, R) = \frac{2}{\pi} \int_0^\infty dk\, k^2 \frac{I^2(k)\, a_m(kR)}{\varepsilon - \varepsilon_{\underline{k}} + i\delta} \tag{B9}$$

where

$$a_m(kR) = \int d\Omega_{\underline{k}}\, Y^*_{\ell m}(\hat{\underline{k}})\, Y_{\ell m}(\hat{\underline{k}})\, e^{-i\underline{k}\cdot\underline{R}} \qquad \text{(B10)}$$

Again expanding the planewave into partial waves the integral involves a complicated product which can be evaluated in terms of Clebsch-Gordon coefficients. The result, with $\ell = 2$, is

$$a_m(kR) = \sum_L (2L+1)\, i^L j_L(kR) \langle L\ell 0m/\ell m\rangle \langle L\ell 00/\ell 0\rangle \qquad \text{(B11)}$$

where j_L is a spherical Bessel function. With (B11) in (B9), the k integral can be evaluated analytically. Dropping terms which decay exponentially with R, we find

$$F_m(\varepsilon,R) = \sum_L (2L+1)\, i^L \langle L\ell 0m/\ell m\rangle \langle L\ell 00/\ell 0\rangle \times \frac{2m}{\hbar^2}\left[-iK I^2(k) h_L(kR)\right] \qquad \text{(B12)}$$

where k is now given by $\hbar^2k^2/2m = \varepsilon$ and h_L is the spherical Hankel function of the first kind. The sum over m in (B1) can be also evaluated using properties of the Clebsch-Gordon coefficients giving

$$F(\varepsilon,R) = (2\ell+1)^2 \left(\frac{2mik}{\hbar^2} I^2(k)\right)^2 \sum_L \left(i^L h_L(kR) \langle \ell\ell 00/L0\rangle\right)^2 \qquad \text{(B13)}$$

The C-G coefficients restrict the sum to $L = 0,2,4,\ldots 2\ell$, so that in this case we need consider only $L = 0,2$ and 4.

Hence we only need the following spherical Hankel functions:

$$h_0(z) = e^{iz}\left(\frac{-i}{z}\right)$$

$$h_2(z) = e^{iz}\left[i\left(\frac{1}{z} - \frac{3}{z^3}\right) - \frac{3}{z^2}\right]$$

$$h_4(z) = e^{iz}\left[-i\left(\frac{1}{z} - \frac{45}{z^3} + \frac{105}{z^5}\right) + \left(\frac{10}{z^2} - \frac{105}{z^4}\right)\right]$$

Substituting these in (B13) we obtain finally

$$F(\varepsilon, R) = 25\,\Delta^2(\varepsilon)\,\frac{e^{i2kR}}{(kR)^2}\,A(kR) \qquad \text{(B14)}$$

where

$$A(x) = \left(1 + \frac{12i}{x} - \frac{102}{x^2} - \frac{576i}{x^3} + \frac{2232}{x^4} + \frac{5940i}{x^5} - \frac{10530}{x^6} - \frac{11340i}{x^7} + \frac{5670}{x^8}\right) \qquad \text{(B15)}$$

and

$$\Delta(\varepsilon) = \frac{128\,m\,V_0^2\,C^2\,k^5}{\hbar^2\left[(q_{sc}+\lambda)^2 + k^2\right]^6} \qquad \text{(B16)}$$

In terms of the isolated impurity width Δ equation (B16) becomes

$$\Delta(\varepsilon) = \Delta\left[\frac{(q_{sc}+\lambda)^2 + k_f^2}{(q_{sc}+\lambda)^2 + k^2}\right]^6\left(\frac{k}{k_f}\right)^5 \qquad \text{(B17)}$$

Part II

Damping of magnetic excitations in singlet-ground-state systems.

(i) Introduction

There has been considerable interest in the dynamics of localized magnetic systems in which the single ion crystal-field-only ground state is a singlet. In these systems ordering occurs by a magnetic polarization of the ground state and this mechanism is fundamentally different from conventional magnets where magnetic order results from the alignments of permanent moments. Recent reviewsof this field are given by Cooper (1972a) and Birgeneau (1973).

In this part of the thesis we examine the scattering of the magnetic excitations in these systems and we will concentrate our attention on the ferromagnetic compound Pr_3Tl. The exchange interaction between the Pr ions in this compound is weak and only just sufficient to induce magnetic order at temperatures below 11.6K. The saturation moment is about $0.8\mu_B$ which is only a quarter of the free ion value (Birgeneau et al (1971)). In Pr_3Tl, the nine-fold degenerate $4f^2\ ^3H_4$ ground multiplet of the Pr^{3+} ion is split by the crystal-field into a singlet Γ_1 lowest state followed by a triplet Γ_4 , a doublet Γ_3 and a triplet Γ_5(Figure 1). The molecular field mixes up these states and splits the degeneracies as shown in Figure 1. The magnetic excitations are now transitions between these levels which propagate through the lattice via the exchange interaction. These

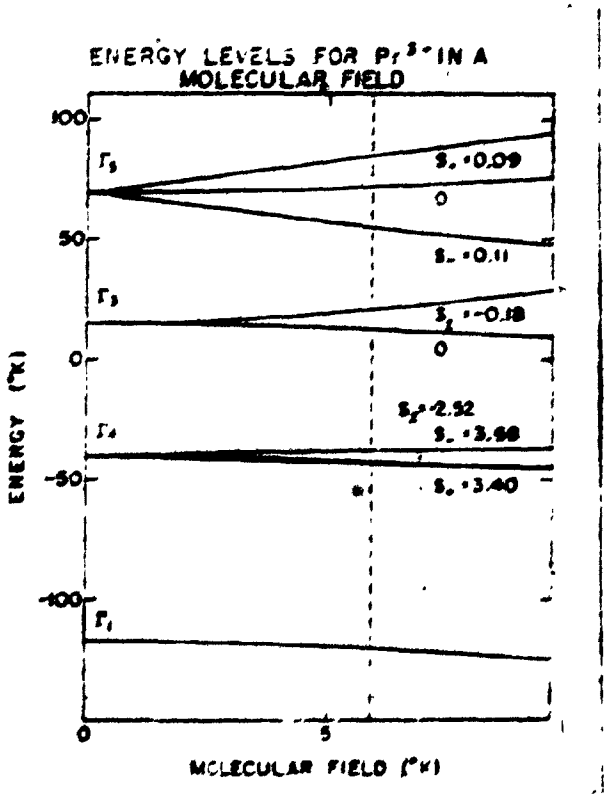

Figure 1

Energy levels of Pr^{3+} ion in a molecular field. The crystal-field only states are denoted by their symmetry labels Γ_n. The broken vertical line gives the molecular field on the Pr^{3+} ion in Pr_2Tl at T=0 (after Holden and Buyers (1974)).

collective excitations are spin waves.

Measurements of the spin wave dispersion relation in polycrystalline material by neutron inelastic scattering have been made by Birgeneau et al (1971) and the striking feature of these results was the insensitivity of the excitation energy to temperature (Figure 2). The simplest theory for singlet-ground-state systems is the singlet-singlet model in which the excited states of the ground multiplet are approximated by a single level. This theory, when solved within the random phase approximation (RPA), predicts that the frequency of the longitudinal zone-centre spin wave mode will fall to zero (i.e. go soft) as the temperature is raised from zero to the transition temperature, and will then rise again as the temperature increases further. This is in marked contrast to the experimental results mentioned above. It was not clear from these measurements (which had to be made at non-zero wavevectors because the specimen was polycrystalline) whether the zone-centre mode does or does not go soft. However, temperature effects predicted by the singlet-singlet theory should have been readily observable at the accessible wavevectors. A refinement of the theory, the singlet-triplet model, is not in significantly better agreement with experiment. In this model four states of the ground multiplet are included, the singlet Γ_1 ground state and triplet Γ_4 excited states.

A shortcoming of these simple model theories is the neglect of the other levels belonging to the ground multiplet.

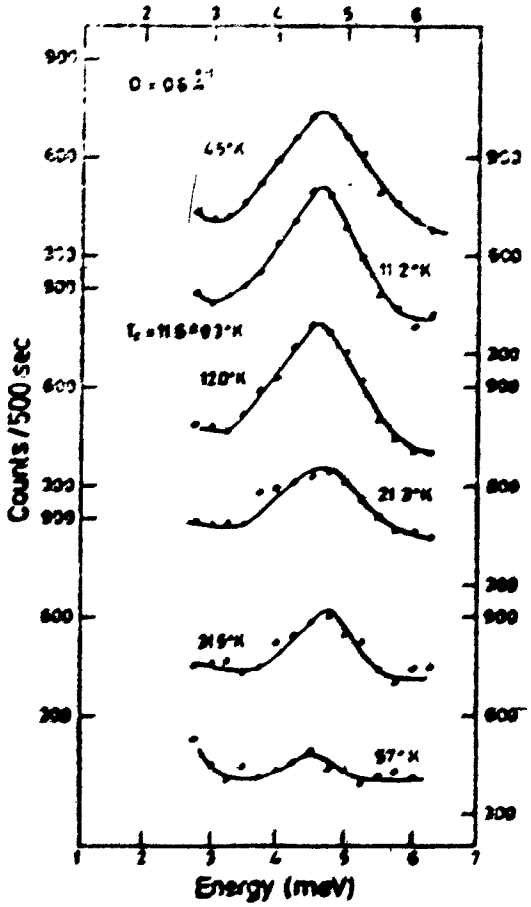

Figure 2

Typical exciton scans in Pr_3Tl as a function of temperature. Similar behaviour is observed at all other wavevectors in both Pr_3Tl and fcc Pr. The instrumental width for these scans was 1.25 mev (after Birgeneau et al (1971)).

The only theories of singlet-ground-state systems in which the real level scheme is considered are based on the pseudoboson theory of Grover (1965). This was applied to Pr_3Tl by Cooper (1972b). The pseudoboson theory is restricted to low temperatures, since only transitions out of the ground state are included and cannot be readily extended to higher temperatures. However, Holden and Buyers (1974) point out that the marked contrast noted by Birgeneau et al (1971) between the experiment and the simple model theories comes from the neglect in the theories of the higher energy levels and the excitations out of these excited states. They suggest a method of obtaining the temperature dependence of the spin waves taking into account the real level scheme and the excitations from all the levels of the ground multiplet. In this case the excitations are obtained from the poles of the dynamic susceptibility. The dynamic susceptibility is evaluated in the random phase approximation (RPA) and this theory is reviewed briefly in section (ii).

The excitations obtained in the RPA are well defined spin waves. At finite temperatures these are damped as a result of scattering from fluctuating fields in the crystal. These fields arise from thermal fluctuations of spins which are coupled by an exchange interaction. In section (iii) we examine the scattering of spin waves by the fluctuating fields using the coherent potential approximation (CPA). The results show that, in addition to the damping, the scattering introduces a shift in the spin wave modes. The frequency and intensity

of the neutron peak is obtained in the CPA and compared with the experimental data of Birgeneau et al (1971) and with the RPA results.

(ii) Magnetic excitations and the random phase approximation.

The Hamiltonian we consider consists of a sum of single-ion crystal-field terms and a Heisenberg exchange interaction term:

$$H = \sum_i V_{CF}(i) - \sum_{ij} J_{ij}\, \underline{S}(i).\underline{S}(j) \qquad (1)$$

In cubic symmetry, the crystal-field potential V_{CF} can be written in terms of the operator equivalents (Hutchings (1964)):

$$V_{CF} = B_4^0\left(O_4^0 + 5O_4^4\right) + B_6^0\left(O_6^0 - 21O_6^4\right) \qquad (2)$$

where O_n^m are the operator equivalents for the total angular momentum and B_4^0 and B_6^0 are the crystal-field parameters which depend on the details of the crystal structure. In the molecular field approximation (Smart (1966)) the Hamiltonian (1) reduces to:

$$H_0 = \sum_i V_{CF}(i) - \sum_i H_z S_z(i) \qquad (3a)$$

where the molecular field H_z is given by

$$H_z = 2\sum_j J_{ij} \langle S_z(j) \rangle$$

The Hamiltonian (3a) is first diagonalized to give a set of molecular field eigenstates $|n\rangle$ and corresponding eigenvalues ω_n. Defining the operators $C_n^+(i)$ and $C_n(i)$ as creation and annihilation operators respectively for the state $|n\rangle$ on site i, the molecular field Hamiltonian can be written as:

$$H_o = \sum_{in} \omega_n \, C_n^+(i) \, C_n(i) \tag{3b}$$

The molecular field results for Pr;Tl are summarized in Figure 1 and Table 1. We note that the molecular field mixes some of the excited states into the ground state thus inducing a moment in the ground state.

Using the equation of motion method, Buyers et al (1975) have derived expressions for the longitudinal and transverse components of the dynamic susceptibility in the random phase approximation (RPA). We now outline briefly their derivation. The dynamic susceptibility is given by the retarded Green's function defined as (Zubarev (1960)):

$$G^{\alpha\beta}(ij,t) = -i\,\theta(t)\langle[S_\alpha(i,t), S_\beta(j)]\rangle$$
$$= \langle\langle S_\alpha(i,t) \,|\, S_\beta(j)\rangle\rangle \tag{4}$$

and its Heisenberg equation of motion is

$$\omega\, G^{\alpha\beta}(ij,\omega) = \langle[S_\alpha(i), S_\beta(j)]\rangle + \langle\langle[S_\alpha(i,t), H] \,|\, S_\beta(j)\rangle\rangle_\omega \tag{5}$$

	Magnetic states						Nonmagnetic states						
n	Δ_n (THz)	$\langle m\|S_z\|n\rangle$	m	$\Delta_m-\Delta_n$ (THz)	$\langle m\|S_y\|n\rangle$	α	n	Δ_n (THz)	$\langle m\|S_z\|n\rangle$	m	$\Delta_m-\Delta_n$ (THz)	$\langle m\|S_y\|n\rangle$	α	
1	0.000	1.009	2	1.792	3.101	+	1	0.000	0.000	2	1.691	3.451		$\Gamma_3-\Gamma_4$
			3	1.611	−2.525	s				3	1.601	−2.582	s	
			4	1.712	3.045	−				4	1.601	3.451	−	
			5	2.797	0					5	2.745	0		
			6	2.923	−0.196	s				6	2.745	0		
			7	3.650	0.116	−				7	3.352	0		
			8	3.905	0					8	3.462	0		
			9	4.262	−0.090	+				9	3.462	0		
2	1.592	0.650	3	0.019	1.932	−	2	1.601	0.500	3	0.000	0.707	−	$\Gamma_4-\Gamma_4$
			4	0.119	0					4	0.000	0		
			5	1.164	3.995	+				5	1.144	3.742	+	$\Gamma_3-\Gamma_4$
			6	1.331	−1.913	−				6	1.144	−2.160	−	
			7	2.056	0					7	2.250	0		
			8	2.403	−1.299	+				8	2.250	−1.871	+	
			9	2.669	−1.130	s				9	2.250	−1.323	s	
3	1.611	0.784	4	0.101	0.464	−	3	1.601	0.000	4	0.000	−0.707	−	$\Gamma_4-\Gamma_4$
			5	1.144	0					5	1.144	0		$\Gamma_3-\Gamma_4$
			6	1.313	−2.693	s				6	1.144	−2.038	s	
			7	2.039	−2.520	−				7	2.250	−1.871	−	
			8	2.384	0					8	2.250	0		
			9	2.651	1.151	+				9	2.250	1.871	+	
4	1.712	−0.256	5	1.045	3.450	−	4	1.601	−0.500	5	1.144	3.742	−	$\Gamma_3-\Gamma_4$
			6	1.211	−1.994	+				6	1.144	−2.160	+	
			7	1.928	1.550	s				7	2.250	1.323	s	
			8	2.262	2.315	−				8	2.250	1.871	−	
			9	2.550	0					9	2.250	0		
5	2.797	0.795	6	0.127	0		5	2.745	0.000	6	0.000	0		
			7	0.593	1.818	+				7	1.136	1.414	+	
			8	1.236	−1.886	s				8	1.136	−2.000	s	
			9	1.505	0.913	−				9	1.136	1.414		
6	2.923	−1.765	7	0.727	1.966	−	6	2.745	0.000	7	1.136	2.449	−	
			8	1.072	0					8	1.136	0		
			9	1.286	2.778	+				9	1.136	2.449	+	
7	3.650	2.286	8	0.345	−2.362	−	7	3.352	2.5	8	0.000	−2.236	−	
			9	0.613	0.0					9	0.000	0		
8	3.905	−0.795	9	0.267	3.678	−	8	3.352	0.000	9	0.000	3.536		
9	4.262	−2.650					9	3.462	−2.5					

Table 1

Energy levels and matrix elements of the total angular momentum $\underline{S}$ in Pr_3Tl (after Holden and Buyers (1974)).

where

$$G^{\alpha\beta}(ij,\omega) = \int_{-\infty}^{\infty} G^{\alpha\beta}(ij,t)\, e^{i\omega t}\, dt \qquad (6)$$

From (1) and (3a), the Hamiltonian H can be rewritten as

$$H = H_0 - \sum_{ij} J_{ij}\left[S_z(i)\left(S_z(j) - 2\langle S_z(j)\rangle\right) + \tfrac{1}{2}\left(S_+(i)S_-(j) + S_-(i)S_+(j)\right)\right] \qquad (7)$$

The spin components $S_\alpha (\alpha = \pm, z)$ can be expressed in terms of the molecular field operators C_n as:

$$S_\alpha = \sum_{mn} S_{\alpha mn}\, C_m^{\dagger}\, C_n \qquad (8)$$

where the matrix elements $S_{\alpha mn}$ are given by

$$S_{\alpha mn} = \langle m | S_\alpha | n \rangle \qquad (9)$$

and are tabulated in Table 1 for Pr,Tl. It is convenient to substitute for S_α given by (8) into $G^{\alpha\beta}$ and define an inter-level susceptibility $\hat{G}$ by:

$$G^{\alpha\beta}(ij,t) = \sum_{mn} S_{\alpha mn}\, \hat{G}^{\beta}(mn,ij,t) \qquad (10)$$

where

$$\hat{G}^{\beta}(mn,ij,t) = \langle\langle C_m^{\dagger}(i,t)\, C_n(i,t) \,|\, S_\beta(j) \rangle\rangle \qquad (11)$$

and its equation of motion is

$$\omega\, \hat{G}^{\beta}(mn, ij, \omega) = \left\langle \left[C_m^{+}(i) C_n(i),\, S_\beta(j) \right] \right\rangle + \left\langle\!\!\left\langle \left[C_m^{+}(i,t) C_n(i,t), H \right] \middle| S_\beta(j) \right\rangle\!\!\right\rangle_{\omega} \qquad (12)$$

Using (3b) and (8) the Hamiltonian H in (7) can be written entirely in terms of the operators C_n and hence the commutators in (12) can be easily evaluated. Some terms from the second commutator involve products of four C_n operators. These give rise to a higher order Green's functions whose equations of motion generate, in a similar way, Green's functions of an even higher order. The resulting hierachy of Green's function equations may be decoupled in the RPA by replacing a product of four operators by terms involving only two operators as follows:

$$\begin{aligned} C_m^{+}(i) C_s(i)\, C_q^{+}(l) C_p(l) &= \left\langle C_m^{+}(i) C_m(i) \right\rangle C_q^{+}(l) C_p(l)\, \delta_{ms} \\ &\quad + \left\langle C_q^{+}(l) C_q(l) \right\rangle C_m^{+}(i) C_s(i)\, \delta_{pq} \\ &= f_m\, C_q^{+}(l) C_p(l) \delta_{ms} + f_q C_m^{+}(i) C_s(i) \delta_{pq} \end{aligned} \qquad (13)$$

where $f_m = \langle C_m^{+}(i)\, C_m(i) \rangle$ is the Boltzmann occupation factor for the level m and is independent of the site. Substituting into (12) and taking Fourier transforms, it can easily be shown that

$$\begin{aligned} G^{\alpha\beta}(q,\omega) &= g^{\alpha\beta}(\omega) + g^{\alpha+}(\omega) J(q) G^{-\beta}(q,\omega) \\ &\quad + g^{\alpha-}(\omega) J(q) G^{+\beta}(q,\omega) + 2 g^{\alpha z}(\omega) J(q)\, G^{z\beta}(q,\omega) \end{aligned} \qquad (14)$$

where

$$G^{\alpha\beta}(\underline{q},\omega) = \frac{1}{N}\sum_{ij} G^{\alpha\beta}(ij,\omega)\, e^{i\underline{q}\cdot(\underline{R}_i - \underline{R}_j)} \tag{15}$$

and the single-ion susceptibility $g^{\alpha\beta}(\omega)$ is given by

$$g^{\alpha\beta}(\omega) = \sum_{mn} S_{\alpha mn} S_{\beta nm} \frac{(f_n - f_m)}{\omega - (\omega_n - \omega_m)} \tag{16}$$

For Pr^{3+} ion in cubic symmetry, it is found that if any one of S_+, S_- or S_z has a non-zero matrix element between the levels m and n, then the other two have zero matrix elements. Hence, from (16), the only non-zero components of the single-ion susceptibility are g^{+-}, g^{-+} and g^{zz}. With this simplification equation (14) reduces to:

$$G^{+-}(\underline{q},\omega) = g^{+-}(\omega) + g^{+-}(\omega) J(\underline{q})\, G^{+-}(\underline{q},\omega) \tag{17a}$$

$$G^{-+}(\underline{q},\omega) = g^{-+}(\omega) + g^{-+}(\omega) J(\underline{q})\, G^{-+}(\underline{q},\omega) \tag{17b}$$

$$G^{zz}(\underline{q},\omega) = g^{zz}(\omega) + 2g^{zz}(\omega) J(\underline{q})\, G^{zz}(\underline{q},\omega) \tag{17c}$$

The components of the dynamic susceptibility are thus given by:

$$G^{+-}(\underline{q},\omega) = \frac{g^{+-}(\omega)}{1 - J(\underline{q})\, g^{+-}(\omega)} \tag{18a}$$

$$G^{-+}(q,\omega) = \frac{g^{-+}(\omega)}{1 - J(q)\,g^{-+}(\omega)} \qquad (18b)$$

and

$$G^{zz}(q,\omega) = \frac{g^{zz}(\omega)}{1 - 2J(q)\,g^{zz}(\omega)} \qquad (18c)$$

Although these equations have a very simple form, most of the information about the complex crystal level structure is contained in the single-ion susceptibility $g^{\alpha\beta}(\omega)$ given by (16). All the transitions between the single-ion levels are contained in (16) and equation (17) tells us how these propagate through the crystal as spin waves via the exchange. The spin wave energies are given by the poles of the Green's function $G(q,\omega)$ and the neutron inelastic scattering cross-section is proportional to

$$\frac{1}{(1 - e^{\beta\omega})}\ Im\, G(q,\omega) \qquad (19)$$

Holden and Buyers (1974) and Buyers et al (1975) have applied this theory to Pr_3Tl and $(Pr, La)_3Tl$ and obtain fairly good agreement with experiment in the temperature dependence of the magnetic excitations in these systems. Some of the results for Pr_3Tl are shown in Figures 3 and 4. Figure 3 shows the dispersion relations at T = 0 where all modes originate from the ground state. Only the three

lowest branches arising from Γ_4-Γ_1 transitions have appreciable dispersion. The higher-frequency branches, since they have small matrix elements (see Table 1), are almost independent of wa vector as expected from equation (18). At finite temperatures the excited states become populated and new modes appear. At 0.9 T_c the dispersion relations of the lowest frequency excitations are as shown in Figure 4.

(iii) Scattering of magnetic excitations and the coherent potential approximation.

The magnetic excitations obtained from the RPA expression for the dynamic susceptibility are undamped. As mentioned earlier, these spin waves are transitions between single-ion molecular field states which propagate through the crystal via the exchange interaction. If the state of an ion were to deviate from the molecular field value, it would be equivalent to introducing a defect at that site which can scatter the spin waves. One way in which the molecular field state of an ion may be changed is by applying a magnetic field. In this work we assume that there is a distribution of fluctuating fields in the crystal which can scatter the spin waves. At any site these fields arise from thermal fluctuations of the spins on neighbouring sites which couple to the central site via the exchange interaction. The scattering of the spin waves is treated in the coherent potential approximation (CPA) and we begin in section (A)

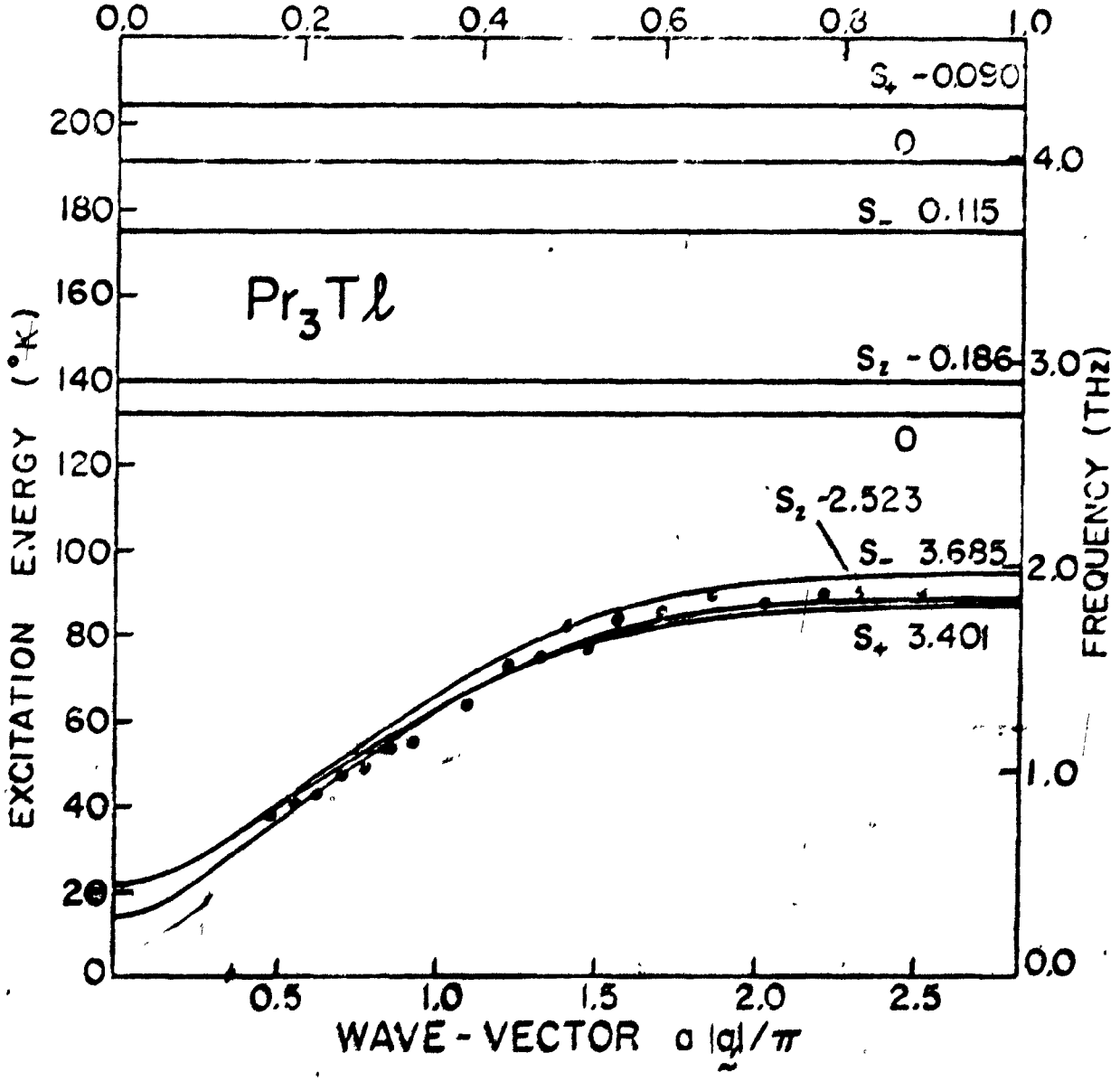

Figure 3

Dispersion relation of spin waves propagating along the [110] direction of Pr_3Tl at T=0. The full circles are the experimental results of Birgeneau et al (1971). The single-ion matrix elements corresponding to each transition 0→n are $S_\alpha \pm S_{\alpha\alpha}$, where $\alpha = \pm, z$ (after Buyers et al (1975)).

Figure 4

Dispersion relation for Pr_3Tl at finite temperature. The symbols m-n identify the single-ion transitions corresponding to the excited state spin waves. (after Buyers et al (1975)).

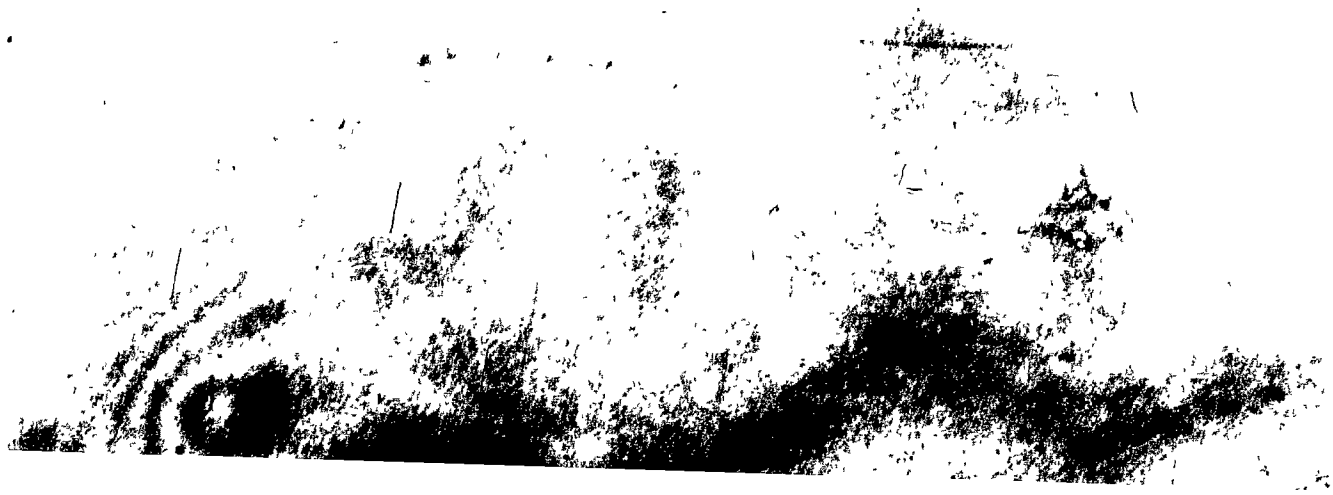

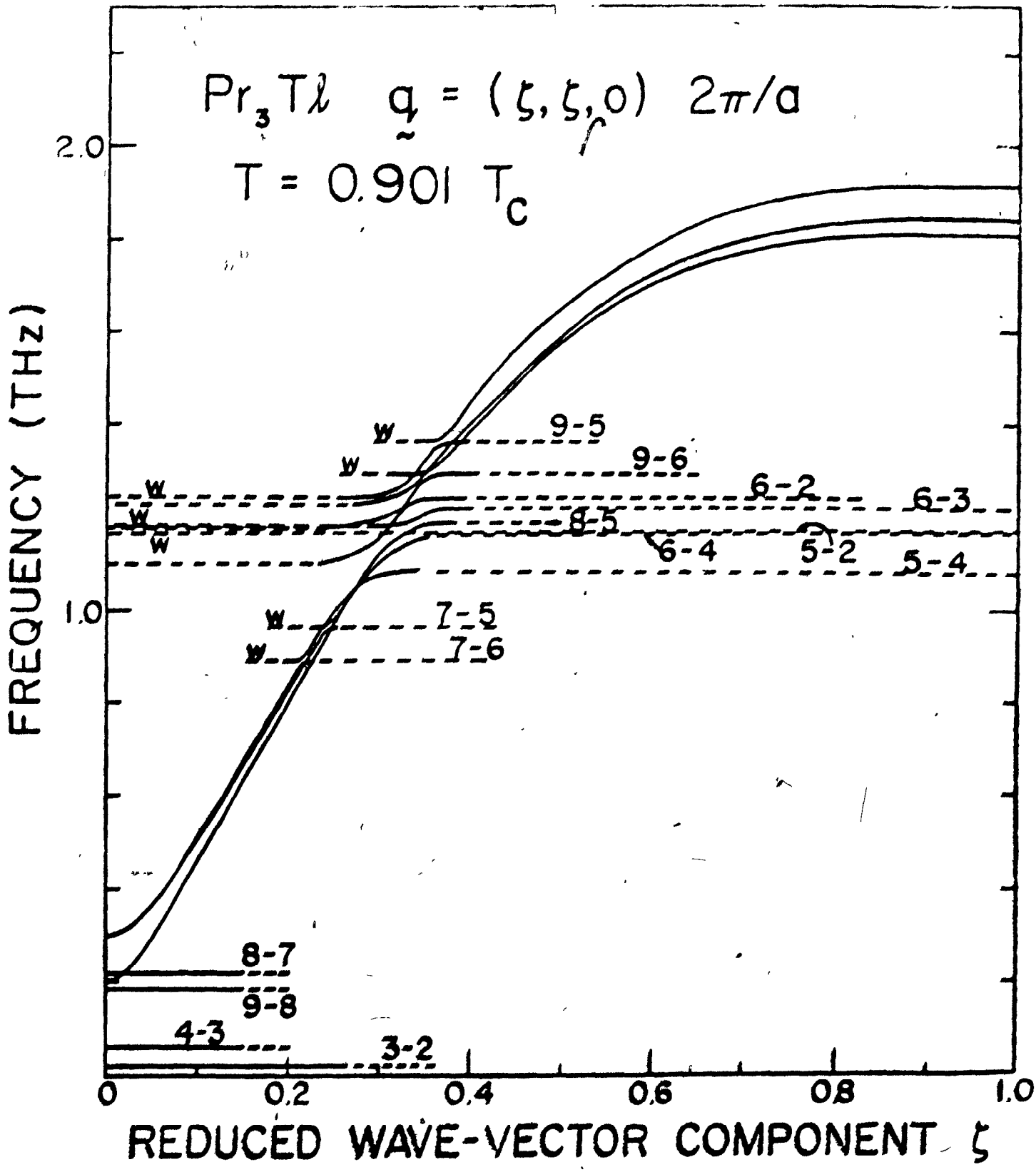
Pr_3Tl $q = (\zeta, \zeta, 0)$ $2\pi/a$
T = 0.901 T_c
FREQUENCY (THz)
2.0
1.0
W
9-5
9-6
6-2
6-3
8-5
6-4
5-2
5-4
7-5
7-6
8-7
9-8
4-3
3-2
0
0.2
0.4
0.6
0.8
1.0
REDUCED WAVE-VECTOR COMPONENT ζ

Figure 4

below with a brief summary of the CPA results. Then in section (B) we obtain an expression for the distribution of fluctuating fields which is used to discuss the scattering of spin waves in section (C). Finally, the results and conclusions are given in section (D).

(A) The Coherent Potential Approximation

The coherent potential approximation (CPA) is an effective medium theory for disordered systems. In the case of a binary metallic alloy the different scattering potentials at the two types of atoms are replaced by the same effective potential at each atomic site. This restores the translational invariance of the lattice and enables the electronic band structure to be calculated. We give here a brief summary of the main results of the CPA and the reader is referred to the papers by Soven (1967, 1969) for further details.

Consider an alloy of N atoms of type A and B with concentration c and 1-c respectively. In the absence of any scattering potentials the empty lattice is represented by a conduction band with a Hamiltonian H_0 given by

$$H_0 = \sum_{\underline{k}} \varepsilon_{\underline{k}} C^{+}_{\underline{k}} C_{\underline{k}} \qquad (20)$$

The corresponding unperturbed Green's function is

$$G^0(\omega) = \frac{1}{\omega - H_0} \qquad (21)$$

or in momentum representation

$$G^{\circ}_{\underline{K}}(\omega) = \frac{1}{\omega - \varepsilon_{\underline{K}}} \qquad (22)$$

In the presence of the potentials, the total Hamiltonian H is written as

$$H = H_0 + H_1 \qquad (23)$$

where H_1 is the contribution due to the potentials and has the following form in the Wannier representation:

$$H_1 = \sum_i V_i C_i^{\dagger} C_i \qquad (24)$$

The atomic potential V_i has the value V_A at the A sites and V_B at the B sites and $C_i^{\dagger}$ and C_i are the creation and annihilation operators for the Wannier function of the i^{th} atomic site. The total Green's function is

$$G(\omega) = \frac{1}{\omega - H} \qquad (25)$$

and is related to the unperturbed Green's function as follows:

$$G = G^{\circ} + G^{\circ} H_1 G \qquad (26)$$

In the Wannier representation this becomes

$$G_{ij} = G^{\circ}_{ij} + \sum_{\ell} G^{\circ}_{i\ell} V_{\ell} G_{\ell j} \qquad (27)$$

The starting point for CPA is to assume an effective potential $\Sigma(\omega)$ at each site i.e. an effective medium with the Hamiltonian

$$H_{eff} = H_o + \sum_i \Sigma(\omega) C_i^\dagger C_i \qquad (28)$$

The potential $\Sigma(\omega)$ is energy dependent and is usually called the electron self-energy. It is determined self-consistently by requiring that the excess single-site scattering is zero. The Green's function for the effective medium is

$$G^{eff}(\omega) = \frac{1}{\omega - H_{eff}} \qquad (29)$$

or in momentum representation

$$G_{\underline{k}}^{eff}(\omega) = \frac{1}{\omega - (\varepsilon_{\underline{k}} + \Sigma(\omega))} \qquad (30)$$

By analogy with (27) the total Green's function is related to the effective Green's function as follows:

$$G_{ij} = G_{ij}^{eff} + \sum_l G_{il}^{eff} V_l G_{lj} \qquad (31)$$

where v_l is the excess potential at site l i.e.

$$v_l = V_l - \Sigma(\omega) \qquad (32)$$

The total scattering of an electron due to this excess potential is given by the single site t-matrix

$$t_\ell = \frac{V_\ell}{1 - G^{eff}_{\ell\ell} V_\ell} \qquad (33a)$$

Because of the translational invariance of the effective medium $G^{eff}_{\ell\ell}$ is independent of the site and we may take ℓ to be the origin ($\ell = 0$). Hence

$$t_\ell = \frac{V_\ell}{1 - G^{eff}_{00} V_\ell} \qquad (33b)$$

In CPA we assume that the average excess scattering is zero i.e.

$$\langle t_\ell \rangle = 0 \qquad (34)$$

Neglecting the remaining scattering terms we find that the Green's function G (which we now denote by G^{CPA}) is that of the effective medium we started with i.e.

$$G^{CPA}_{\underline{k}}(\omega) = \frac{1}{\omega - (\varepsilon_{\underline{k}} + \Sigma(\omega))} \qquad (35)$$

We note that from (22) this can be rewritten as

$$G^{CPA}_{\underline{k}}(\omega) = G^{0}_{\underline{k}}(\omega) + G^{0}_{\underline{k}}(\omega)\,\Sigma(\omega)\,G^{CPA}_{\underline{k}}(\omega) \qquad (36)$$

Thus the CPA condition may be written as

$$\frac{c\left(V_A - \Sigma(\omega)\right)}{1 - G_{oo}^{CPA}(\omega)\left(V_A - \Sigma(\omega)\right)} + \frac{(1-c)\left(V_B - \Sigma(\omega)\right)}{1 - G_{oo}^{CPA}(\omega)\left(V_B - \Sigma(\omega)\right)} = 0 \tag{37}$$

where

$$G_{oo}^{CPA}(\omega) = \frac{1}{N}\sum_{\underline{k}} G_{\underline{k}}^{CPA}(\omega) \tag{38}$$

and the self-energy $\Sigma(\omega)$ is determined self-consistently from (37) and (38).

In the following sections we will apply these results to the scattering of the spin waves discussed earlier. We will show that the propagator equation for the spin waves in real space has the same form as that of electrons (equation(27)). However, instead of two types of scattering potentials we have an infite distribution of fields which scatter the spin waves.

(B) Distribution of fluctuating fields.

The fluctuating fields at a site result from thermal fluctuations of spins of neighbouring atoms which are coupled to the central site by the exchange interaction. Furrer and Heer (1973) extended the molecular field theory for rare-earth metals to include such fluctuating fields and were thus able to obtain a better fit for the magnetization of NdSb as a function of temperature. In this section we present an alternative derivation of the probability distribution of Furrer and Heer for the fluctuating fields. The resulting expression is subsequently used to examine the scattering of

spin waves at non-zero temperatures. The probability for a deviation δS_z in the z-component of a spin is given by (Landau and Lifshitz (1958)):

$$P(\delta S_z) = \frac{1}{\sqrt{2\pi \langle \delta S_z^2 \rangle}} e^{-\delta S_z^2 / 2\langle \delta S_z^2 \rangle} \quad (39)$$

where $\langle \delta S_z^2 \rangle$ is given by the fluctuation dissipation theorem as

$$\langle \delta S_z^2 \rangle = \frac{1}{2\pi} \int_{-\infty}^{\infty} Im\, G^{zz}(ii,\omega) \coth \frac{\omega}{2KT}\, d\omega \quad (40)$$

The Green's function in (40) is the full Green's function of the system which includes the effects of the fluctuating fields self-consistently. A first approximation is to replace G^{zz} in (40) by its RPA value. To simplify this expression we employ the classical approximation and keep only the leading term in $\coth \frac{\omega}{2kT}$. Thus

$$\langle \delta S_z^2 \rangle = \frac{1}{2\pi} \int_{-\infty}^{\infty} Im\, G^{zz}(ii,\omega) \frac{2KT}{\omega}\, d\omega$$

$$= \frac{KT}{\pi} \int_{-\infty}^{\infty} \frac{Im\, G^{zz}(ii,\omega)}{\omega}\, d\omega$$

and using the Kramers-Kronig relation this reduces to

$$\langle \delta S_z^2 \rangle = KT\, G^{zz}(ii,0). \quad (41)$$

where $G^{zz}(ii,0)$ is the local static susceptibility. Using the RPA expression for the susceptibility (equation (18c) we

can write this as

$$G^{zz}(ii,0) = \frac{1}{N}\sum_{\underline{q}} G^{zz}(\underline{q},0)$$

$$= \frac{1}{N}\sum_{\underline{q}} \frac{g^{zz}(0,T)}{1-2J(\underline{q})g^{zz}(0,T)} \qquad (42)$$

where we have now indicated explicitly the temperature dependence of the single-ion susceptibility. The Curie temperature for the transition to an ordered state is given in the RPA by the pole of the $\underline{q} = 0$ component of the static susceptibility in (42) i.e.

$$1 - 2J(0)g^{zz}(0,T_c) = 0 \qquad (43)$$

Using this we can rewrite (42) as:

$$G^{zz}(ii,0) = \frac{1}{2J(0)} W(T) \qquad (44)$$

where

$$W(T) = \frac{1}{N}\sum_{\underline{q}} \frac{1}{1+y(T)-\gamma(\underline{q})} \qquad (45)$$

For nearest neighbour interaction, $\gamma(\underline{q})$ is a structure factor given by

$$\gamma(\underline{q}) = J(\underline{q})/J(0)$$

$$= \sum_i e^{i\underline{q}\cdot\underline{R}_i} \qquad (46)$$

In equation (45), all the temperature dependence is in y(T) which is defined as:

$$y(T) = \frac{g(0,T_c) - g(0,T)}{g(0,T)} \qquad (47)$$

At the transition temperature y = 0 and W is of the order of unity. We now make a further simplifying assumption by neglecting the temperature dependence of W and replacing it by unity. With this approximation we finally obtain

$$\langle \delta S_z^2 \rangle \sim \frac{kT}{2J(0)} \qquad (48)$$

The field h at a given site due to fluctuations δS_z of spins of neighbouring atoms is

$$h = \lambda \delta S_z \qquad (49)$$

where $\lambda = 2J(o)$. From (39), (48) and (49) the probability for a field h at a site is

$$P(h) = \frac{1}{\sqrt{2\pi kT/\lambda}} e^{-h^2/2\lambda kT} \qquad (50)$$

This is the same expression as that obtained by Furrer and Herr (1973).

(C) Damping of the magnetic excitations.

We now consider, in the CPA, the scattering of the spin waves by the fluctuating fields. To do this we write the susceptibility equation (17) in real space formally as:

$$G(ij,\omega) = g(i,\omega)\delta_{ij} + \sum_{l} g(i,\omega) J_{il} G(lj,\omega) \qquad (51)$$

In the presence of the fluctuating fields h distributed at the atomic sites with a distribution given by (50) this equation becomes

$$G(ij,\omega,h) = g(i,\omega,h)\delta_{ij} + \sum_{l} g(i,\omega,h) J_{il} G(lj,\omega,h) \qquad (52)$$

To simplify matters, we now change the notation slightly and rewrite equations (51) and (52) respectively as:

$$G^{\circ}(ij,\omega) = g^{\circ}(i,\omega)\delta_{ij} + \sum_{l} g^{\circ}(i,\omega) J_{il} G^{\circ}(lj,\omega) \qquad (53)$$

and

$$G(ij,\omega) = g(i,\omega)\delta_{ij} + \sum_{l} g(i,\omega) J_{il} G(lj,\omega) \qquad (54)$$

We now define a new function F as

$$F(ij,\omega) = G(ij,\omega)/g(i,\omega) \qquad (55)$$

so that, substituting this in (54) gives

$$F(ij,\omega) = \delta_{ij} + \sum_{l} J_{il}\, g(l,\omega)\, F(lj,\omega) \qquad (56)$$

To obtain an equation with single-site scattering terms we introduce another function Q defined as

$$Q(ij,\omega) = \sum_{l} F(il,\omega)\, J_{lj} \qquad (57)$$

It can easily be shown that Q satisfies the following equation

$$Q(ij,\omega) = Q^{\circ}(ij,\omega) + \sum_{l} Q^{\circ}(il,\omega)\left(g(l,\omega) - g^{\circ}(l,\omega)\right) Q(lj,\omega) \qquad (58)$$

where Q° is evaluated in the absence of the scattering fields. The propagator equation (58) should be compared with equation (27) for an electron scattered by a series of potentials. Within the CPA we look for the self-consistent Q which minimizes the scattering. Following the arguments of section (A) the single-site t-matrix is

$$t_l = \frac{g(l,\omega) - g^{\circ}(l,\omega) - \Sigma(\omega)}{1 - Q(00,\omega)\left(g(l,\omega) - g^{\circ}(l,\omega) - \Sigma(\omega)\right)} \qquad (59)$$

If h is the field at site ℓ then this t-matrix may be written as:

$$t(h) = \frac{\delta g(\omega) - \Sigma(\omega)}{1 - Q(00,\omega)\left(\delta g(\omega) - \Sigma(\omega)\right)} \qquad (60)$$

where $\delta g(\omega)$ is the difference in the single-ion susceptibility

in the presence and absence of the field h. The CPA condition is then

$$\int P(h)\, t(h)\, dh = 0 \qquad (61)$$

The 'self-energy' $\Sigma(\omega)$ relates the self-consistent CPA solution Q to the mean field solution Q° via the equation (compare with (36)):

$$Q(\underline{q},\omega) = Q^\circ(\underline{q},\omega) + Q^\circ(\underline{q},\omega)\Sigma(\omega)\, Q(\underline{q},\omega) \qquad (62)$$

where

$$Q(\underline{q},\omega) = \frac{Q^\circ(\underline{q},\omega)}{1 - Q^\circ(\underline{q},\omega)\,\Sigma(\omega)} \qquad (63)$$

with

$$Q^\circ(\underline{q},\omega) = \frac{J(\underline{q})}{1 - J(\underline{q})\, g^\circ(\omega)} \qquad (64)$$

The last equation is easily obtained from the Fourier transforms of equations (56) and (57). Finally, the single-site function in (60) is

$$Q(00,\omega) = \frac{1}{N}\sum_{\underline{q}} Q(\underline{q},\omega) \qquad (65)$$

Hence (61) is an implicit function for $\Sigma(\omega)$ which can be solved by an iterative procedure and thus obtain $Q(\underline{q},\omega)$. This

can then be inverted, using (57) and (55), to give us the CPA susceptibility

$$G(q,\omega) = \frac{g^0(\omega) + \Sigma(\omega)}{1 - J(q)(g^0(\omega) + \Sigma(\omega))} \qquad (66)$$

Using this G we can obtain the spin wave spectrum and the neutron scattering cross-section in the CPA.

(D) Results and Conclusions.

We have applied the scattering theory described above to the damping of the magnetic excitations in Pr_3Tl. This compound has the Cu_3Au structure which is equivalent to fcc Pr with the corner Pr atoms replaced by Tl. Birgeneau (1972) points out that if the charge of the Tl ion is taken equal to that of the Pr^{3+} ion, then in the point charge model the effective symmetry at the Pr site is cubic. It then follows that the ratio of the crystal-field parameter B_4^4/B_4^0 given by the point charge model is -149.4 (Holden and Buyers (1974)). The magnitudes of B_4^0 and B_4^4 are chosen to reproduce the observed crystal-field splitting. The average crystal-field splitting between the ground state and the first excited state triplet is Δ = 77K and the crystal field parameters chosen to fit this are $B_4^0 = -1.04 \times 10^{-3}$THz and $B_4^4 = 6.9 \times 10^{-6}$THz (1THz = 48K). Assuming only nearest neighbour interaction, the exchange coupling $J(-5.8 \times 10^{-3}$THz) is chosen to give the observed saturation moment in Pr_3Tl (Holden and Buyers (1974)).

To evaluate the CPA propagator (66) we solve the coupled equations (61) and (65) for the self-energy $\Sigma(\omega)$ by an iterative procedure. To facilitate numerical calculation we replace the continuous distribution in (61) by a finite number of discrete fields with the Gaussian distribution given by (50). We found that we can obtain good convergence with a fairly small number of fields (in our calculations we have considered 13 fields).

The broadening of the spin wave modes due to scattering is shown in Figure 5. In this figure the lineshape of the transverse spin wave modes is shown for 3 values of the wavevector. We note that the $\vec{q} = 0$ mode is shifted upwards from 0.3 THz to 0.65 THz and is also broadened in the CPA compared to the RPA. The 0.02 THz width in the RPA case is the Lorentzian width artificially introduced to simplify numerical computation. This was done by adding to the frequency a small imaginary part $\epsilon = 0.01$ THz. In the CPA, the width is 0.05 THz which means that the broadening due to scattering is 0.03 THz. At very low temperatures this broadening disappears as expected since as $T \to 0$ the fluctuating fields disappear. As the temperature increases the damping width increases and then remains fairly constant at 0.03 THz from 4.5 to 57 K (the highest temperature considered). The large shift of the $\vec{q} = 0$ mode is due to the fact the scattering fields are quite large. For example at $T = 0.9\ T_c$ the average scattering field is twice as large as the molecular field. The magnitudes of the fields increase rapidly as $T^{1/2}$

at low temperatures(equation (48)) and hence the scattering is expected to increase rapidly at low temperatures. As the temperature increases further the scattering would tend to saturate and this could explain why the damping remains fairly constant above 4.5 K.

In Figure 6 we show the dispersion of the longitudinal spin waves at a finite temperature (T=15K). The upper part is the RPA result which shows the main dispersion curve mixing with 2 weak dispersionless modes originating from the excited states. The lower CPA picture is in marked contrast. Here the main dispersion curve is shifted upwards with maximum shift occuring at small wavevectors. In addition, new weak modes appear which are fairly dispersionless and they also mix with the main dispersion curve. In the RPA the spin wave modes may be identified as arising from transitions between pairs of molecular field levels by examining the level structure of Figure 1 and the matrix elements of Table 1. In the CPA the inclusion of the fluctuating fields changes the level structure and it becomes difficult to identify the new weak modes.

Figure 7 shows the temperature dependence of the $q = 0$ main spin wave modes arising from the Γ_4-Γ_1 transitions. In the RPA, the energies of both the transverse and longitudinal modes decrease as the temperature increases. Although they exhibit soft mode behaviour, the modes do not become soft at the transition temperature. Their energies fall off to a finite value at T_c and then increase again as the temperature

increases further. In contrast, in the CPA, the energies of these modes increase with temperature and show no tendency toward softening. The splitting between the transverse and longitudinal modes above T_c is due to the fact that we have only considered fluctuating fields in the z-direction. The sharp linear rise at low temperatures in the CPA modes is due to the sharp increase in the magnitudes of the scattering fields at low temperatures. We note that the temperature distribution of the fields (equation (48)) was obtained in the classical approximation which is not applicable at low temperatures.

Figure 8 indicates the temperature dependence of the main modes at finite wavevector and shows that their behaviour with temperature is qualitatively the same as the $q = 0$ modes.

Finally in Figure 9 we plot the frequency and intensity of the neutron peak as a function of temperature and compare them with the experimental results of Figure 2. For the frequency, the CPA results are not as good as those in the RPA while agreement with experiment for the intensity is better in CPA.

Recently Bak (1975) introduced a new scheme for calculating damping effects in the spin excitation spectra of singlet-ground-state systems by use of the lowest order self-consistent corrections to the RPA. These corrections also correspond to spin wave scattering by single site fluctuations. It is at present difficult to compare Bak's scheme with the

CPA method of this section since he considered only the singlet-doublet excitations in paramagnetic dhcp Praseodimium whereas the CPA was applied to Pr^{3+} excitations in Pr_3Tl. We hope to apply the CPA and related methods to dhcp Pr^{3+} for this purpose.

In conclusion, we have presented a method of calculating the damping of the magnetic excitations in singlet-ground-state systems using the coherent potential approximation. Some of the results are difficult to interpret and more experimental information is needed to give us a better understanding. In particular detailed measurements are required of the spin wave spectra on single-crystal Pr_3Tl which would distinguish the various modes (especially the modes near the zone-centre) and would thus allow direct comparison with the CPA results to be made.

Figure 5

Lineshape for transverse spin waves in Pr_3Tl in RPA and CPA.

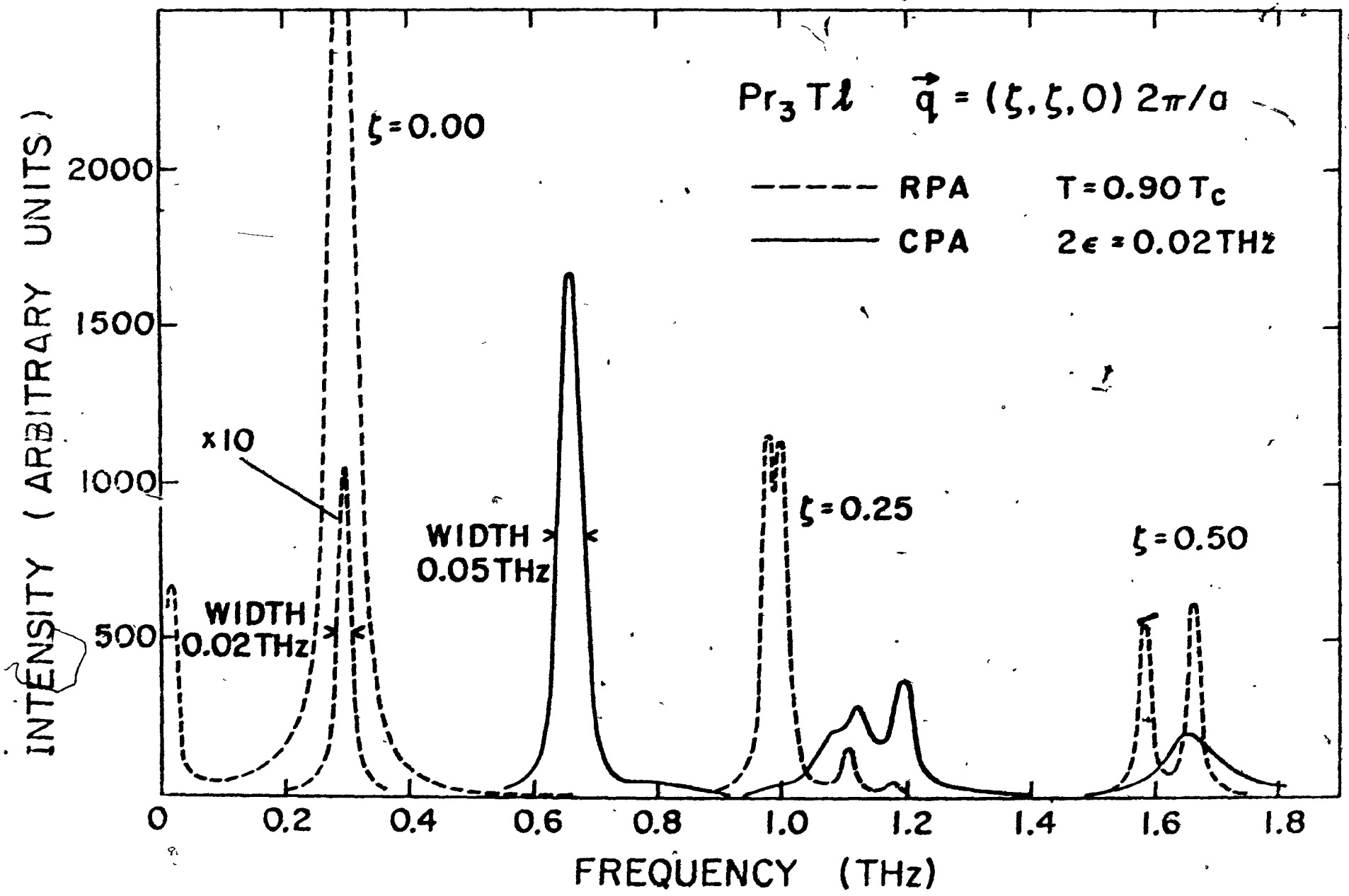
Pr_3Tl $\vec{q} = (\zeta, \zeta, 0)\, 2\pi/a$
RPA
CPA
T = 0.90 T_c
2ϵ = 0.02THz
ζ = 0.00
ζ = 0.25
ζ = 0.50
x10
WIDTH 0.02THz
WIDTH 0.05THz
INTENSITY (ARBITRARY UNITS)
FREQUENCY (THz)
0
0.2
0.4
0.6
0.8
1.0
1.2
1.4
1.6
1.8
500
1000
1500
2000

Figure 5

Figure 6

Dispersion of longitudinal spin waves in Pr_3Tl at finite temperature in RPA and CPA.

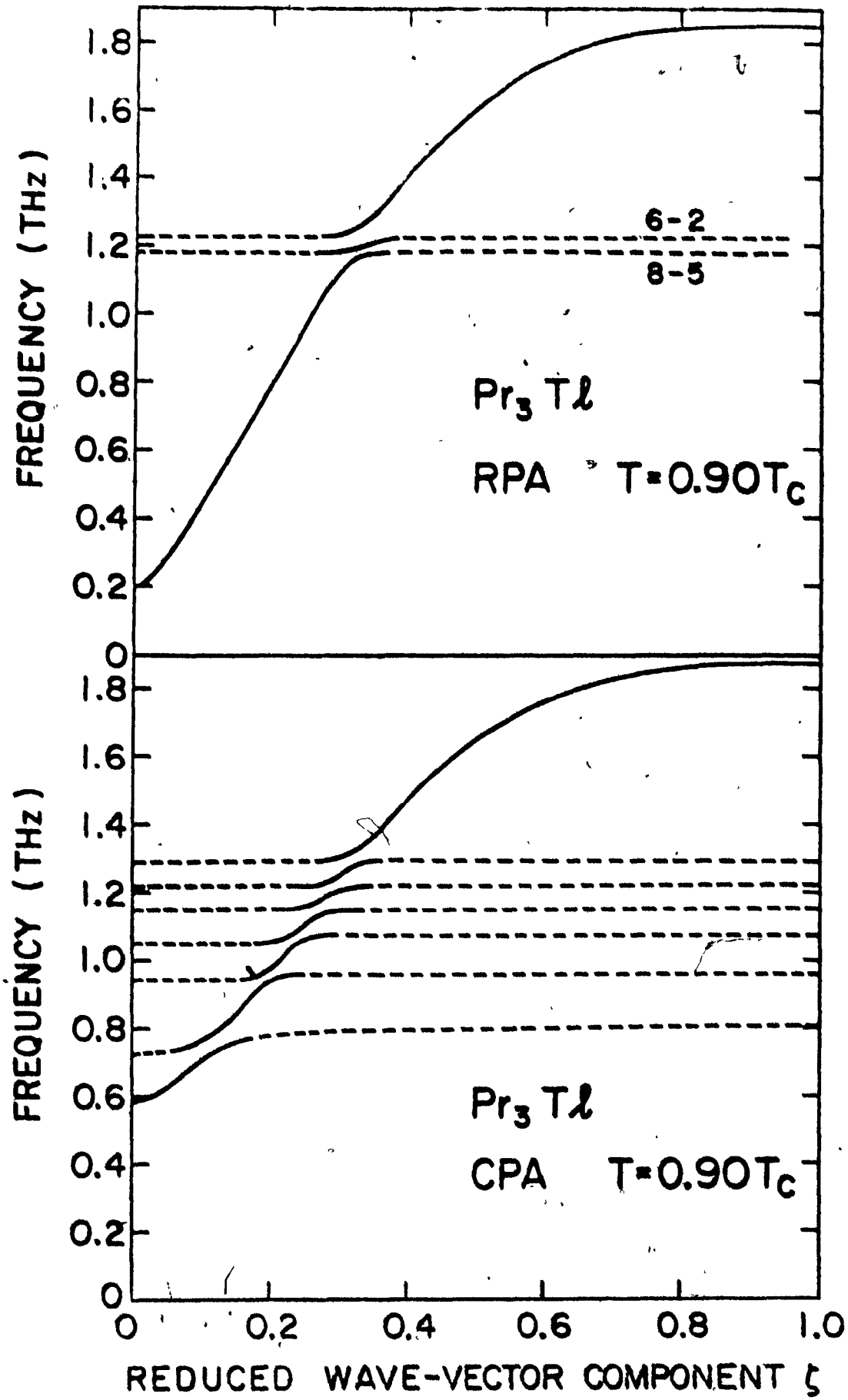
FREQUENCY (THz)
1.8
1.6
1.4
1.2
1.0
0.8
0.6
0.4
0.2
0
6-2
8-5
Pr3 Tl
RPA T=0.90Tc
FREQUENCY (THz)
Pr3 Tl
CPA T=0.90Tc
0
0.2
0.4
0.6
0.8
1.0
REDUCED WAVE-VECTOR COMPONENT ζ

Figure 6

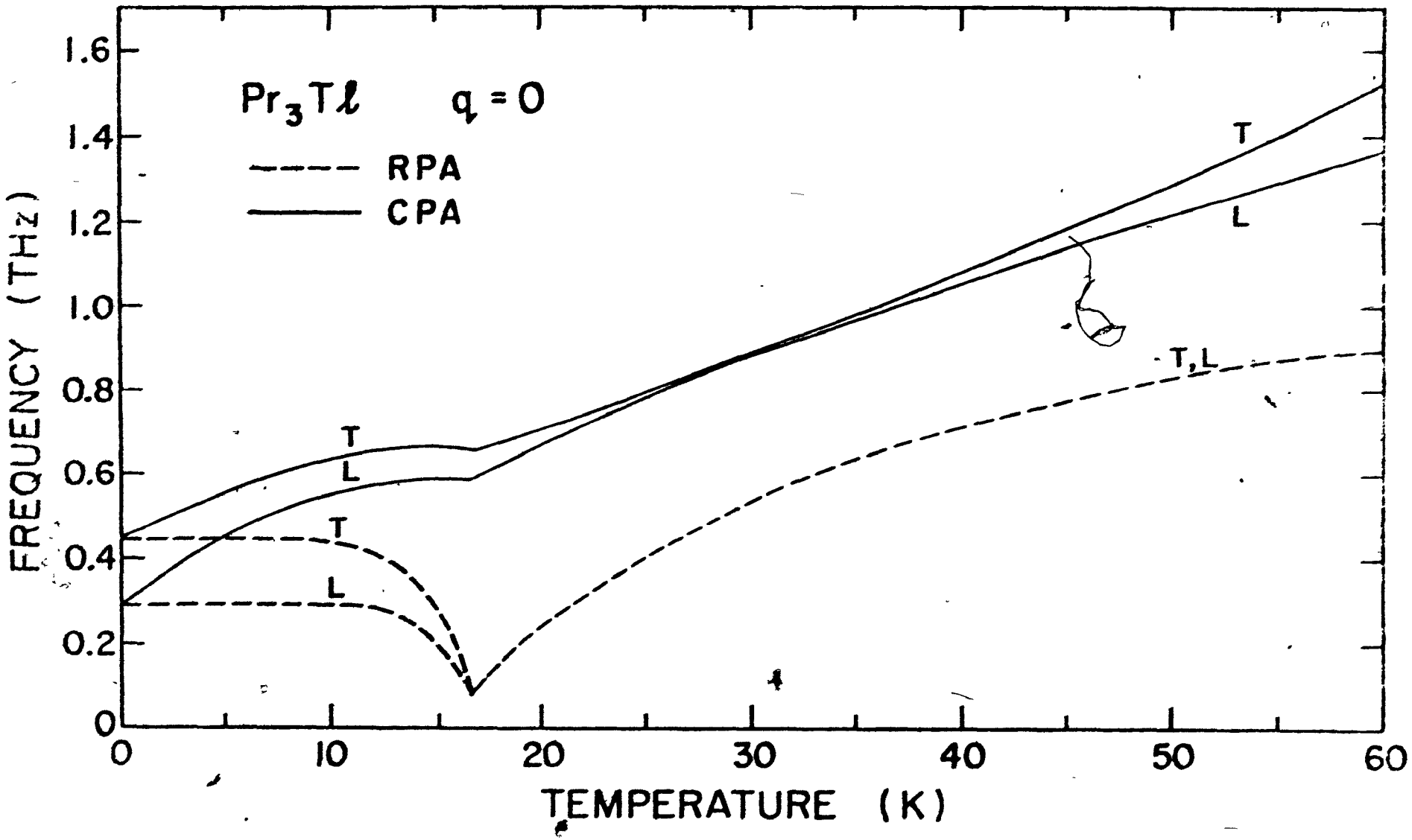

Figure 7

Temperature dependence of the zone-centre spin waves in RPA and CPA

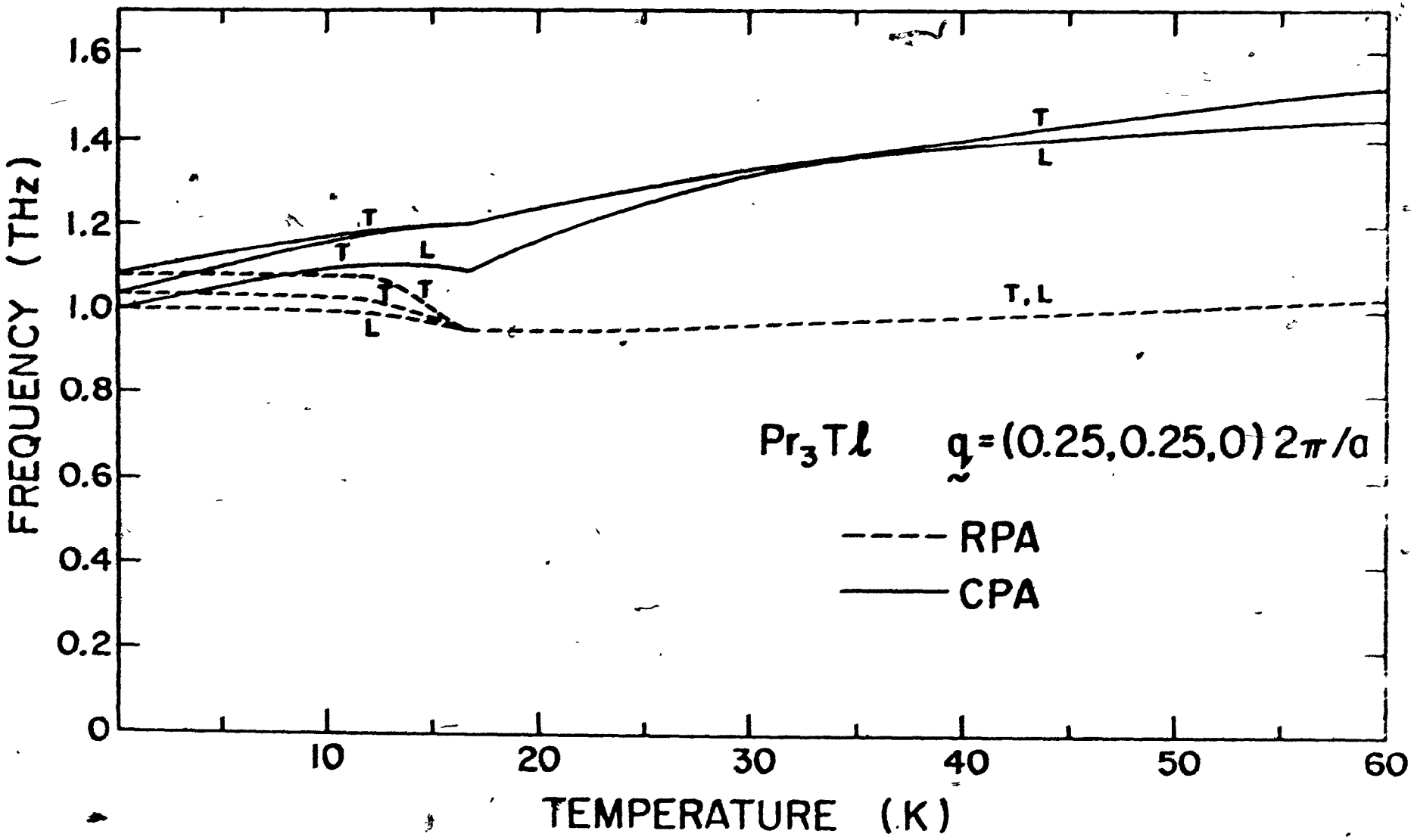

Figure 8

Temperature dependence of spin waves of finite wave vector in RPA and CPA

Figure 9

Temperature dependence of the frequency (top) and intensity (bottom) of the peak in the neutron scattering in RPA and CPA. The full circles are the experimental results of Birgeneau et al (1971).

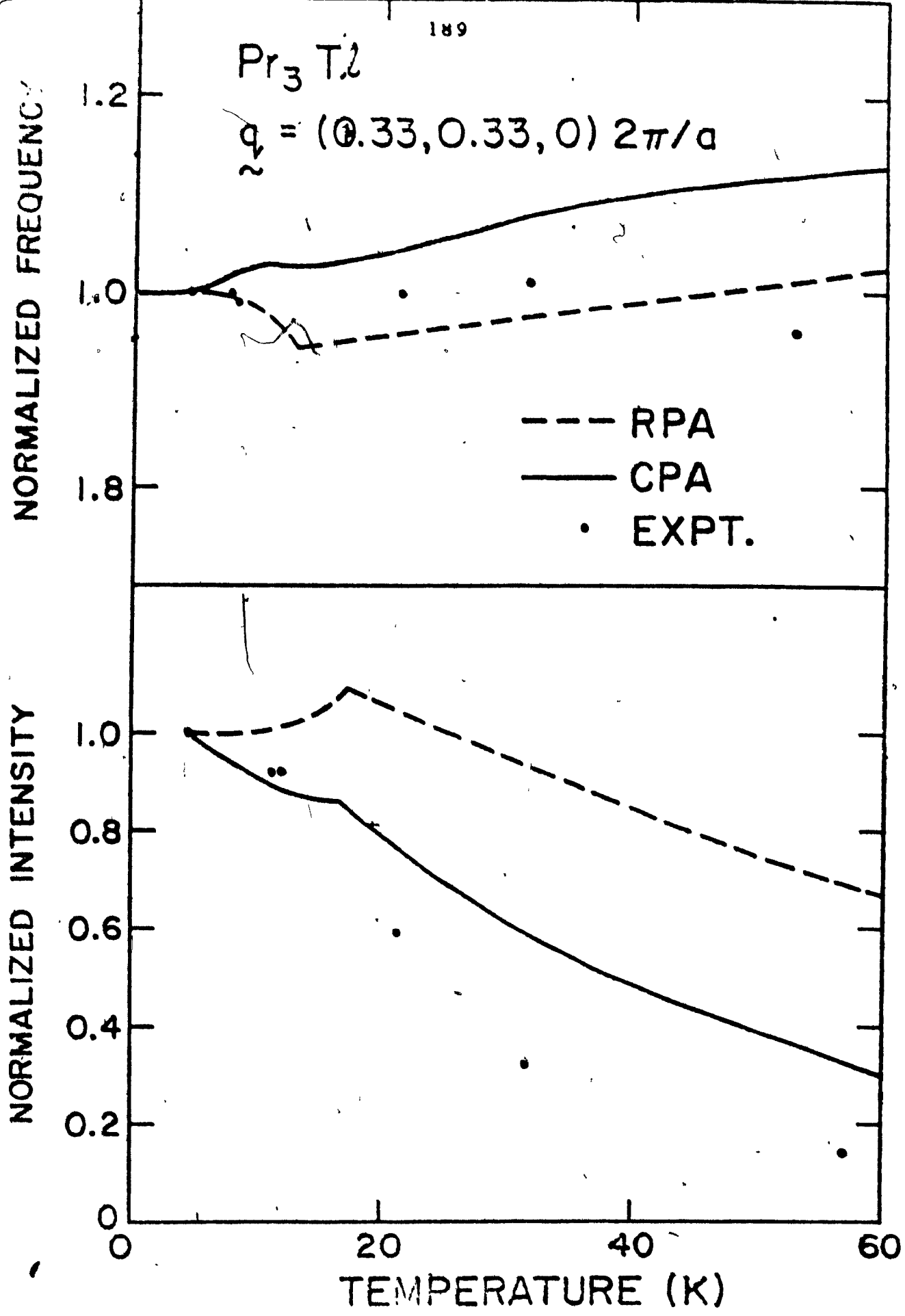
Pr_3Tl
$\underset{\sim}{q}$ = (0.33, 0.33, 0) $2\pi/a$
NORMALIZED FREQUENCY
1.2
1.0
1.8
RPA
CPA
EXPT.
NORMALIZED INTENSITY
1.0
0.8
0.6
0.4
0.2
0
0
20
40
60
TEMPERATURE (K)

Figure 9

Abrikosov A.A., Gorkov L.P. and Dzyaloshinski I.E., Methods of Quantum Field Theory in Statistical Physics (Prentice-Hall, 1963).

Anderson P.W., Phys. Rev. 124, 41 (1961).

Andres K. and Jensen M.A., Phys. Rev. 165, 533 (1968).

Bahurmuz A.A. and Zuckermann M.J., Solid State Commun. 15, 1225 (1974).

Bak P., Phys. Rev. Letters 34, 1230 (1975).

Berk N.F. and Schrieffer J.R., Phys. Rev. Letters 17, 433 (1966).

Birgeneau R.J., AIP Conf. Proc. 10, 1664 (1973).

Birgeneau R.J., Als-Nielson J. and Bucher E., Phys. Rev. Letters 27, 1530 (1971).

Bloch F., Z. Phys., 61, 206 (1930).

Bradley A.J. and Rodgers J.W., Proc. Roy. Soc. A144, 340 (1934).

Buyers W.J.L., Holden T.M. and Perreault A., Phys. Rev. B11, 266 (1975).

Caroli B., J. Phys. Chem. Solids 28, 1427 (1967).

Clogston A., Matthias B., Peter M., Williams H., Corenzwit E., and Sherwood R., Phys. Rev. 125, 541 (1962).

Coles B.R., Hume-Rothery W. and Myers H.P., Proc. Roy. Soc. A196, 125 (1949).

Cooper B.R., Magnetic Properties of Rare Earth Metals, edited by R.J. Elliot (Plenum, London, 1972a), p.17.

Cooper B.R., Phys. Rev. B6, 2730 (1972b).

Coqblin B., J. Phys. (Paris), Colloq. 32, C1-599 (1971).

Daniel E., Solid State Commun. 9, 1359 (1971).

Doniach S. and Engelsberg S., Phys. Rev. Letters 17, 750 (1966).

Doniach S., Proc. Phys. Soc. 91, 86 (1967).

Elliot J.F., Levgold S. and Spedding F.H., Phys. Rev. 91, 28 (1953).

Fallot M., Ann. Phys. (Paris), 6, 305 (1936).

Felcher J.P., Cable J.W. and Wilkinson M.K., J. Phys. Chem. Solids 24, 1663 (1963).

Friedel J., Nuovo Cimento Suppl. 7, 287 (1958).

Furrer A. and Heer H., Phys. Rev. Letters 31, 1350 (1973).

Griffith J.S., The Theory of Transition-Metal Ions, (Cambridge University Press, 1961), p. 104.

Grover B., Phys. Rev. 140, A1944 (1965).

Herring C. and Kittel C., Phys. Rev. 81, 869 (1951).

Holden T.M. and Buyers W.J.L., Phys. Rev. B9, 3797 (1974).

Holstein T. and Primakoff H., Phys. Rev. 58, 1098 (1940).

Hubbard J., Proc. Roy. Soc., 276A, 238 (1963).

Hutchings M.T., Solid State Physics, edited by F. Seitz and D. Turnbull (Academic, New York, 1964), p.227.

Ishikawa Y. and Noda Y. (Private Communication).

Izuyama T., Prog. Theor. Phys., Japan, 23, 969 (1960).

Izuyama T. and Kubo R., J. Appl. Phys. 35, 1074 (1964).

Izuyama T., Kim D.J. and Kubo R., J. Phys. Soc. Japan 18, 1025 (1963).

Jullien R. and Coqblin B., Phys. Rev. B8, 5263 (1973).

Kaiser A.B. and Doniach S., Int. J. Magnetism 1, 11 (1970).

Katzman H. and Mydosh J.A., Phys. Rev. Lett. 29, 998 (1972).

King E., Lee J.A., Harris I.R. and Smith T.F., Phys. Rev. B1, 1380 (1970).

Kishore R. and Joshi S.K., Phys. Rev. B2, 1411 (1970).

Kittel C., Introduction to Solid State Physics, Wiley (1971).

Kubo R., J. Phys. Soc. Japan 12, 570 (1957).

Landau L.D. and Lifshitz E.M., Statistical Physics (Pergamon Press, London, 1958), Ch. XII.

Lederer P. and Mills D.L., Phys. Rev. 165, 837 (1968).

MacPherson M.R., Everett G.E., Wohleben D. and Maple M.B., Phys. Rev. Lett. 26, 20 (1971).

Manohar C., Solid State Commun. 9, 2025 (1971).

Matsubara T., Prog. Theor. Phys. 14, 351 (1955).

Mattis D.C., Phys. Rev. 132, 2521 (1963).

Mills D.L. and Lederer P., J. Phys. Chem. Solids 27, 1805 (1966).

Ratto C.F., Coqblin B., and Galleaui d'Agliano E., Adv. Phys. 18, 489 (1969).

Rice M.J., Phys. Rev. 159, 153 (1967).

Sarachik M.P., Phys. Rev. 170, 679 (1968).

Schindler A.I. and Rice M.J., Phys. Rev. 164, 759 (1967).

Sinclair R.N. and Brockhouse B.N. Phys. Rev. 120, 1638 (1960).

Smart J.S., Effective Field Theories of Magnetism (W.B. Saunders Company, Philadelphia & London, 1966), Chapter 3.

Soven P., Phys. Rev. 156, 809 (1967).

Soven P., Phys. Rev. 178, 1136 (1969).

Stoner E.C., Proc. Roy. Soc., A165, 372 (1938).

Sugibuchi K. and Endo K., J. Phys. Chem. Solids 25, 1217 (1964).

Webster P.J., J. Phys. Chem. Solids 32, 1221 (1971).

Webster P.J., Contemp. Phys. 10, 559 (1969).

Weiss P., Phys. Theor. Appl.[4], 6, 661 (1907).

Wohlfarth E.P., Rev. Mod. Phys. 25, 211 (1953).

Ziman J.M., Electrons and Phonons (Oxford 1960) Ch. VII.

Zubarev D.N., Sov. Phys. Uspekhi. 3, 320 (1960).